

Dissertation zur Erlangung des Doktorgrades
der Fakultät für Chemie und Pharmazie
der Ludwig-Maximilians-Universität München

Structural view on 60S ribosome biogenesis: remodeling and quality control mechanisms



Clara Barrio García
aus
Madrid, Spanien

2016

Dissertation zur Erlangung des Doktorgrades
der Fakultät für Chemie und Pharmazie
der Ludwig-Maximilians-Universität München

Structural view on 60S ribosome biogenesis: remodeling and quality control mechanisms

Clara Barrio García
aus
Madrid, Spanien

2016

Erklärung

Diese Dissertation wurde im Sinne von § 7 der Promotionsordnung vom 28. November 2011 von Herrn Prof. Dr. Roland Beckmann betreut.

Eidesstattliche Versicherung

Diese Dissertation wurde eigenständig und ohne unerlaubte Hilfe erarbeitet.

München,

Clara Barrio García

Dissertation eingereicht am: 12.08.2016

1. Gutachter: Prof. Dr. Roland Beckmann

2. Gutachter: Dr. Daniel N. Wilson

Mündliche Prüfung am: 19.09.2016

Parts of this thesis have been published or submitted to scientific journals:

“Architecture of the Rix1–Rea1 checkpoint machinery during pre-60S-ribosome remodeling”

Clara Barrio-Garcia*, Matthias Thoms*, Dirk Flemming, Lukas Kater, Otto Berninghausen, Jochen Baßler, Roland Beckmann** and Ed Hurt**

* These authors contribute equally to the work

** Corresponding Author

Published on Nature Structural and Molecular Biology 23, 37–44. 2016.

Parts of this thesis have been presented at international conferences:

Poster presented at EMBO Conference on Ribosome Synthesis in Brussels, Belgium, 2015

“Coupled checkpoint-remodelling machinery operative on pre-60S ribosomes prior to nuclear export”

Clara Barrio-Garcia*, Matthias Thoms*, Dirk Flemming, Lukas Kater, Jochen Baßler, Ed Hurt and Roland Beckmann

* These authors contribute equally to the work

Summary

Eukaryotic ribosomes undergo a complex maturation process through which the ribosomal RNA (rRNA) must bind to ribosomal proteins (r-proteins) and fold into its native state. This requires numerous auxiliary factors responsible of rRNA processing, remodeling, intracellular transport and quality control checkpoints.

Impairments in the process of ribosome production can lead to different diseases known as ribosomopathies. However, little is known about which defects in the ribosome biogenesis pathway can escape all quality checkpoints and what targets these faulty ribosomes and their putative products for degradation. The first part of this thesis constitutes a first attempt to address these questions, focusing on a specific impairment of the 60S biogenesis pathway that leads to the production of structurally deficient 80S ribosomes. Here, using cryo-EM and biochemical analysis, it is shown that large structural defects in the ribosome may bypass all quality control mechanisms in the nucleus, but are recognized in the cytoplasm after faulty ribosomes engage in translation. Then, the resulting proteins are targeted for degradation by the ribosome quality-control complex (RQC) after subunit splitting is carried out.

The second part of this thesis focuses on a nucleoplasmic step of 60S ribosome biogenesis in which both the Rix1 complex and the dynein related AAA⁺ ATPase Rea1 bind to maturing pre-60S particles. Rea1 is required for the ATP-dependent dissociation of the assembly factor Rsa4 and may be involved in rearranging the Central Protuberance (CP). Several cryo-electron microscopy (cryo-EM) structures of native pre-60S particles bound to the Rix1-Rea1 machinery are presented in this thesis. Overall, the Rix1-Rea1 particle is similar to the earlier intermediate, the so-called Arx1 particle. However, a 180° rotation of the CP required to reach the final conformation of the 60S, has already happened in the Rix1-Rea1 state, constituting the largest remodeling step at the end of the maturation pathway. By performing cryo-EM analysis on two similar particles that were mutated on either Rix1 or Rea1 and by comparing the structures of the Arx1 and Rix1-Rea1 particles, a mechanistic model for the transition between the two intermediates is provided.

Contents

1	Introduction	1
1.1	Ribosome structure	1
1.2	Translation mechanism	4
1.3	Quality control of nascent peptides	6
1.4	Ribosome biogenesis	7
1.5	60S biogenesis pathway	11
1.5.1	Nucleolar intermediates	12
1.5.2	Nucleoplasmic intermediates	13
1.5.3	Cytoplasmic intermediates	15
1.6	Quality control of ribosomal subunits	15
1.7	Ribosome biogenesis and human diseases	16
1.8	Motivation	17
2	Materials and Methods	21
2.1	Tandem affinity purification of biogenesis intermediates	21
2.2	Cryo-electron microscopy	22
2.2.1	Sample and grid preparation	22
2.2.2	Data collection	23
2.2.3	Data pre-processing	23
2.2.4	Automated particle picking	24
2.2.5	3D refinement and sorting with SPIDER	24
2.2.6	3D refinement and sorting with FREALIGN	27
2.2.7	Resolution determination	28
2.3	Rix1-Rea1 particle model building	29
2.4	Figures	31
3	Results	33
3.1	Translation by structurally impaired ribosomes	33
3.1.1	Impairment of foot processing by Las1 depletion	33

3.1.2	Cryo-EM structures of the Nop53 Las1-depleted sample	34
3.2	Remodeling-checkpoint activity of Rix1-Rea1	40
3.2.1	Rix1-Rea1 interaction and Rix1 complex characterization	40
3.2.2	Cryo-EM structure of the Rix1-Rea1 particle	42
3.2.3	Biogenesis factors on the Rix1-Rea1 particle	44
3.2.4	rRNA remodeling from the Arx1 particle to the mature 60S	48
3.2.5	CP rotation from the Arx1 to the Rix1-Rea1 particle	49
3.2.6	Cryo-EM structure of the Rix1-Rea1 K1089A particle	50
3.2.7	Cryo-EM structure of the Rix1 Δ C particle	53
4	Discussion	57
4.1	Structurally impaired ribosomes can engage in translation	57
4.2	Biogenesis factors in the Rix1-Rea1 particle	60
4.3	Model improvement using high-resolution structures of pre-60S inter- mediates	63
4.4	Remodeling mechanism of the CP	65
4.5	Foot removal in the transit from the Arx1 to Rix1-Rea1 particle	68
5	Conclusions	71
6	Future Perspective	73
	Appendix	78
	List of Abbreviations	79
	References	83
	Acknowledgements	97
	Curriculum Vitae	99

List of Figures

1.1	Structural evolution of the ribosome	2
1.2	The RQC machinery	6
1.3	Eukaryotic ribosome biogenesis overview	8
1.4	Yeast pre-rRNA processing	10
1.5	60S biogenesis pathway	12
1.6	Las1 cleaves 27SB pre-rRNA at site C2	13
3.1	Purification of the Nop53 Las1-depleted 80S particle	33
3.2	FSCs of the first Nop53 Las1-depleted 3D classes	34
3.3	Classification of the Nop53 Las1-depleted particle	35
3.4	Resolution of the Nop53 Las1-depleted 80S particle	36
3.5	Cryo-EM structure of the Nop53 Las1-depleted 80S particle	37
3.6	Hybrid states on Nop53 Las1-depleted 80S particle	38
3.7	The Nop53 Las1-depleted 60S particle	39
3.8	Overall arrangement of the Rix1-Rea1 complex	41
3.9	Cryo-EM structure of the Rix1-Rea1 particle	42
3.10	Resolution of the Rix1-Rea1 reconstruction	43
3.11	Classification of the Rix1-Rea1 dataset	44
3.12	Identification of biogenesis factors in the Rix1-Rea1 particle	46
3.13	Interactions of biogenesis factors in the Rix1-Rea1 particle	47
3.14	rRNA maturation from the Arx1 particle to the mature 60S	48
3.15	Comparison between Arx1 and Rix1-Rea1 particles provides insights into rotation mechanism.	50
3.16	Cryo-EM structure of the Rix1-Rea1 K1089A particle	51
3.17	Resolution of the Rix1-Rea1 K1098A reconstruction	52
3.18	Classification of the Rix1-Rea1 K1098A dataset	53
3.19	Cryo-EM structure of the Rix1 Δ C particle	54
3.20	Resolution of the Rix1 Δ C reconstruction	55

3.21	Classification of the Rix1 Δ C dataset	55
4.1	Foot obstructing the path of ES27	58
4.2	Foot clashing within polysomes	59
4.3	Rsa4's UBL domain interacts with an unexplained density of Rea1 . .	61
4.4	Model of the Rix1 complex organization	63
4.5	Biogenesis factors identified or improved using recent high resolution structures	64
4.6	Nucleoplasmic 60S ribosome biogenesis	67
4.7	The Rpf2-Rrs1 complex stabilizes the immature conformation of the CP	68
A.1	Alignment between Rea1's AAA ⁺ modules and Dynein AAA1 module .	75
A.2	Sda1 secondary structure and sequence conservation	76
A.3	Rsa4 secondary structure and sequence conservation	77

List of Tables

2.1	Cryo-EM structures presented in this dissertation.	28
2.2	Biogenesis factors from <i>S. cerevisiae</i> modeled in the Rix1-Rea1 particle.	30

1 Introduction

Proteins are large biomolecules involved in practically every biological process that takes place in a living organism. They perform a wide range of tasks, such as providing structural and mechanical support to the cell, catalysing reactions or communicating chemical signals. Proteins consist of amino acid chains and with the assistance of molecular chaperones, fold in a defined three-dimensional structure which determines their final role. The amino acid sequence of every protein is encoded by a gene, i.e. a specific nucleotide sequence in the DNA. RNA polymerases synthesize RNA molecules using the genetic information stored in the DNA in a process known as transcription. Different classes of RNA molecules fulfil distinct functions, including scaffolding, enzymatic and expression regulation activities. In particular, messenger RNAs (mRNAs) act as information carriers and are used by the ribosome as templates to synthesize proteins.

1.1 Ribosome structure

Ribosomes are the molecular machines responsible of protein biosynthesis. They are made out of rRNA and r-proteins and their function and overall structure are conserved throughout all domains of life. They have two subunits, each of them harbouring specific functional sites. The small subunit contains the mRNA tunnel and the decoding center (DC), where nucleotide triplets of mRNA are decoded and assigned to a particular amino acid with the mediation of transfer RNAs (tRNAs). The large subunit accommodates the peptidyl transferase center (PTC), where ribosomes catalyze peptide bond formation; and the polypeptide tunnel exit (TE), an elongated cavity that goes from the PTC to the solvent side of the large subunit which serves as a path for the nascent protein chain (NC). In the space between the two subunits, tRNAs have three binding sites known as aminoacyl, peptidyl and exit sites (A- P- and E-sites respectively).

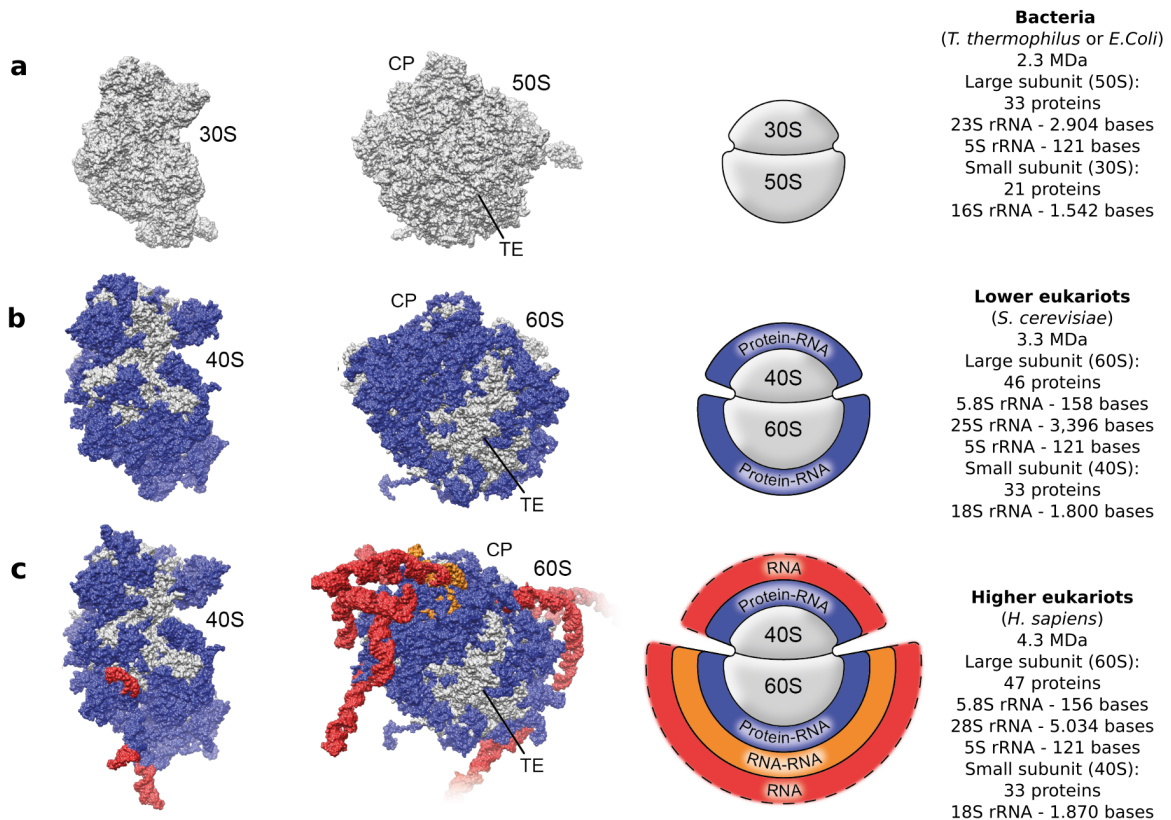


FIGURE 1.1: **Structural evolution of the ribosome.** Comparison between bacterial (a), lower (b) and higher (c) eukaryotic ribosomes showing a conserved core (gray) in both small and large subunits. Eukaryote-specific r-proteins form a network of interactions with the rRNA expansion segments, giving rise to a protein-RNA layer (blue). In higher eukaryotes, there are two additional RNA layers: a rigid inner layer (orange) that results from multiple RNA-RNA interactions, and a flexible outer layer, arising from flexible extensions of the rRNA. CP, Central Protuberance; TE, Tunnel Exit. Adjusted from Anger et al., 2013 and Melnikov et al., 2012.

Although the overall architecture and function of prokaryotic (70S) and eukaryotic (80S) ribosomes are conserved, they differ considerably in size and structural features (see FIG 1.1). Their molecular weight varies from 2.3 MDa in bacteria to 4.3 MDa in higher eukaryotes, and even within eukaryotes the size of the 80S ribosome may vary within 1 MDa. The small subunit of the *E. coli* ribosome (30S) contains 21 r-proteins and one 16S rRNA and the large subunit (50S) has 33 r-proteins and 5S and 23S rRNAs. Eukaryotic 80S ribosomes are larger and more complex. They

contain large portions of rRNA not present in prokaryotes known as expansion segments (ES), in addition to a number of new r-proteins and r-protein extensions. For example, the large subunit (60S) of *S. cerevisiae* contains 46 r-proteins and 3 rRNAs (5S, 5.8S, and 25S rRNA) and the small subunit (40S) 33 proteins and one 18S rRNA (reviewed for instance by Wilson and Cate, 2012 and Melnikov et al., 2012).

The structure of the ribosome has been extensively studied by X-Ray crystallography and cryo-EM. The first atomic resolution structures were obtained with X-Ray crystallography on archaeal and bacterial subunits (Ban et al., 2000; Nissen et al., 2000; Wimberly et al., 2000; Schluenzen et al., 2000) and the crystal structure of the complete bacterial ribosome was available few years later (Selmer et al., 2006). Importantly, these structures showed that r-proteins are absent from the PTC, confirming that the ribosome is a ribozyme with RNA at the core of its enzymatic activity (Nissen et al., 2000). R-proteins are mostly located on the solvent side and many of them have long basic extensions that reach to the center of the subunits, suggesting that they have a primary role in RNA binding, ribosome biogenesis and maintenance of the overall structure of the ribosome (Ban et al., 2000; Lafontaine and Tollervey, 2001). These structures form the basis for further research the translation mechanism (reviewed by Steitz, 2008; Schmeing et al., 2009; Voorhees and Ramakrishnan, 2013).

Eukaryotic ribosomes were for many years mostly studied by cryo-EM, bringing important insights into the architecture of eukaryotic specific components such as ES (Spahn et al., 2001; Armache et al., 2010). In 2011, the X-ray structures of the individual subunits from *T. thermophila* (Klinge et al., 2011; Rabl et al., 2011) as well as the full 80S from *S. cerevisiae* (Ben-Shem et al., 2011) provided an atomic model for the eukaryotic ribosome. Consistent with the universally conserved function of the PTC, these structures confirmed the overall absence of bacteria- and eukaryote-specific elements on the core of the ribosome. Moreover, they contributed immensely to a better understanding of the eukaryotic translation apparatus (reviewed by Melnikov et al., 2012; Wilson and Cate, 2012). Even though some differences between bacterial and eukaryotic ribosomes reflect known particularities in their respective translation mechanisms (Melnikov et al., 2012), the role of ES on eukaryotic translation is still unclear. Cryo-EM structures have repeatedly shown that ES are flexible and perform dynamic rearrangements (Beckmann et al., 2001; Armache et al., 2010; Anger et al., 2013). In particular ES27 adopts two different conformations, one of them towards L1-stalk and the other one towards the TE (Beckmann et al., 2001).

In addition, ES27 has been shown to interact with factors binding to the TE site, including the export factor Arx1 (Bradatsch et al., 2012; Greber et al., 2012), and the ribosome associated complex (RAC; Leidig et al., 2013), suggesting that ES27 has an relevant role in coordinating access of ribosomal ligands to the TE. Furthermore, deletion of ES27 in *T. thermophila* was shown to be lethal (Jeeninga et al., 1997; Sweeney et al., 1994), stressing that some ES such as ES27 have essential duties during translation and ribosome biogenesis which remain to be understood.

1.2 Translation mechanism

mRNAs are organized in nucleotide triplets known as codons, determining either which amino acid should be added to the NC or when translation should start and terminate. Translation of mRNAs into polypeptides is divided into four different phases: Initiation, Elongation, Termination and Recycling. This process is regulated by many auxiliary and regulatory factors, of which eukaryotes require a much larger number than prokaryotes. Elongation is the most conserved step, whereas Initiation and Recycling differ considerably between the three domains of life.

Initiation. Eukaryotes and bacteria have different approaches to recognize start codons (Sonenberg and Hinnebusch, 2009). In bacteria, this is mediated by three initiation factors (IF1, IF2 and IF3) and the Shine Dalgarno sequence, which is located upstream of the start codon (Shine and Dalgarno, 1974). It establishes base pair interactions with the anti-Shine-Dalgarno sequence at the 3' end of the 16S rRNA ensuring correct placement of the start codon in the P-site. Initiation in eukaryotes is much more complex. It involves at least twelve initiation factors (Hinnebusch and Lorsch, 2012) and the formation of the 43S preinitiation complex, consisting of the small subunit, initiator tRNA (Met-tRNAⁱ) and the initiation factors eIF1, eIF1A, eIF3, GTP bound eIF2 and probably eIF5 (Jackson et al., 2010). Once the preinitiation complex is formed, it binds to mRNA through a unique cap feature at the 5' end of eukaryotic mRNAs, which may be several codons upstream the start codon. Therefore mRNAs need to be scanned on the 5'-3' direction until the start codon is reached. Then eIF5 and eIF5B promote the hydrolysis of eIF2-bound GTP, which leads to large subunit joining and moving to the elongation phase after the initiation factors are released (Jackson et al., 2010).

Elongation. During elongation aminoacyl-tRNAs are delivered and accommodated to the A-site by either EF-Tu in prokaryotes or its homologue eEF1 α in eukaryotes. Only if the aa-tRNA displays the correct anticodon for the mRNA codon on the

A site, EF-Tu/eEF1 α hydrolyses GTP causing a conformational change that leads to its dissociation from the tRNA. After proper accommodation of the aa-tRNA to the PTC, peptide bond formation occurs and the growing NC is linked to the last delivered tRNA on the A-site, leaving a deacetylated tRNA on the P-site. This state is dynamic (Blanchard et al., 2004) and the tRNAs move with respect to the large subunit getting into the so called A/P and P/E hybrid states. The formation of tRNA hybrid states during translocation is shown to be coupled to a rotation of the subunits relative to one another (Frank and Agrawal, 2000). Elongation factor G (EF-G) in prokaryotes or elongation factor 2 (eEF-2) in eukaryotes, preferentially bind the hybrid state of the ribosome, whereas the other complexes favour the non-rotated (or canonical) state (Dever and Green, 2015). These factors catalyze translocation to the next mRNA codon, which brings the deacetylated tRNA to the E-site and the peptidyl-tRNA to the P-site. After GTP hydrolysis, EF-G/eEF2 is released from the ribosome, leaving an empty A-site for the next aa-tRNA to come. The elongation process is repeated until the stop codon is reached, which leads to translation termination.

Termination. When a stop codon is positioned on the A-site, tRNAs cannot decode it. Instead, it is recognized by a class-I release factor. In eukaryotes eRF1 can recognize all three stop codons, while prokaryotes have two class-I release factors: RF1 identifies UAA/UAG and RF2 UAA/UGA. All these proteins contain a conserved GGQ motif that catalyzes the hydrolysis of the ester bond in the peptidyl-tRNA by selectively positioning water molecule on the PTC. In prokaryotes class-II RF3 removes RF1 and RF2 from the ribosome in a GTP dependent manner (reviewed by Petry et al., 2008). In contrast, eukaryotic class-II release factor eRF3 delivers eRF1 to the ribosome and stimulates its action (Preis et al., 2014).

Recycling. After release of the NC, the ribosomal subunits need to be recycled before they can be used in the next round of translation. In prokaryotes, the post-termination complex (consisting of the ribosome bound to mRNA with a stop codon in the A-site and a deacetylated tRNA in the P-site) is split into 50S and 30S-tRNA-mRNA by the concerted action of recycling factor RRF and EF-G. T-RNA and mRNA disassociation is achieved with the mediation of IF3 (Zavialov et al., 2005; Peske et al., 2005). In Eukaryotes, peptide release and subunit dissociation is coupled through the combined action of ABCE1 and eRF1 (Becker et al., 2012). In addition, this is further linked to re-initiation, since initiation factors such as eIF3, eIF1 and eIF1A bind the small ribosomal subunit as recycling is completed (Pisarev et al., 2007).

1.3 Quality control of nascent peptides

Protein synthesis may fail for a number of causes, such as poor availability of aa-tRNAs, damaged mRNA and genetic errors. Organisms have developed mechanisms that identify stalled ribosomes and set up specific pathways for quality control, recycling and stress signalling (Brandman and Hegde, 2016). Proteins produced without a stop codon and other stalled NCs are recognized by the RQC machinery and targeted for proteasomal degradation (FIG. 1.2, Brandman et al., 2012; Defenouillère et al., 2013). This complex, consisting on Ltn1 (a E3 ubiquitin ligase also known as Listerin), Rqc2 (Tae2), Rqc1, and Cdc48; binds to the 60S subunit after splitting of the stalled ribosome and mediates the ubiquitylation and proteasomal degradation of the stalled NC (Brandman et al., 2012; Defenouillère et al., 2013). Recent structures have revealed that Rqc2 binds to the peptidyl-tRNA and recruits Ltn1, which curves around the large subunit and positions its ligase domain close to the TE (Lyumkis et al., 2014; Shao et al., 2015; Shen et al., 2015). Importantly, Rqc2 recruits tRNA^{Ala} and tRNA^{Thr}, and adds in an mRNA-independent manner a C-terminal Ala/Thr sequence (CAT tail) to the NC (Shen et al., 2015). These CAT tails activate a heat shock response through a mechanism that is not determined yet (Shen et al., 2015). Deletion of the E3 ubiquitin ligase Ltn1 causes stalled proteins to form aggregates and inclusions in a process linked to the CAT tails, demonstrating the important role of the RQC in maintaining proteostasis (Choe et al., 2016).

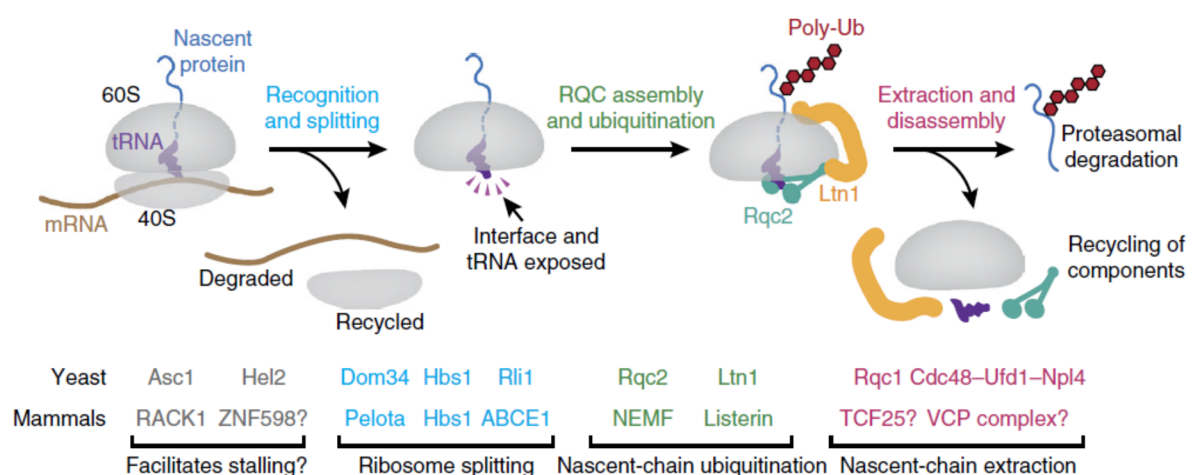


FIGURE 1.2: **The RQC machinery.** Main steps involved in NC degradation by the RQC. From Brandman and Hegde, 2016.

1.4 Ribosome biogenesis

The production of mature and functional ribosomes is a highly regulated process that involves several key steps common for prokaryotes and eukaryotes, including: transcription of a polycistronic precursor rRNA (pre-rRNA), covalent modifications of the pre-rRNA, processing the pre-rRNA, translation and modification of r-proteins and assembly of the rRNA with the r-proteins (Lafontaine and Tollervey, 2001; Shajani et al., 2011). Nonetheless, the differences in ribosome and cell structure between eukaryotes and bacteria correlate to distinct ribosome biogenesis pathways.

Bacterial Ribosome Biogenesis. In bacteria, *in vitro* reconstitution of ribosomal subunits from purified components led to the assumption that bacterial ribosome biogenesis is a self assembly process, mainly driven by rRNA and r-proteins (Traub and Nomura, 1968; Nierhaus and Dohme, 1974). In addition, most bacterial biogenesis factors are not essential (Connolly and Culver, 2009). However, these *in vitro* experiments were done in rather non-physiological conditions, using high Mg^{2+} and/or high temperatures (Cruz et al., 2015). Therefore, assembly factors that decrease the activation energy of rate-limiting reactions are needed (reviewed by Fromont-Racine et al., 2003). Even though genetic and structural studies have been carried out, the specific function of biogenesis factors in bacteria need to be studied in more detail (see for instance reviews by Shajani et al., 2011; Connolly and Culver, 2009).

Eukaryotic Ribosome Biogenesis. In contrast, eukaryotic ribosome biogenesis is a extremely regulated process that requires high amounts of energy, a large number of auxiliary factors (>200 in *S. cerevisiae*) and about 75 small nucleolar RNAs (snoRNAs) responsible of rRNA modifications. Although it is highly conserved, our knowledge about eukaryotic ribosome biogenesis is largely based on *S. cerevisiae* (see for instance reviews by Fromont-Racine et al., 2003; Henras et al., 2008; Kressler et al., 2010). Cellular compartmentalization introduces an extra level of complexity, requiring r-protein import to the nucleus and pre-ribosome export to the cytoplasm (FIG. 1.3).

Hence, most r-proteins need to be imported to the nucleus. This is mediated by importins (part of the karyopherin- β protein family) and transport adaptors, which recognize their nuclear localization signals (NLS) and interact with the hydrophobic phenylalanine-glycine (FG) repeats of the nuclear pore complex (NPC). Once in the nucleus, the cargo r-proteins are generally released through an interaction with Ran-GTP (reviewed by Bange et al., 2013). Nevertheless, a release mechanism independent of Ran-GTP has been recently identified for eS26 (Schütz et al., 2014).

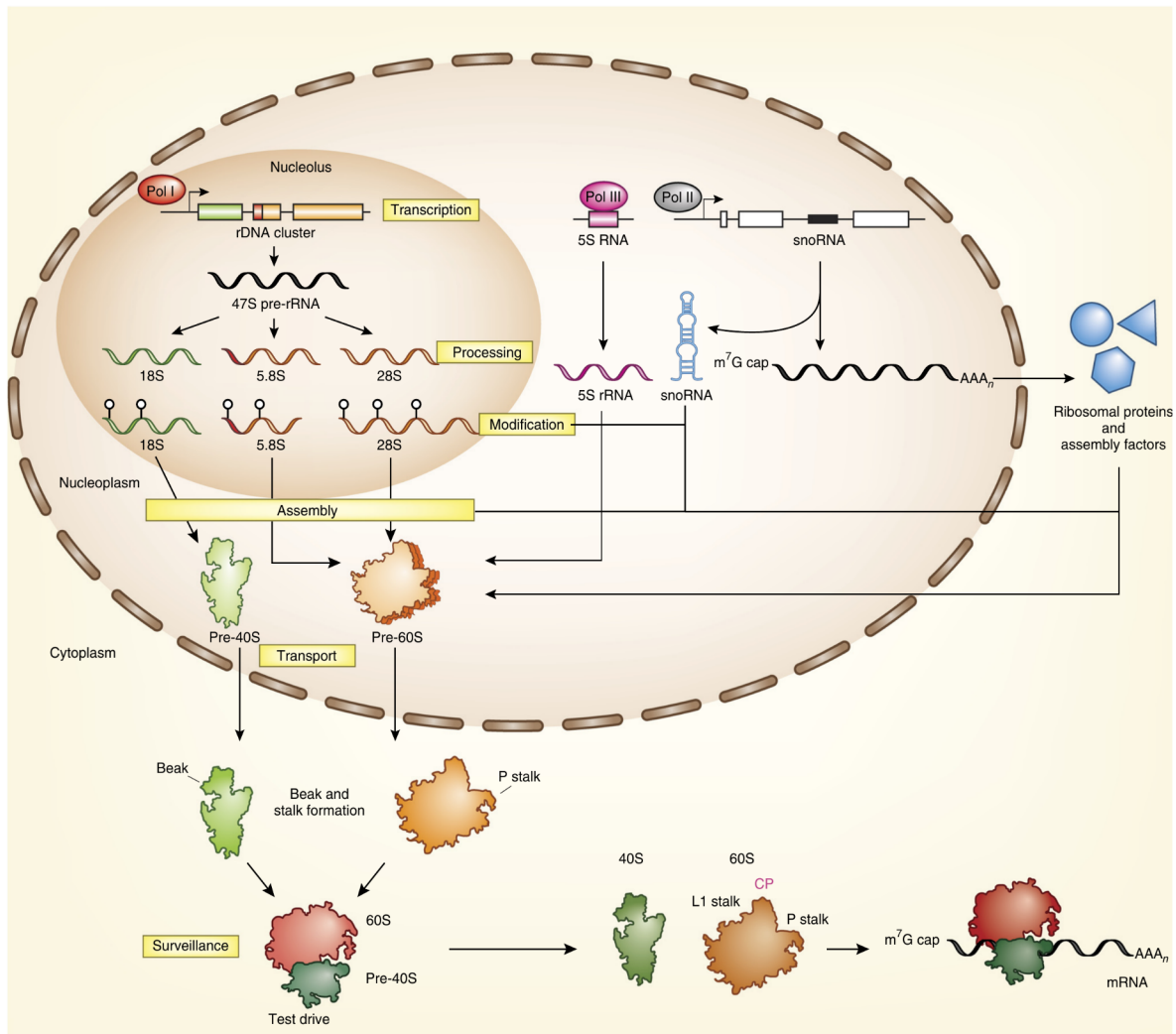


FIGURE 1.3: **Eukaryotic ribosome biogenesis overview.** Highlighted in yellow are shown the most relevant phases of eukaryotic ribosome production: transcription; pre-rRNA processing; pre-rRNA modifications; assembly of r-proteins with pre-rRNA; transport of the pre-ribosomal subunits to the cytoplasm and final surveillance steps. From Lafontaine, 2015.

Reflecting the need for a tight temporal and spatial regulation of r-protein import, it has been demonstrated that specific r-proteins require coordinated nuclear import (Kressler et al., 2012a). This suggests that nuclear co-import of related cargo could be a widespread strategy to integrate assembly of macromolecular complexes in the nucleus (Bange et al., 2013). In particular, Syo1 simultaneously imports uL18 (note that throughout this study the nomenclature for r-proteins used is as suggested in

Ban et al., 2014) and uL5 (Kressler et al., 2012a), the two r-proteins which bind to the 5S rRNA to form the 5S ribonucleoprotein (5S RNP). Interestingly, Syo1 has been suggested to serve as an assembly platform for 5S RNP formation (Calviño et al., 2015).

In contrast to the bacterial case, the majority of assembly factors are essential in yeast (Dinman, 2009; Fromont-Racine et al., 2003). Among them, 20% are nucleoside triphosphate hydrolyzing enzymes such as GTPases, ATPases, and kinases (reviewed by Kressler et al., 2010; Strunk and Karbstein, 2009). Remodeling, intracellular transport, quality control mechanisms and integration with other cellular activities are some of the most relevant causes for such energy need (Strunk and Karbstein, 2009; Kressler et al., 2012b). In addition, altering the free energy of the pre-ribosomal complexes provides directionality to the process (Kressler et al., 2010). As a consequence, ribosome production needs to be adjusted to the cellular environment. Indeed, it is tightly connected to cell growth rates: dividing cells rely on effective ribosome biogenesis, while starving cells stop the production of new ribosomes (Warner, 1999).

In *S. cerevisiae* 10% of the entire genome contains the rRNA genes in a single tandem array of about 150 identical repeats (Warner, 1999). RNA polymerase I transcribes (5' to 3') the 35S primary transcript in the nucleolus. This initial pre-rRNA contains RNAs destined for both small and large subunits (18S, 5.8S, and 25S) separated by internal transcribed spacers (ITS1 and ITS2) and flanked by 5' and 3' external transcribed spacers (ETS1 and ETS2; see FIG. 1.4a). All the transcribed spacers need to be removed as they are not part of the mature rRNA. The remaining 5S rRNA is independently produced by RNA polymerase III and is later incorporated in the pre-60S particle as the 5S RNP. The subsequent pre-rRNA processing steps consist of a set of exonucleolytic and endonucleolytic cleavages which are summarized in FIG. 1.4b and have been reviewed, for example, by Fromont-Racine et al., 2003 and Woolford and Baserga, 2013.

The primary pre-rRNA starts to fold and interact with snoRNAs, assembly factors and early joining r-proteins while transcription is still ongoing, producing the 5'-end terminal knob structures in the nascent 35S pre-rRNA which can be seen in "Miller chromatin spreads" (Mougey et al., 1993; Henras et al., 2008; Cruz et al., 2015). This gives rise to the small subunit processome or 90S particle (Kos and Tollervey, 2010), which contains many biogenesis factors of the small subunit as well as the U3 small nucleolar RNP (snoRNP) and the modular subcomplexes UTP-A, UTP-B and UTP-C (Grandi et al., 2002). Notably, the cryo-EM structure of the 90S particle at 7.3

Å has been recently published, revealing that the co-translational folding of the rRNA is mediated by its insertion into a mold-like structure formed by the above mentioned subcomplexes (Kornprobst et al., 2016). The 66S pre-60S particle is obtained after the binding of the remaining pre-rRNA with large subunit r-proteins and biogenesis factors. After cleavage at the A₂ site, the two precursor particles corresponding to the small and large subunits are processed independently in the nucleolus, nucleoplasm and cytoplasm (Henras et al., 2008).

The formation of the pre-40S particle involves a great compositional change, as many of the biogenesis factors present on the 90S particle are released and few novel biogenesis factors and r-proteins are recruited (Schäfer et al., 2003). Export to the cytoplasm occurs through NPCs, involving RanGTPase system, Crm1 and additional factors (Moy and Silver, 2002; Oeffinger et al., 2004). Once in the cytoplasm, the 40S "beak" structure is formed in parallel with the association of uS3 through a phosphorylation/dephosphorylation event, which involves the protein kinase Hrr25 and the Enp1–Ltv1– uS3 complex (Schäfer et al., 2006).

Cleavage at the D-site (FIG. 1.4) produces the mature 18S rRNA (Udem and Warner, 1973). This final rRNA processing step is dependent on a number of non-ribosomal factors such as Fap7, Rio1, Tsr1 and Rio2 (Kressler et al., 2010); and is catalyzed by Nob1 (Pertschy et al., 2009), which has the typical PIN domain of endonucleases (Fatica et al., 2004). So far, only a low-resolution structure of a native pre-40S has revealed some structural insights into its cytoplasmic maturation (Strunk et al., 2011). The last step before obtaining functional 40S subunits consists on a translation-like cycle, that is carried out as a quality control mechanism (Strunk et al., 2012).

1.5 60S biogenesis pathway

Because of the compact nature of the RNA structures seen in the ribosomal subunits, assembly factors must bind in a strict temporal order to allow access to processing (Lafontaine and Tollervey, 2001). Tandem affinity purification (TAP; Rigaut et al., 1999) combined with sensitive mass spectrometry allow the isolation and compositional analysis of maturing pre-60S and pre-40S particles (Tschochner and Hurt, 2003). Since some trans-acting factors bind to the evolving subunits for a long period of time, only specific biogenesis factors are used as bait in order to obtain defined intermediates. The ones being part of the pre-60S maturation pathway will be described in the following sections and are displayed in FIG. 1.5.

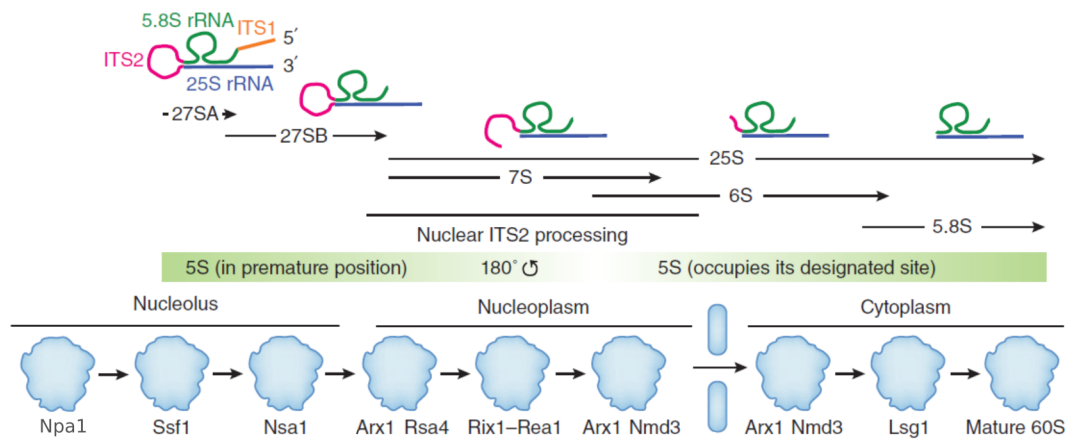


FIGURE 1.5: **60S biogenesis pathway.** Main pre-60S intermediates and the different rRNA species are highlighted. Adjusted from Shchepachev and Tollervey, 2016.

1.5.1 Nucleolar intermediates

Three distinct particles have been identified in the nucleolus. The Npa1 particle mostly contains 27S-A₂ pre-rRNA, meaning that ITS1 and ITS2 were not processed yet and that this particle is the earliest purified so far. Deletion of Npa1 leads to premature cleavage on C₂ site within ITS2 (Dez et al., 2004). Npa1 co-purifies with about 40 non-ribosomal factors, including: a number of H/ACA and C/D snoRNAs which modify rRNA residues in the vicinity of the PTC; eight RNA helicases; several snoRNP components and many early biogenesis factors, some of them even found to be associated with 90S particles (Dez et al., 2004).

The next distinct intermediate is the Ssf1 particle, which is associated with different early pre-rRNA species (27S-A₂, 27S-A₃, and 27S-B pre-rRNA) in addition to about 23 large subunit and 21 other proteins implicated in ribosome biogenesis. These included the four Brix family proteins, Ssf1, Rpf1, Rpf2, and Brx1 (Fatica et al., 2002). Interestingly, Rpf2 and Rrs1 are involved in the incorporation of the 5S RNP to the pre-60S particle (Zhang et al., 2007) and the crystal structure of the Rpf2-Rrs1 complex was recently solved (Kharde et al., 2015; Asano et al., 2015; Madru et al., 2015). According to the existence of an earlier particle, snoRNPs could not be found within the Ssf1 intermediate (Kressler et al., 2010).

The last nucleolar particle is purified through Nsa1, which in addition to the already incorporated 5S rRNA, contains almost exclusively 27S-B rRNA, indicating that 5' trimming of the 27S-A₃ pre-rRNA has already been done. This requires the mediation of the Ytm1–Erb1–Nop7 subcomplex and the rest of the A3 factors (Cic1, Nop15,

Rpl7 and Rrp1; Granneman et al., 2011). Three AAA-type ATPases are needed for pre-60S biogenesis, triggering structural rearrangements and shifting the composition of pre-ribosomal assembly intermediates (Kressler et al., 2012b). Two of them participate in nucleolar maturation: Rix7, which is required for the release of Nsa1 from pre-60S particles (Kressler et al., 2008); and the dynein-related Rea1, responsible of releasing the Ytm1–Erb1 complex, a step that coincides with transition of the pre-60S particles from the nucleolus to the nucleoplasm (Baßler et al., 2010).

1.5.2 Nucleoplasmic intermediates

The first nucleoplasmic particle found so far is the "early" Arx1 particle. The fact that this particle mostly contains 7S and 25S RNA, reveals that the first step required for ITS2 processing, i.e. endonucleolytic cleavage by Las1, has already happened (Gasse et al., 2015). Las1 acts in complex with Grc3, Rat1 and Rei1 and produces a 2', 3' cyclic phosphate on the 7S pre-rRNA and a 5' OH on 26S pre-rRNA (FIG. 1.6, Gasse et al., 2015). Subsequently, Grc3 phosphorylates 26S rRNA for efficient processing by Rat1-Rai1 (Gasse et al., 2015). Importantly, a mutation in human Las1 was recently related to a congenital motor neuron disease (Butterfield et al., 2014).

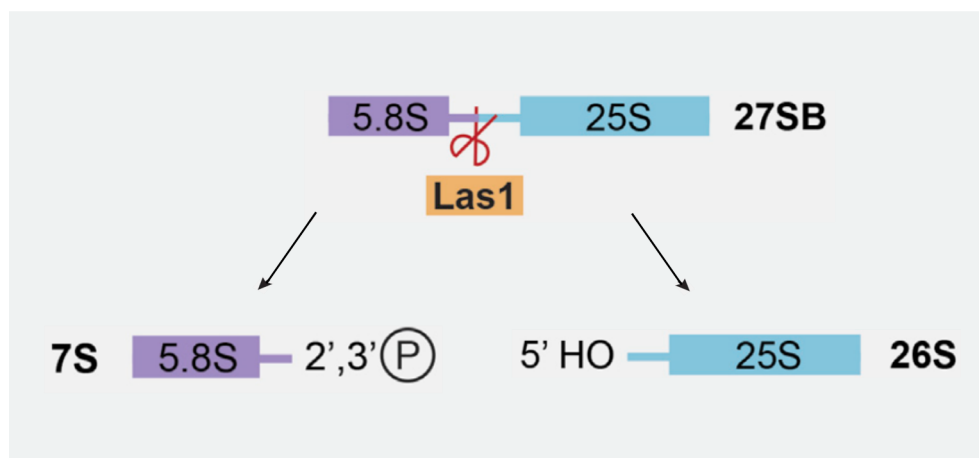


FIGURE 1.6: **Las1 cleaves 27SB pre-rRNA at site C2.** Figure adjusted from Gasse et al., 2015.

Because Arx1 has a role in nuclear export (Bradatsch et al., 2007), this particle was initially thought to be formed late in the nucleoplasm before being exported (Bradatsch et al., 2012). However, Arx1 binds to the pre-60S particle during a long period of the maturation process, so it can be part of several intermediates. Indeed, affinity-purification of the Arx1 particle via the bait protein Alb1 enriches two distinct particles: the first one contains the biogenesis factor Rsa4 and the second one has

the expected export factors Nmd3 and Mex67 (Leidig et al., 2014). The cryo-EM structure of the Arx1 particle at sub-nanometer resolution (8.7 Å) enriched the earlier subpopulation of particles, as Rsa4 among other early biogenesis factors could be found (Leidig et al., 2014). Here, the foot structure was identified for the first time, which consist of biogenesis factors Nop15, Cic1 (Nsa3), Nop7, Rlp7 and Nop53 as well as partially processed ITS2 (7S RNA). Strikingly, the 5S RNP (as well as the rRNA helices on the CP) shows a completely immature conformation, rotated by almost 180° when compared with the mature subunits (Leidig et al., 2014). This result was rather unexpected and it was suggested that the 5S RNP may function as a RNA chaperone (Leidig et al., 2014). However, the mechanism of rotation to the mature position remained an open question.

A recent high-resolution structure of the same particle, purified through the GTPase Nug2, has provided large amounts of structural information about it (Wu et al., 2016). Previously unassigned densities have been assigned to their corresponding biogenesis factors, including: Nug2, Nsa2, Nop15, Cic1, Nop7, Rlp7 and Nop53. Furthermore, extensions of the factors that were already localized could be traced for the first time, including the C-terminal domain of Nog1, which is deeply inserted into the tunnel (Wu et al., 2016).

The next distinct intermediate is the Rix1 particle, which compared to the Arx1 particle has incorporated new factors, including the Rix1–Ipi3–Ipi1 subcomplex, Sda1, and the AAA-ATPase Rea1. Here, the 27SB pre-rRNA has been nearly completely processed into 25S and 7S/5.8S rRNAs (Nissan et al., 2002). Importantly, Rea1 promotes Rsa4 release in a similar manner to Ytm1 removal. In this case, the C-terminal MIDAS domain of Rea1 binds Rsa4 and ATP hydrolysis triggers a mechanochemical mechanism that leads to Rsa4 dissociation from the pre-60S particle (Baßler et al., 2010; Ulbrich et al., 2009). Moreover, this step is monitored by the regulatory GTPase Nug2, which upon GTP hydrolysis is released from the pre-ribosome in coordination with Rea1's ATPase activity, suggesting that both Nug2 and Rea1 act as coupled checkpoint machinery prior to nuclear export (Matsuo et al., 2014). Nevertheless, the state of maturation inspected by these two energy consuming enzymes is unknown. 2D classes of electron microscopy images revealed that the Rix1 particle exhibits a tadpole-like structure and pointed out the suitability of this particle for further structural studies (Nissan et al., 2002).

The last nucleoplasmic particles contain export factors like Crm1, Nmd3, Arx1 and the Mex67-Mtr2 subcomplex which are needed in order to export pre-60S subunits to the cytoplasm (Gadal et al., 2001; Bradatsch et al., 2007).

1.5.3 Cytoplasmic intermediates

Cytoplasmic maturation includes the incorporation of the remaining r-proteins and the release of the last trans-acting factors. On a first step, the third AAA+ ATPase acting in 60S maturation, Drg1, releases Rlp24 for the incorporation of uL24 (Pertschy et al., 2007; Kappel et al., 2012). After this, maturation is branched into two different pathways that can occur at the same time since they concern different sites of the pre-60S. The formation of the P-stalk needs the replacement of the assembly factor Mrt4 by Yvh1, a phosphatase which is eventually removed by the binding of P0 (Rodríguez-Mateos et al., 2009; Kemmler et al., 2009; Lo et al., 2009). In parallel, the final maturation events near the TE can take place, such as the release of Arx1 and Alb1 modulated by Rei1, Jjj1 and Ssa (Hung and Johnson, 2006; Lebreton et al., 2006; Meyer et al., 2010; Demoinet et al., 2007). A recent cryo-EM structure of rebound Rei1, Arx1 and Alb1 to the 60S subunit shows how Rei1 deeply inserts into the TE, ensuring its integrity (Greber et al., 2016).

The completion of these events is a requirement for the two last cytoplasmic steps. Release of Nmd3 is carried out by the GTPase Lsg1 in a process coupled to the recruitment of uL16 (Gadal et al., 2001; Hedges et al., 2005; West et al., 2005). eIF6 (Tif6 in yeast) prevents premature assembly of 80S ribosomes by binding to the inter-subunit side and it is released by Sdo1 and the GTPase Efl1 (Senger et al., 2001; Lo et al., 2010; Bussiere et al., 2012). Recent cryo-EM structures of native *D. discoideum* 60S subunits containing endogenous eIF6 rebound to human SBDS (Sdo1 in yeast) and Efl1, revealed mechanistic details about eIF6 release (Weis et al., 2015). It was first suggested that the release of eIF6 is a prerequisite for the release of Nmd3 (Lo et al., 2010). However, the fact that uL16 establishes crucial contacts with SBDS in the above mentioned structures, supports the hypothesis that SBDS is recruited to an eIF6-bound pre-60S particle after uL16 loading and Nmd3 removal. Therefore, release of eIF6 would constitute the final step of 60S-subunit maturation (Weis et al., 2015).

1.6 Quality control of ribosomal subunits

Because of the complexity of ribosomes and the pathways that produce them, it is expected that some of them could become damaged or get incorrectly assembled. Surveillance mechanisms should be in charge of detecting non-functional ribosomes or pre-ribosomes, recruiting the corresponding degradation machineries and eventually degrading them and their possible products (Kressler et al., 2010). Compared to

the extensive knowledge about mRNA decay (Shoemaker and Green, 2012), to date only little information is available about the degradation of rRNA (LaRiviere et al., 2006). In yeast, some improperly processed pre-rRNAs end up restricted to the nucleus, and are rapidly targeted by a degradation mechanism known as the nucleolar surveillance pathway. This involves the polyadenylation of the faulty pre-ribosomes by the TRAMP (Trf4/5, Air1, Mtr4 polyadenylation) complex and their degradation by the exosome (Dez et al., 2006). Another known nuclear pre-rRNA surveillance pathway happens in the absence of pre-rRNA dimethylation. In this case Dim1p blocks pre-rRNA processing steps required for maturation of 18S rRNA (Lafontaine et al., 1998).

In addition to nucleolar degradation, a late-acting quality control process for eukaryotic rRNAs containing functionally deleterious mutations has been identified (LaRiviere et al., 2006). Termed as “non-functional rRNA decay” or “NRD”, this mechanism involves the elimination of translationally defective ribosomes (LaRiviere et al., 2006). NRD can be divided into two distinct and independent pathways: one related to the small subunit (18S NRD) and one dealing with the large subunit (25S NRD; Cole et al., 2009). Interestingly, 25S NRD requires a ubiquitin E3 ligase component Rtt101p and its associated protein Mms1p, which possibly mediate the ubiquitination of r-proteins (Fujii et al., 2009). Moreover, the proteasome is needed for initiating 25S degradation in 25S NRD (Fujii et al., 2012). On the other hand, 18S NRD is dependent on translation elongation and utilizes Dom34, Hbs1, the exonuclease Xrn1, and the exosome recruitment factor Ski7 similarly to no-go decay of mRNAs (Cole et al., 2009). Even though some of the proteins involved in NRD have been found, a detailed mechanism of ribosome degradation by this system is so far unknown.

1.7 Ribosome biogenesis and human diseases

Because of the essential role of ribosomes in every living organism, defects on ribosome biogenesis that escape all checkpoints and quality control mechanisms may lead to ribosomopathies. Indeed, a number of diseases linked to ribosome biogenesis have been already discovered (Freed et al., 2010). Four out of the 14 ribosomopathies identified so far are specifically related to impairments of the 60S subunit or its assembly pathway, including: the Diamond-Blackfan anaemia, which is linked to mutations in several r-proteins including the ones belonging to the 5S RNP (uL18 and uL5); the Shwachman-Diamond syndrome, linked to deficient removal of eIF6

by SBDS; a motor neuron disease linked to a mutation in *Las1*; and T-cell acute lymphoblastic leukemia, linked to mutations in *uL18*, *uL16*, *eL22* (for a recent and comprehensive review see Armistead and Triggs-Raine, 2014). Surprisingly, these diseases often display tissue specificity, many of them being bone marrow failure syndromes, characterized by reduced numbers of blood cells and predisposition to cancer (Kressler et al., 2010).

Moreover, several cancer cell lines display an increased expression of factors related to ribosome biogenesis. This could be expected since dividing cells need higher amounts of ribosomes (Dai and Lu, 2008). In addition, a number of tumor suppressors play regulatory roles in ribosomal biogenesis (Dai et al., 2007b). For instance, it has been recently demonstrated that the 5S RNP, in particular *uL5* acts as a feedback regulator of *c-Myc*, an oncoprotein that promotes cell growth and proliferation by enhancing ribosomal biogenesis and protein translation (Oskarsson and Trumpp, 2005; Dai et al., 2007a). Furthermore, *uL5* plays a crucial role in the activation of the tumor suppressor *p53* by inhibiting its major regulator *Mdm2* (Donati et al., 2013; Zheng et al., 2015). It remains a challenge in the field to elucidate the molecular activities underlying all these diseases and their coordination with ribosome biogenesis and cell proliferation. This will only be achieved with a deeper structural and mechanistic understanding about 5S RNP and ribosome maturation.

1.8 Motivation

Given that eukaryotic ribosome biogenesis is a highly regulated process involving many quality control checkpoints, it is generally assumed that only properly processed pre-ribosomes gain nuclear export competence. Yet some defects in the production of ribosomes lead to detectable human diseases, a rather unexpected fact since nearly all assembly factors and r-proteins are essential for cell survival (Freed et al., 2010). Up to now, only point mutations at important rRNA functional sites have been identified as NRD substrates (LaRiviere et al., 2006). Recently, it has been shown that ribosomes containing unprocessed 7S RNA are exported to the cytoplasm and engage in translation (Rodríguez-Galán et al., 2015). However, it is not known whether ribosomes having big structural defects are also exported to the cytoplasm and become NRD substrates, how faulty ribosomes are recognized in the first place and how their protein products are targeted for degradation. In an attempt to answer these questions, the first part of this thesis focuses on the characterization of an anomalous 80S ribosome which arises from the depletion of the endonuclease *Las1*,

responsible of cleaving 27SB pre-rRNA at C₂ site. Without Las1, ITS2 processing and removal of the foot structure do not take place. Since a mutation in human Las1 was found in a patient with a motor neuron disease (Butterfield et al., 2014), understanding the mechanisms underlying the recognition and degradation of these faulty particles is of particular interest.

The second part of this thesis focuses on the molecular mechanisms required for 60S maturation. For many years the field of eukaryotic ribosome biogenesis has focused on the identification of biogenesis factors and their possible roles in pre-rRNA processing by genetic essays (Woolford and Baserga, 2013). In order to obtain a mechanistic understanding about such a complicated cellular process, structural information of single proteins and pre-ribosomal particles has to be obtained. However, only in the recent years, few cryo-EM structures have been generated, mostly of 60S subunits and artificially rebound biogenesis factors (Gartmann et al., 2010; Sengupta et al., 2010; Greber et al., 2012; Weis et al., 2015; Greber et al., 2016). Even though these structures revealed fundamental details about the latest steps of cytoplasmic maturation, this method is not optimal for earlier phases of ribosome biogenesis where the rRNA is not processed yet or has a different fold compared to the mature state. Using TAP and cryo-EM seems to be the most promising strategy in generating a comprehensive picture of ribosome assembly. Nevertheless, to date only two native pre-ribosomal intermediates (the early Arx1 particle and the 90S particle) have been studied structurally (Bradatsch et al., 2012; Leidig et al., 2014; Wu et al., 2016; Kornprobst et al., 2016).

The main goal of the second project presented in this thesis is to provide a deeper understanding in the remodeling and checkpoint activities carried out within the intermediate following the Arx1 particle in the pre-60S maturation pathway, i.e. the Rix1-Rea1 particle, using the combination of TAP and cryo-EM single particle reconstruction. This particle is of great importance for several reasons. Firstly, the structure of the Arx1 particle revealed that the whole CP, including the 5S RNP, needs to rotate about 180° to reach the mature state (Leidig et al., 2014). Even though it was suggested that some assembly factor would have to provide a substantial power stroke to promote such conformational change, the precise mechanism of rotation remained unclear (Leidig et al., 2014). Since the 5S RNP has an important role in the p53–MDM2 and Myc regulation pathways and is related to some genetic diseases (see above), the molecular activities underlying its maturation and integration in the ribosome are of great interest. Secondly, release of assembly factors from the pre-ribosomal subunits is crucial for proper maturation. It was previously shown

that Rea1 releases the biogenesis factor Rsa4 from the pre-60S particle upon ATP hydrolysis (Ulbrich et al., 2009). Concomitantly, it may be involved in remodeling the rRNA helices of the 60S subunit (Baßler et al., 2014). Finally, Rea1 together with the GTPase Nug2 act as a coupled checkpoint machinery before pre-ribosomal particles are allowed to be exported to the cytoplasm (Matsuo et al., 2014). However, the state of maturation being checked by these two energy consuming enzymes was not known. In order to address all these questions, several cryo-EM structures of the Rix1-Rea1 particle are presented here. Since the Arx1 and the Rix1-Rea1 are two consecutive particles, a model for the transition between them is provided, contributing to the greater goal of understanding how pre-ribosomes are remodeled in their transit through the different intermediates before mature and functional ribosomes are produced.

2 Materials and Methods

2.1 Tandem affinity purification of biogenesis intermediates

All samples presented in this thesis were purified by Matthias Thoms (Heidelberg University Biochemistry Center, BZH) from *S. cerevisiae*. The following description of the procedure followed to purify the Rix1-Rea1, Rix1–Rea1 K1089A and Rix1 Δ C particles is adjusted from Barrio-Garcia et al., 2016.

Standard TAPs were done using a buffer that contained 100 mM NaCl, 50 mM of Tris-HCl at pH 7.5, 1.5 mM MgCl₂, 0.1% NP-40, 5% glycerol and 1 mM DTT. A planetary mill (from Fritsch) was used for cell lysis. Two centrifugation steps were performed in order to clear the lysate. The first one at 4,000 r.p.m. during 10 minutes; the second one at 17,500 r.p.m. during 25 minutes. Incubation of the supernatant in IgG Sepharose 6 Fast Flow (from GE Healthcare) was done for 90 minutes at 4 °C. Then the lysis buffer was used to wash the beads and elution from the beads by TEV cleavage at 16 °C for 90 minutes was done. Eluates were incubated at 4° C for 1 hour with Flag agarose beads (Anti-Flag M2 Affinity Gel, from Sigma Aldrich). The lysis buffer was used to wash the Flag beads, and elution of the samples was performed using a buffer that contained 0.15 mg/ml of Flag peptide (from Sigma-Aldrich). TCA at a final concentration of 10% was used to precipitate the samples, which were resuspended in SDS sample buffer. A 4–12% polyacrylamide gel (NuPAGE, Invitrogen) was used to separate proteins.

Split purifications were done in order to purify the samples used for cryo-EM of the Rix1–Rea1 K1089A and the Rix1–Rea1 WT particles. Here the *rea1* K1089A mutant or *REA1* WT sequences, having an N-terminal Flag-tag sequence, were transformed into a Rix1-TAP strain under control of the GAL1-10 promoter. Overexpression of the *REA1* alleles was done in yeast extract peptone glycerol (YPG) for 6 to 7 hours. The first purification step was done to for Rix1 enrichment and the second one enriched for Flag-Rea1.

In the case of the purification of the Rix1 Δ C particle, the plasmid-based rix1 Δ C allele bearing a FTpA-tag sequence in its C terminus, was transformed into a RIX1-HA-aid degtron strain. Yeast extract peptone dextrose (YPD) was used to grow cells overnight. 500 μ M auxin (final concentration) was added and incubated (90 minutes) in order to devoid the sample from endogenous Rix1 (Rix1-HA-aid; Nishimura et al., 2009). TAP was done as described above. For Flag agarose binding, the IgG purification step and TEV cleavage, a buffer that contained 100 mM NaCl, 50 mM Tris-HCl pH 7.5, 1 mM DTT, 5 mM MgCl₂, 0.1% NP-40 and 5% glycerol was used. A buffer that did not have neither NP-40 neither glycerol was used for the Flag peptide elution and the final washing step.

In the case of the Nop53 Las1-depleted sample, the TAP procedure was the same as described above. N-terminal TAP Flag for Nop53 and C-terminal HA-aid tag for Las1 were genomically integrated. In order to deplete Las1, the culture was treated with 500 μ M of auxin (final concentration) for 2 hours before harvesting.

Gene disruption and C-terminal tagging were performed with established procedures (Janke et al., 2004; Longtine et al., 1998). *Escherichia coli* DH5a was used for cloning and plasmid propagation.

2.2 Cryo-electron microscopy

All the grids were prepared by Charlotte Ungewickell. Cryo-EM data was collected by Dr. Otto Berninghausen. Pre-processing and 3D classification of the Rix1-Rea1 WT particle was carried out by Lukas Kater during his student internship in the Beckmann Lab.

2.2.1 Sample and grid preparation

Samples were express shipped on ice from Heidelberg to the Gene Center (LMU Munich), where the Rix1-Rea1 samples were concentrated on a 50 kDa MWCO concentrator and the Nop53 Las1-depleted sample was diluted.

Carbon-coated holey grids (from Quantifoil) with a carbon thickness of about 2 nm were glow discharged under a pressure of 2.2×10^{-2} torr during 30 seconds. 3.5 μ l of sample was applied to the grids. The concentrations of each sample were the following: the Rix1-Rea1 particle was 2.06 OD₂₆₀ ml⁻¹, the Rix1-Rea1 K1089A particle was 0.548 OD₂₆₀ ml⁻¹, the Rix1 Δ C particle had 0.8 OD₂₆₀ ml⁻¹ and the Nop53 Las1-depleted sample had 2.64 OD₂₆₀ ml⁻¹ (where OD refers to optical density).

Then, using a Vitrobot Mark IV (form FEI Company), all samples were blotted (for 3 seconds) and vitrified.

2.2.2 Data collection

Cryo-EM data was collected using 300 keV on Titan Krios TEM microscope (from FEI Company). For the Rix1-Rea1 and Rix1 Δ C particles, micrographs were recorded with a TemCam F816 camera (TVIPS) under low-dose conditions (about 20 e⁻/Å²). In the case of the Rea1 K1089A mutant and the Nop53 Las1-depleted particles, a Falcon II Direct Detector (form FEI) was used, having an accumulated dose of near 34 e⁻/Å² and 30 e⁻/Å² respectively.

All the data was collected using automated software. For the data recorded on the TemCam F816 camera, EM-TOOLS (TVIPS) was used. In the case of the Falcon II Direct Detector, EPU software (FEI) was used for data collection. The final pixel sizes on the object scale were the following: 1.0345 Å for the Rix1–Rea1 and Rix1 Δ C particles; 1.376 Å the Rix1–Rea1 K1089A particle and 1.084 Å for the Nop53 Las1-depleted sample. The final defocus ranges used were 1.1-4.2 μ m for the Rix1-Rea1 data, 1.26-3.58 μ m for the Rix1-Rea1 K1089A data, 1.29-3.39 μ m for the Rix1 Δ C data and 9,35 to 3,28 μ m for the Nop53 Las1-depleted data.

For the Rix1-Rea1 K1089A dataset, movie frames were obtained and grouped into seven segments, the sum of the first six segments was used for the final map reconstruction. The Nop53 Las1-depleted data set was collected in 17 movie frames of which only 11 were used. Motion correction was done on the Nop53 Las1-depleted and Rix1–Rea1 K1089A data sets using the MotionCorr software (Li et al., 2013).

2.2.3 Data pre-processing

Processing was done using the SPIDER software (Frank and Radermacher, 1996) in the case of the Rix1-Rea1 particle project and FREALIGN (Grigorieff, 2007) for the Nop53 Las1-depleted project.

For SPIDER processing, raw images were converted into SPIDER format using the 'CP FROM RAW' command and skipping the image header. Then the defocus and contrast transfer function (CTF) of each micrograph was obtained with the SPIDER command 'TF ED' using the previously calculated power spectra ('PW' command). Power spectra quality was determined by calculating their rotational symmetry based on the cross-correlation (CC, value that measures the similarity of two images) that the same power spectrum has at 0° and 90° rotation. Only those micrographs with

a highly symmetric power spectrum were further used. The remaining micrographs were manually checked for good quality using jweb.

In contrast, for FREALIGN processing of the Nop53 Las1-depleted data, CTF-FIND4 (Rohou and Grigorieff, 2015) was used for defocus, resolution and astigmatism estimation. This information was used to omit all micrographs having more than 6% of astigmatism and a resolution estimate worse than 5 Å.

2.2.4 Automated particle picking

SIGNATURE (Chen and Grigorieff, 2006) was used to pick particles automatically, based on the CC to reference projections. This was done on band-pass filtered and 4x binned micrographs (the size of the micrographs was 4 times reduced by averaging neighbouring pixels). Thus, the pixel size for this step was 4.138 Å for the Rix1-Rea1 and Rix1 Δ C data; 5.504 Å for the Rix1-Rea1 K1089A data; and 4.336 Å for the Nop53 Las1-depleted data. Templates used to create the reference projections were the following: an Arx1-particle for the Rix1 Δ C data, a structure containing both Rix1 and Rea1 (obtained in a previous collection) for the Rix1-Rea1 data, the final Rix1-Rea1 3D reconstruction for the Rix1-Rea1 K1089A and a 80S RNC map for the Nop53 Las1-depleted particle. CC between the images and the template was calculated within SIGNATURE and the coordinates of the highest CC values were used to window out single particles with SPIDER (for the Rix1-Rea1 project) or RELION (for the Nop53 Las1-depleted particle; Scheres, 2012).

The following boxsizes were used: 492 voxels for the Rix1-Rea1, Rix1-Rea1 K1089A and Rix1 Δ C particles; and 384 voxels for the Nop53 Las1-depleted particle. For the Rix1-Rea1 particle, in order to see Rea1's tail, particles were windowed out again with a box of 800 voxels. Then these particles were back projected using the alignment parameters obtained during refinement of the data with the smaller box.

2.2.5 3D refinement and sorting with SPIDER

Data processing of all the datasets belonging to the Rix1-Rea1 project was done with the SPIDER software, parallelized and calculated on the in-house Linux cluster. In this case, particles were organized in defocus groups of similar defocus values. The first processing steps were done on a 3x binned dataset, giving rise to the following pixel sizes: 3.1035 Å for the Rix1-Rea1 and Rix1 Δ C datasets; 4.128 Å for the Rix1-Rea1 K1089A data; and 3.252 Å for the Nop53 Las1-depleted data. Initial

alignment was performed using projection matching to 83 reference projections of the following initial references (all of them filtered with the Butterworth low-pass filter in SPIDER). For the Rix1–Rea1 data, a Rix1–Rea1 3D reconstruction that did not contain neither Rea1 nor the Rix1 complex and that was filtered to 25 Å was used. In the case of the Rix1–Rea1 K1089A particle, a Rix1–Rea1 map that was filtered to 45 Å was provided as initial reference. Finally, a sorted reconstruction of the Rix1–Rea1 data that did not have the Rix1–Rea1 complex and that contained the 5S RNP in its mature conformation was tried at first for the Rix1 Δ C data. The resulting reconstruction was similar to the Arx1 structure, displaying the 5S RNP in its non-rotated position. Therefore, initial alignment was repeated, giving as initial reference the Arx1 structure filtered to 30 Å (as described in Barrio-Garcia et al., 2016).

Initial alignment was done using the 'AP MQ' command; reference projections were CTF-distorted in order to match the data. Then a 3D reconstruction of each defocus group was made, backprojecting the particles with their corresponding Euler angles and x/y shifts, both obtained during the alignment procedure. Each map was CTF-corrected and finally combined using the Wiener Filter.

The quality of the map was improved during refinement, a process in which the projection matching procedure described above is performed in an iterative way. Each refinement round consisted on the alignment of all the particles to the reference projections of the map created in the previous round (using the 'AP MD', 'AP RQ', 'AP RN', or 'AP RD' commands); and their backprojection to create a new 3D reconstruction (using the 'BP 32F' command). In order to improve the accuracy of Euler angles and x/y shifts for each particle, the angular search and the decimation (the reduction of the image size by averaging neighbouring pixels) were decreased as refinement progressed. To avoid potential over-fitting, a constant filter at approximately the resolution was applied during the entire refinement and sorting process by using the 'FQ' command and selecting the Butterworth low-pass filter. With the goal of avoiding noise alignment, during the latest stages of refinement the references were multiplied with a smooth mask (consisting of pixels valued at either 1 or 0) which was created by low-pass filtering one of the output structures to a low resolution (20 to 50 Å) and using the 'TH M' command in SPIDER. The reconstructions created for each defocus group were CTF corrected, weighted according particle amount on each of them and combined to create the final map by using the 'TF CTS' command.

Particles were classified in order to obtain homogeneous datasets that contained the factors of interest. To that end, iterative multireference projection alignment was

performed in 3x and 2x binned images; aligning the particles to different references and assigning them to the class where they had the highest CC to the reference projections. This process was also iterative and stopped when the number of particles on each class converged. All three datasets on the Rix1-Rea1 project went through a similar classification procedure as described in Barrio-Garcia et al., 2016. In a first step, contaminations and non-ribosomal particles were removed by providing a non-ribosomal or "edge" counter-reference, originally made by assigning random Euler angles to non-ribosomal particles and back-projecting them into a 3D structure. Then, in order to classify the different subpopulations of each data set, 3D reconstructions that differed in factor occupancy and/or in intrinsic conformations, were provided as references.

In the case of the Rix1-Rea1 data, always two classes were calculated on each sorting round. In the first classification step after "edge" sorting, particles that did not contain neither Rix1 nor Rea1 were sorted out. In the next one, particles that only contained Rix1 but not Rea1 were separated from those that contained both factors. Then, with the aim to obtain different conformational states, particles that had both factors were subclassified again using two previously obtained reconstructions of the Rix1-Rea1 particle. Nevertheless, only few non-alignable particles were sorted out this way.

After sorting out non-alignable particles of the Rix1 Δ C data, a classification step intended to enrich the presence of the Rix1 Δ C complex was performed. However, the two outputs contained the Rix1 Δ C complex in two different and flexible conformations, but they differed in the rigidity of the CP and Rsa4. The class on which the CP and Rsa4 were more stable contained 39% of the particles and was further refined to obtain the final structure of the Rix1 Δ C particle (FIG. 3.21). The more flexible class was further sorted into four different subclasses, which provided the other two subpopulations displayed in figure FIG. 3.21 plus two other classes representing contaminations and non-alignable particles.

Regarding Rix1-Rea1 K1089A data, the particles that did not contain neither Rix1 nor Rea1 were sorted out in a first step. Then, since it was previously observed a correlation between the inward conformation of L1 and the enrichment of Rix1-Rea1, two classes were calculated in the second sorting step with the aim to enrich L1 in its inward conformation. The class that had the Rix1-Rea1 K1089A complex and L1 pointing towards it was chosen for further refinement.

The main classes obtained after 3D classification of the datasets belonging to the Rix1-Rea1 project are shown in FIG. 3.11, FIG. 3.18 and FIG. 3.21.

Once stable classes were obtained, the refinement procedure was repeated using 2x binned and non-binned images for all datasets except the Rix1–Rea1. In this case, the refinement with non-binned images was not performed because such a big box (800 voxels) could not be handled by the SPIDER software. Given the limited resolution of this reconstruction, refinement with non-binned images would not have provided a big improvement in the alignment accuracy. Therefore, refinement of the Rix1-Rea1 dataset was only done with 3x and 2x binned images. The Rix1-Rea1 and the Rix1 Δ C data displayed signs of "projection bias", meaning that some projections were overrepresented in comparison to others. This was healed by analysing how many particles were assigned to each projection and by reducing the number of particles in those projections that contained too many. In order to improve the resolution, the CC of each particle to the assigned projection was calculated, and particles having a lower CC than a certain threshold were eliminated. The final maps were obtained by refining those subpopulations that enriched for the presence of biogenesis factors: 15,749 particles in the Rix1–Rea1 structure; 16,341 particles in the Rea1 K1089A mutant and 26,082 particles in the case of the Rix1 Δ C particle.

2.2.6 3D refinement and sorting with FREALIGN

FREALIGN (Grigorieff, 2007) was used to reconstruct the Nop53 Las1-depleted particle. On a parallel attempt, SPIDER was also tried but since FREALIGN was able to sort out particles that were burnt or had signal to noise problems (see FIG. 3.3), FREALIGN was chosen in the end.

In order to create a single stack that contains all particles (as FREALIGN requires), particles were first extracted in RELION (Scheres, 2012) from 3x binned images. Within the extraction process in RELION, a file containing all the information about each particle (defocus, coordinates, particle identifiers etc.) is written. This was converted to a FREALIGN-readable file (referred as the parameter file in the following) using the conversion script provided in the FREALIGN webpage (grigoriefflab.janelia.org/frealign_conversion_scripts). Then the single stack was created using EM2EM (www.imagescience.de/em2em.html).

Once the parameter file and the single stack were obtained, FREALIGN refinement was started. The initial reference was an 80S RNC. During the refinement and classification procedure a high-resolution limit for particle alignment was set above the resolution of the previous output. As mentioned above, during an initial classification step non-alignable particles were sorted out. The complete processing procedure is found in FIG. 3.3. Finally, in an attempt to improve the resolution, the

two final classes were refined using a stack containing non-binned images that were dose-corrected with the software Summovie (Grant and Grigorieff, 2015).

2.2.7 Resolution determination

Overall structure resolution calculations were done through the Fourier Shell Correlation (FSC). Cut-off at 0.5 (Frank, 2002) was used for the Rix1-Rea1 project, obtaining 9.5 Å resolution for the Rix1-Rea1 map, 8.9 Å for the Rea1 K1089A map and 11 Å for the Rix1 Δ C map. In this case the command RF 3 from the SPIDER software was used to calculate the CC between two Fourier transformed maps, arising from the back-projection of two semi-independent half-sets of the data.

For the Nop53 Las1-depleted data the FSC cut-off at 0.143 was used (Rosenthal and Henderson, 2003), leading to an overall resolution of 7.3 Å in the case of the Nop53 Las1-depleted 80S particle and 7.7 Å in the case of the Nop53 Las1-depleted 60S particle.

Since resolution varies within the different areas of a map (mostly because of intrinsic flexibility and heterogeneity of the sample), local resolution was calculated using ResMap (Kucukelbir et al., 2014) in the split-binned mode. In order to avoid including the noise surrounding the particles in the resolution estimations, both ResMap and FSC calculations were done after applying a smooth mask to the half-reconstructions.

FSC curves and maps colored according to local resolution can be found in FIG. 3.4, FIG. 3.7, FIG. 3.10, FIG. 3.17 and FIG. 3.20.

TABLE 2.1: Cryo-EM structures presented in this dissertation.

Sample	Resolution (Å)	n° of particles	Detector
Rix1-Rea1 WT	9.5 (FSC _{0.5})	15,749	TemCam-F816
Rix1-Rea1 K1089A	8.9 (FSC _{0.5})	16,341	Falcon II
Rix1 Δ C	11.2 (FSC _{0.5})	26,083	TemCam-F816
Nop53 Las1-depleted - 80S class	7.3 (FSC _{0.143})	4,869	Falcon II
Nop53 Las1-depleted - 60S class	7.7 (FSC _{0.143})	8,602	Falcon II

2.3 Rix1-Rea1 particle model building

In a first step, a model for the rRNA was generated. The structure of the Arx1 pre-60S particle was used as a starting point (PDB 3J64; Leidig et al., 2014). The crystal structure of the yeast 80S ribosome (PDB 3U5D; Ben-Shem et al., 2011) was taken as initial model for the rRNA helices of the CP. Differing regions were docked independently into their corresponding densities with UCSF Chimera (Pettersen et al., 2004). A final flexible fit was performed using molecular dynamics flexible fitting (MDFF; Trabuco et al., 2008).

Once the rRNA densities were assigned, the densities corresponding to proteins were identified. The r-proteins were modeled also on the base of the crystal structure of the yeast 80S ribosome and the Arx1 particle structure (PDB 3U5E, PDB 3J64, Ben-Shem et al., 2011; Leidig et al., 2014). R-proteins uL16, eL24, eL29, eL40, eL41, eL42, uL10, P1 and P2 were absent from the Rix1-Rea1 particle and therefore are not included in the model. The same r-proteins were not present in the Arx1 particle (Leidig et al., 2014).

Regarding the biogenesis factors, those for which there was a previous structure or model available assigned to densities of the Arx1 particle -namely eIF6, Mrt4, Nog1, Arx1 and Rpl24- were docked in the map using Chimera (Leidig et al., 2014; Greber et al., 2012; Groft et al., 2000). For the newly identified factors, homology models were created as described below. Sequences were obtained on the UniProt Database (www.uniprot.org). All biogenesis factors identified in the Rix1-Rea1 and their corresponding templates are summarized in TABLE 2.2.

A homology model for Rea1's AAA⁺ ring domain was made with MODELLER (Eswar et al., 2006) using as template the crystal structure of dynein (PDB 3QMZ; Kon et al., 2012). Each AAA⁺ module was modeled individually and the whole ring was assembled using the structure of dynein as a guide. The distant homology between Dynein and Rea1 AAA⁺ modules is shown in FIG. A.1.

The model for Sda1 was done using the homology detection and structure prediction tool HHpred (<https://toolkit.tuebingen.mpg.de/hhpred>; Söding et al., 2005). After homology was detected to several proteins the "best multiple templates" option was selected in order to automatically select the best templates and create a homology model based on them. All helices of this model were docked into a rod-like density of the cryo-EM map. Because it was not possible to find an unambiguous orientation of Sda1 in the map, the sequence of the Sda1 model was mutated to alanines and the connections between the helices were removed from the final structure. The

secondary structure prediction and conservation of Sda1 is displayed in FIG. A.2.

In Rsa4's case, the crystal structure from *C. thermophilum* (PDB 4WJS; Baßler et al., 2014) was used as a template to make a homology model using MODELLER, which had to be adjusted manually in order to fit its ubiquitin-like domain (UBL) into the map. The conservation of this factor and its secondary structure obtained from the *C. thermophilum* structure is shown in FIG. A.3. All the manual adjustments and fits of the models were done using UCSF Chimera (Pettersen et al., 2004) and improved using MDFF (Trabuco et al., 2008) and Phenix (Adams et al., 2010). The nomenclature for r-proteins recently suggested (Ban et al., 2014) was used throughout this study.

TABLE 2.2: Biogenesis factors from *S. cerevisiae* modeled in the Rix1-Rea1 particle.

Protein	Size (aa)	Modeled (aa)	Chain ID	Source
Rsa4	515	28-515	q	Rsa4 crystal structure (4WJS)
Sda1	767	α -helices	r	HHpred best templates
eIF6	245	1-224	m	Arx1 particle (3J65)
Mrt4	236	25-236	n	"
Nog1	647	347	o	"
Rlp24	199	1-63	t	"
Arx1	593	15-109; 129-197; 215-260; 298-326; 384-394; 416-439; 440-465; 500-558	u	"
Rea1	4910	287-1024; 1055-1323; 1344-1684; 1720-1988; 2028-2416	s	Dynein crystal structure (3QMZ)

2.4 Figures

All the figures that display electron densities and molecular models were generated using UCSF Chimera (Pettersen et al., 2004).

PyMOL Molecular Graphics System Version 1.7.4 (www.pymol.org/) was used to make the figure showing transition vectors. In order to color according to the distance between two coordinates, the scripts `rmsd-b.py` and `color-b.py` by Robert L. Campbell were used (©2009 Robert L. Campbell and ©2004 Robert L. Campbell respectively). In the case of `color-b.py`, only the color gradient function was used adding it to `modevectors.py`. These scripts can be found at pldserver1.biochem.queensu.ca/~rlc/work/pymol/.

Alignments shown in the Appendix were made with Clustal Omega (www.ebi.ac.uk/Tools/msa/clustalo/) and displayed with Jalview Desktop (www.jalview.org/).

3 Results

3.1 Translation by structurally impaired ribosomes

3.1.1 Impairment of foot processing by Las1 depletion

With the purpose of gaining a deeper understanding into how the foot structure is being processed, purifications of mutant pre-60S particles on which the foot cannot be removed were carried out in the Hurt Lab by Matthias Thoms and Anshuk Sharkar (Heidelberg University). More precisely, using the aid-degron system (Nishimura et al., 2009, see Materials and Methods) these particles were devoided of the endonuclease Las1, which is required for endonucleolytic cleavage at site C₂ (FIG. 1.6, Gasse et al., 2015).

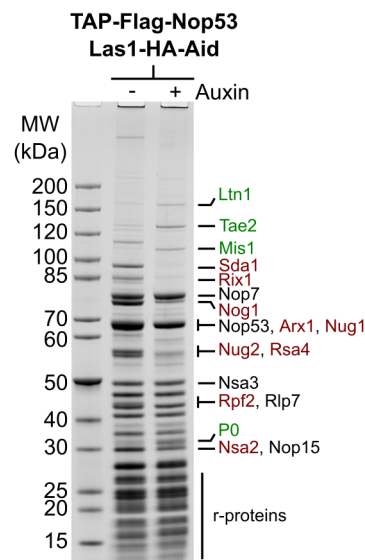


FIGURE 3.1: **Purification of the Nop53 Las1-depleted particle**, SDS-PAGE and Coomassie staining were used for the analysis of the sample. Only the sample obtained after depletion of Las1 (+ Auxin) was used for cryo-EM analysis. Main bands are labelled, in red and green are shown, respectively, those biogenesis factors that are lost and acquired after the Las1 depletion step.

By performing TAP through an N-terminal TAP-Flag tag on Nop53, they obtained particles on which all biogenesis factors except the ones that are part of the foot (namely Nop15, Nsa3, Nop7, Rlp7 and Nop53; see FIG. 3.1) were lost or substoichiometric. Surprisingly, these particles also contained r-proteins that are normally assembled in the cytoplasm (such as P0; FIG. 3.1), meaning that they escaped all surveillance checkpoints and underwent nuclear export. Moreover, RQC factors Ltn1 and Tae2 were substoichiometrically recruited to these mutant intermediates (FIG. 3.1), suggesting that: i) these impaired 60S subunits can form 80S ribosomes which eventually engage in translation and ii) the products of this deficient machinery are degraded by the RQC.

3.1.2 Cryo-EM structures of the Nop53 Las1-depleted sample

In order to structurally characterize the above mentioned intermediates, cryo-EM analysis was performed on the Nop53 Las1-depleted particle. In this case, the quality of the grids was not ideal, leading to a situation on which a high percentage of the collected data was burnt due to thin ice. However, by performing 3D classification with FREALIGN (Grigorieff, 2007), those particles that did not contribute to the signal were efficiently sorted out (FIG. 3.2).

Through further classification of the "good" particles (class 5 after the first sorting step), five different classes were obtained (see FIG. 3.3). Importantly, two of these classes reconstructed an 80S ribosome. The main difference between them was the presence or absence of tRNAs (classes 1 and 4, FIG. 3.3).

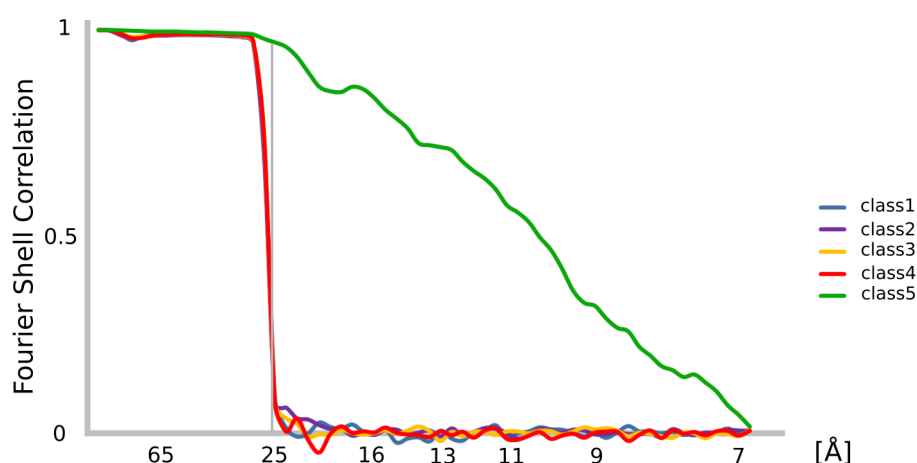


FIGURE 3.2: **FSCs of the first Nop53 Las1-depleted 3D classes.** 3D classification was performed using FREALIGN and only class 5 was used for further classification and refinement.

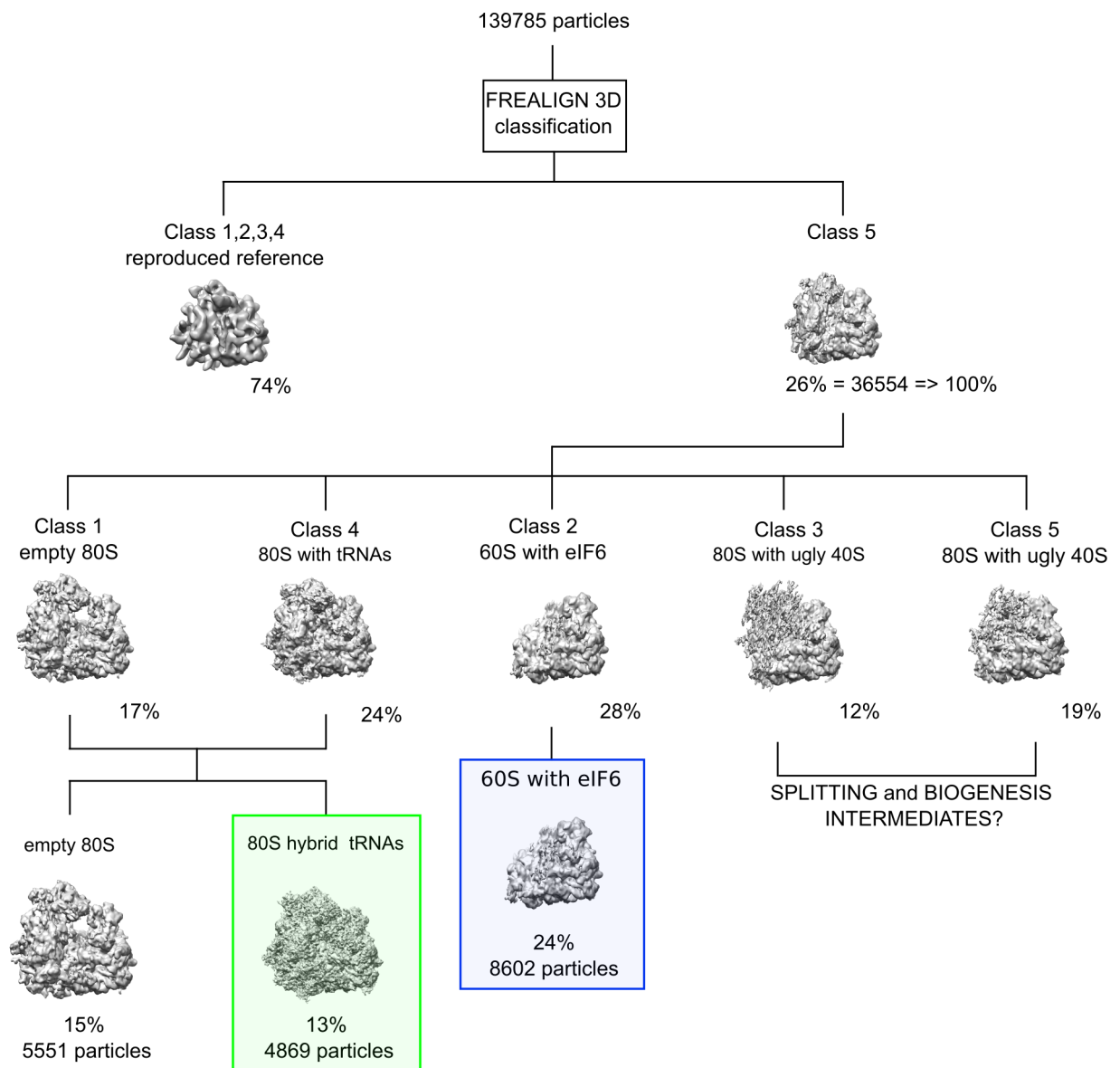


FIGURE 3.3: Classification of the Nop53 Las1-depleted particle. Sorting scheme of the Nop53 Las1-depleted dataset. 74% of the particles were sorted out in the first step as they did not contribute to the signal (see FSCs in FIG. 3.2). In green and blue are highlighted, respectively, the classes corresponding to the 80S map that contains tRNAs in hybrid states and the 60S map that has eIF6. The percentages shown in the two first sorting steps indicate the amount of particles assigned to each class, whereas the percentages displayed in the last round represent the amount of particles included in the final reconstruction.

The three remaining classes showed a strong density for the 60S subunit, but were very noisy on the 40S area (classes 2, 3 and 5, FIG. 3.3). These could correspond to

a mixture of splitting intermediates and pre-60S subunits that still contained biogenesis factors. The cleanest among them (class 2) displayed an extra density near the binding site of the anti-association and biogenesis factor eIF6 (FIG. 3.3). This class and the one corresponding to a programmed 80S ribosome were chosen for further refinement and in the following will be referred to as the Nop53 Las1-depleted 60S and Nop53 Las1-depleted 80S particles, respectively.

Even though the final amount of particles in the Nop53 Las1-depleted 80S cryo-EM structure was relatively low (4869) the overall resolution measured by the $FSC_{0.143}$ criterion was 7.3 Å (FIG. 3.4a). The local resolution varied again between 5 and 14 Å, and the core of the 80S was mostly resolved between 7 and 9 Å. Thus, secondary structure visualization was possible in these areas (FIG. 3.4b).

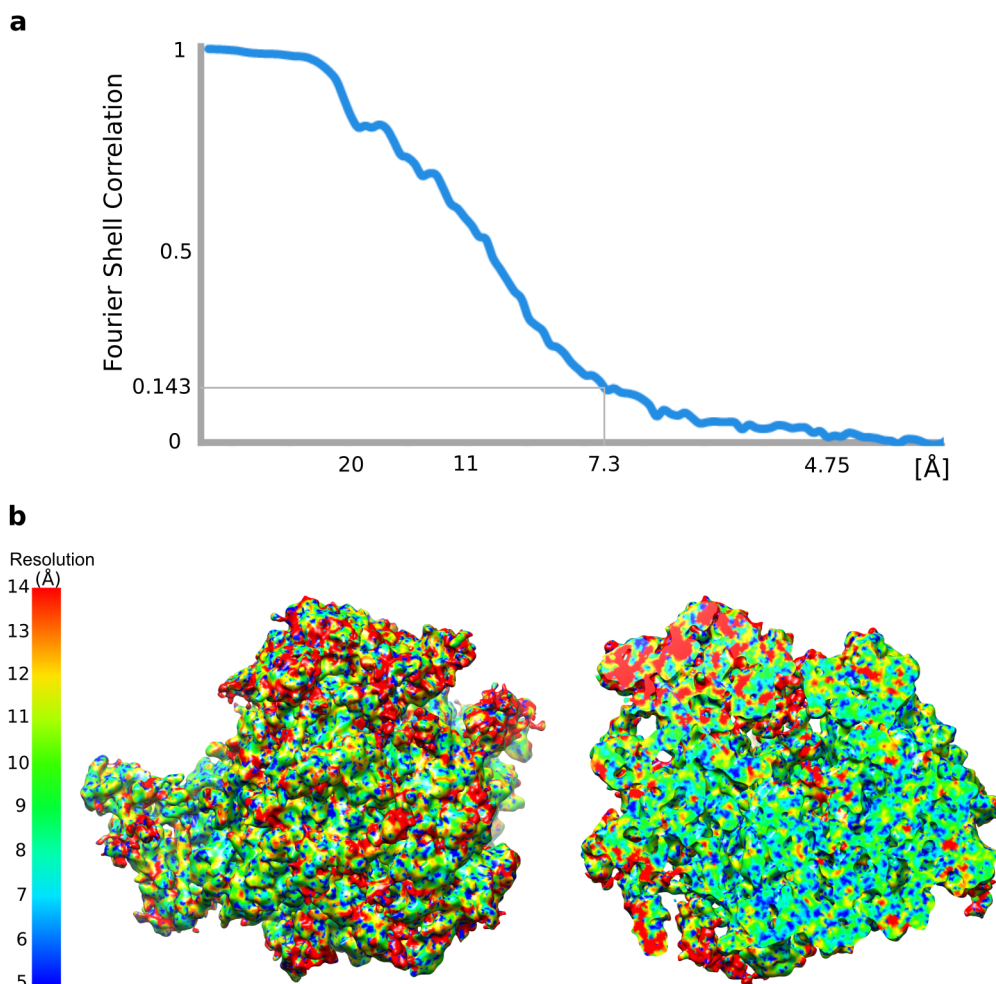


FIGURE 3.4: **Resolution of the Nop53 Las1-depleted 80S particle.** (a) Overall resolution measured at the 0.143 cut-off of the FSC from two independent datasets. (b) Nop53 Las1-depleted 80S map colored according to its local resolution.

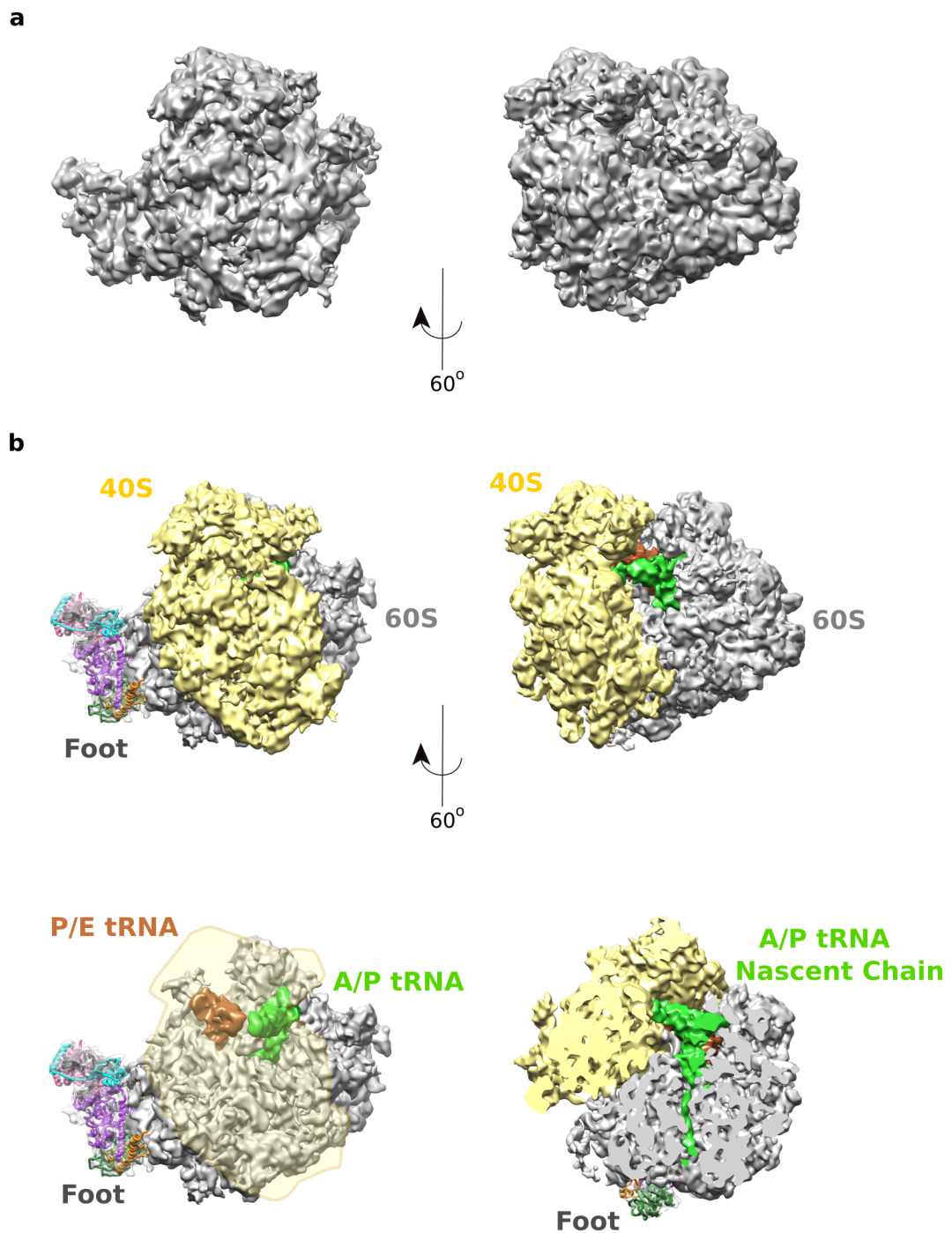


FIGURE 3.5: Cryo-EM structure of the Nop53 Las1-depleted 80S particle. (a) Cryo-EM map filtered to 8 Å. (b) Segmentation of the map highlighting the small subunit (yellow), large subunit (gray), A/P tRNA (green), NC (green) and P/E tRNA (brown). The foot structure coordinates from Wu and colleagues are shown fitted to their corresponding density (Wu et al., 2016, PDB 3JCT).

Strikingly, the 80S particle displayed a strong density for the foot, which accommodated all biogenesis factors that are part of it (Nop15, Nsa3, Nop7, Rlp7 and Nop53) as well as ITS2 (FIG. 3.5). In addition, density for a NC could be traced all throughout the TE, meaning that these faulty 80S ribosomes are nevertheless able to perform several rounds of translation (FIG. 3.5b). Moreover, the two tRNAs in this particle were in their A/P and P/E hybrid conformations (FIG. 3.6, A/P meaning that the tRNA is on the A site on the small subunit and on the P-site on the large subunit; Moazed and Noller, 1989), correlating with a pre-translocation state. This is a rather surprising result, since through cryo-EM analysis of normally translating human ribosomes, it was found that the hybrid state constitutes only about 24% of the ribosomes on the polysomal fraction (Behrmann et al., 2015).

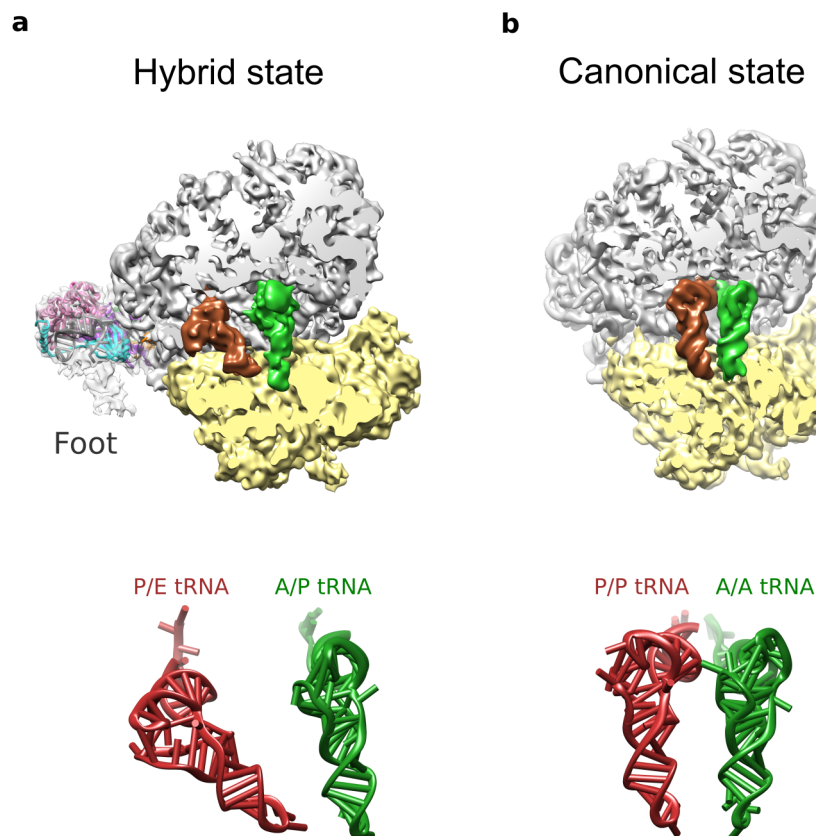


FIGURE 3.6: **Hybrid states on the Nop53 Las1-depleted 80S particle.** A comparison between the tRNAs in hybrid states appearing in the Nop53 Las1-depleted 80S particle (a) and the canonical position of A- and P- site tRNAs (b) is shown.

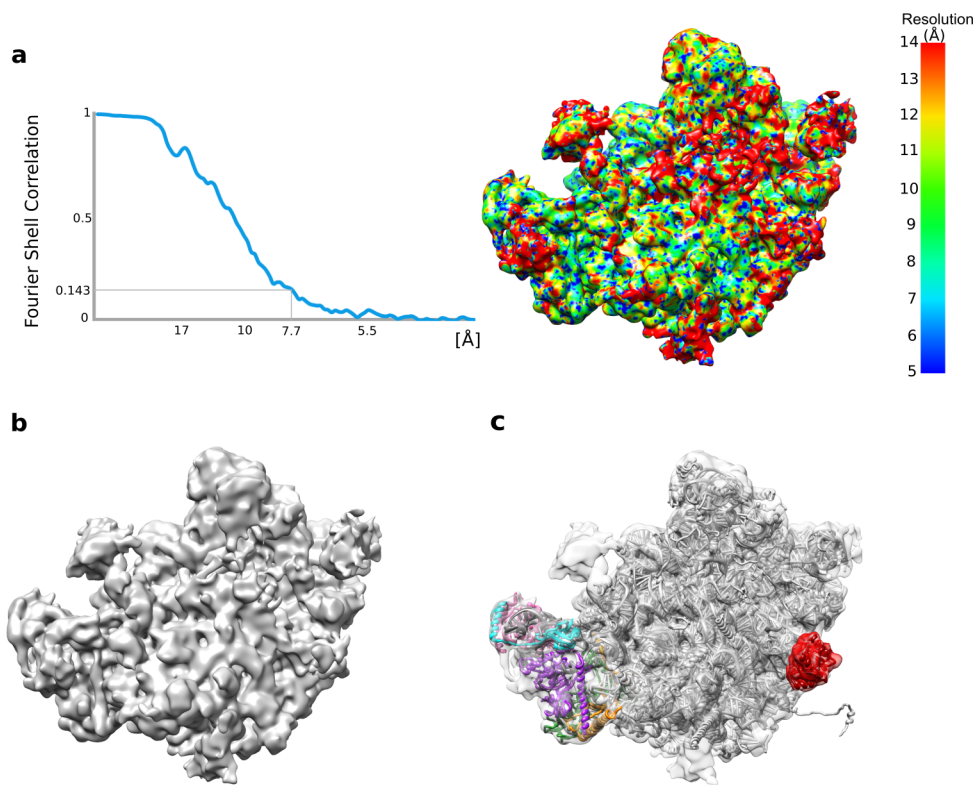


FIGURE 3.7: The Nop53 Las1-depleted 60S particle. (a) Overall resolution measured at the 0.143 cut-off of the FSC from two independent datasets and Nop53 Las1-depleted 60S map colored according to its local resolution. (b) The cryo-EM structure of the Nop53 Las1-depleted 60S particle. (c) Models for the foot structure (3JCT; Wu et al., 2016), the mature 60S subunit (gray, 3U5D, Ben-Shem et al., 2011) and eIF6 (red, PDB 3J65; Leidig et al., 2014) are shown fitted into their corresponding densities.

Interestingly, after fitting the model of the foot structure by Wu and colleagues (PDB 3JCT, Wu et al., 2016), a fuzzy density that protrudes from it was left out unrepresented by the model (FIG. 3.6a). Since only 64 residues out of 235 are modeled for ITS2 in the fitted structure, this additional density could be interpreted as the remaining nucleotides of the completely unprocessed ITS2, which appears to be flexible since the resolution of this region was lower than in the rest of the particle.

Finally, the Nop53 Las1-depleted 60S class was analyzed. This time the overall resolution was measured to be 7.7 Å using the $FSC_{0.143}$ criterion (FIG. 3.7a). Although it still contained the foot and all its associated factors, the core of this intermediate represented a mature 60S (FIG. 3.7b). Importantly, an additional density that fits to the anti-association factor eIF6, was found near the usual binding site of this protein (FIG. 3.7c).

Thus, this particle could constitute both a biogenesis or a post-splitting intermediate, being the later in agreement with the fact that the RQC was substoichiometrically found in this sample, since this machinery only binds to the 60S after subunit dissociation (Brandman et al., 2012). However, the factors belonging to the RQC could not be distinguished in the structures presented here. This is probably because the sample was very heterogeneous and due to the low particle amount, some states could not be properly classified (see FIG. 3.3).

Summarizing, the results described here showed that specific structural defects can be disregarded by all quality control checkpoints and thus, structurally impaired ribosomes are able to engage in translation. Consequently, translational stress is sensed by the cell so that these ribosomes are recognized as faulty and a surveillance system is activated. This system triggers first subunit splitting and then targeting of the proteins manufactured by these ribosomes for degradation by the RQC.

3.2 Remodeling-checkpoint activity of Rix1-Rea1

3.2.1 Rix1-Rea1 interaction and Rix1 complex characterization

The dynein-like N-terminal domain of Rea1 consists of a hexameric AAA⁺ ATPase ring, containing helix 2 (H2) insertion motifs in its domains D2, D4 and D6. This is followed by a linker domain (260 kDa), a D/E-rich domain (approximately 70 kDa) and a C-terminal domain (30 kDa) that possesses a MIDAS (metal ion-dependent adhesion site), which is homologous to the I-domain of integrins (Garbarino and Gibbons, 2002, FIG. 3.8).

With the aim of understanding how Rea1 promotes maturation of the nascent 60S subunit, potential docking partners were screened by yeast 2-hybrid using Rea1's AAA⁺ ring domain as bait. These investigations carried out by Matthias Thoms in Heidelberg University revealed that Rea1's ring domain exhibits a specific 2-hybrid interaction with Rix1, but not with the two other components of the conserved Rix1 complex: Ipi1 and Ipi3. Truncation analyses combined with either 2-hybrid assays or biochemical reconstitution showed that Rea1 and Rix1 interact through the H2 insertion motif of Rea1's D2 (residues 704-800) and the last 100 C-terminal residues of Rix1, which are predicted to be unstructured (residues 663-763; Barrio-Garcia et al., 2016). The functional importance of these sequences was analyzed by *in vivo* complementation, which showed that expression of Rea1 Δ 704-800 or Rix1 Δ C100 in the otherwise lethal *rea1* Δ and *rix1* Δ strains, induced no or only inefficient complementation (Barrio-Garcia et al., 2016). Importantly, affinity purification of Rix1-Rea1

pre-60S particles on which this interaction was impaired (either Rea1 lacked its H2 insertion motif of D2 or Rix1 its last 100 C-terminal residues) demonstrated that the interaction between Rix1 and Rea1 is crucial for the recruitment of Rea1 to the Rix1 pre-ribosomal particle (Barrio-Garcia et al., 2016).

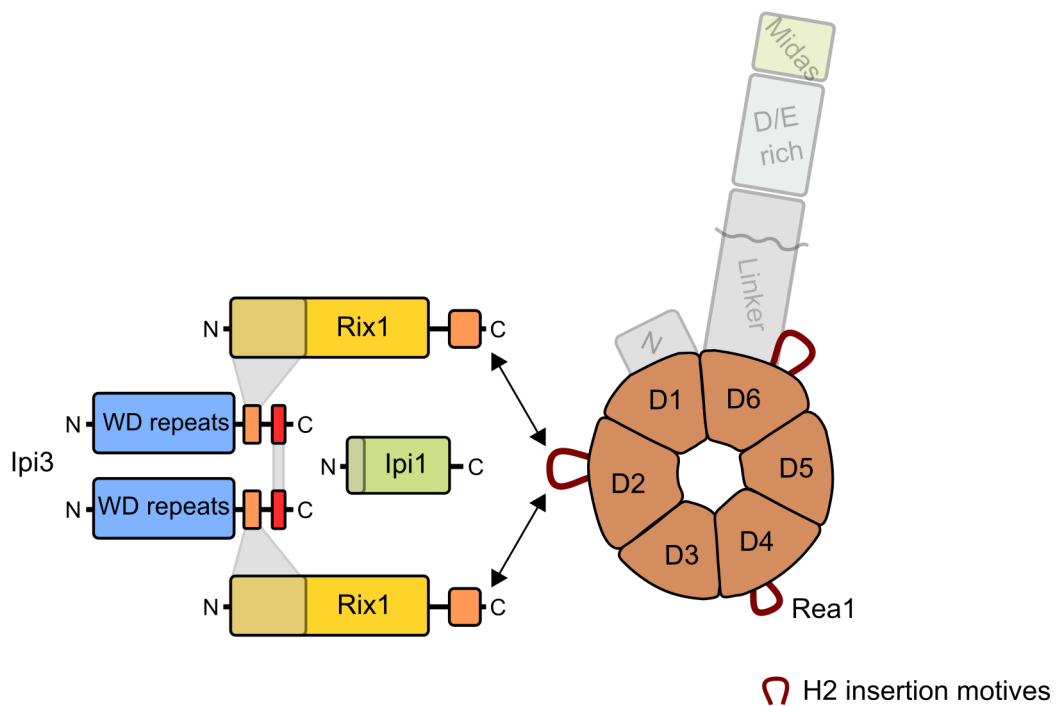


FIGURE 3.8: Overall arrangement of the Rix1-Rea1 complex. Summary of the interactions found within the Rix1-Rea1 complex by yeast 2-hybrid analysis, biochemical reconstitution and XL-MS. Rea1's long flexible tail is depicted in gray, its AAA⁺ protomers D1 to D6 are shown in brown and H2 motifs in red. Rix1 α -helical domain is shown in yellow and ochre and the C-terminal domain involved in its interaction with Rea1 is depicted in orange. Ipi3's β -propeller domain is shown in blue; residues responsible of its interaction with Rix1 are depicted in orange and its coiled-coil C-terminal helix in red. Ipi1 has an α -helical domain shown in light green and its N terminus is shown in dark green. Gray shadows and arrows indicate interactions between different factors. Figure adjusted from Barrio-Garcia et al., 2016.

Further structural and biochemical characterization of the Rix1 complex was carried out in the Hurt Lab. Cross-linking of the purified Rix1-Ipi1 Δ N50-Ipi3 complex combined with mass-spectrometry (XL-MS), provided a valuable insight into the overall arrangement of the complex, which requires two copies of both Rix1

and Ipi3, and one copy of Ipi1. Moreover, the negative-stain EM structure of the Rix1-Ipi1 Δ N50-Ipi3 (obtained by Dirk Flemming, Heidelberg University) revealed its semi-hollowed globular shape (Barrio-Garcia et al., 2016). A description of the domain organization of each component of the complex and the summary of the interactions found can be seen in FIG. 3.8.

3.2.2 Cryo-EM structure of the Rix1-Rea1 particle

To gain a structural insight into how Rea1 is docked to the Rix1 complex in the context of the pre-60S ribosome, the cryo-EM structure of the Rix1-Rea1 particle was

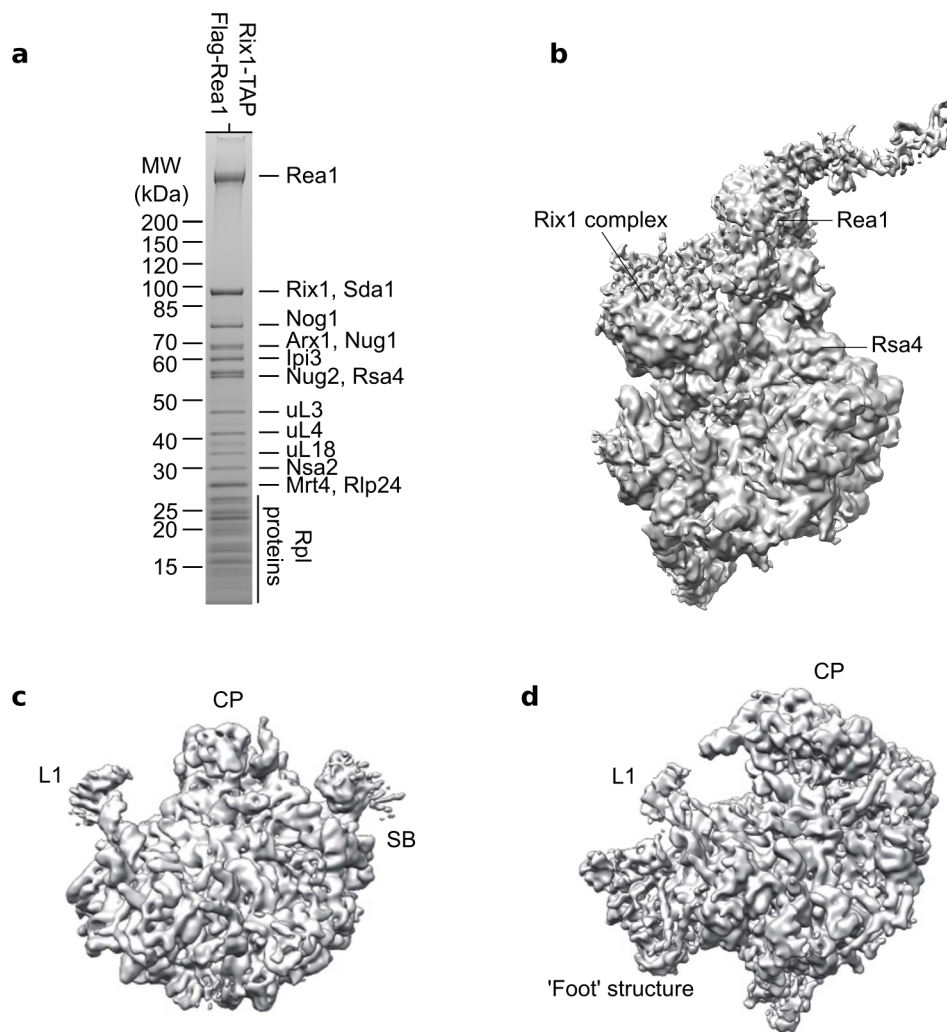


FIGURE 3.9: **Cryo-EM structure of the Rix1-Rea1 particle.** (a) Purification of the Rix1-Rea1 pre-60S particle used for cryo-EM. SDS-PAGE and Coomassie staining were used for the analysis of the sample. (b) Cryo-EM structure of the Rix1-Rea1 particle. The structures of the mature 60S subunit (c) and the Arx1-particle (d) are shown for comparison. Adjusted from Barrio-Garcia et al., 2016 and Leidig et al., 2014.

obtained. For efficient purification of this assembly intermediate, TAP based on a split tag approach was performed, using Rix1-TEV-ProtA in the first, and Flag-Rea1 affinity-purification in the second step (see Materials and Methods).

Analysis of the sample with SDS-PAGE and Coomassie staining (FIG. 3.9a), revealed that the obtained pre-60S particle highly enriched the Rix1-Ipi1-Ipi3 complex, Rea1 and all the other 60S assembly factors typically found on the Rix1 particle (Ulbrich et al., 2009), including: Arx1, Nog1, Nug1, Nug2, Rsa4, Nsa2, Mrt4, Rlp24 and Sda1.

A comparison of the Rix1-Rea1 map with the upstream Arx1 particle and the mature 60S subunit showed that this particle contains huge additional densities, mainly in the intersubunit space, that were not seen before. Essentially, these correspond to the Rea1-Rix1 complex (FIG. 3.9b). Moreover, two large processing steps had happened in the transition from the Arx1 particle to the Rix1-Rea1 particle: i) the CP has been remodeled towards the mature conformation, involving a 180° rotation of the 5S RNP and rRNA helices H81 to H87; and ii) the foot structure has already been removed (FIG. 3.9).

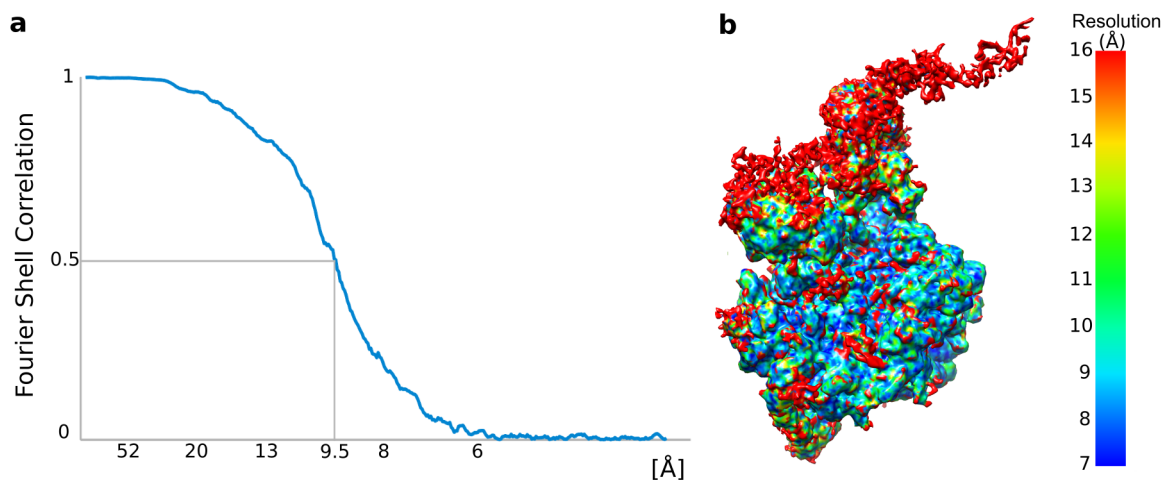


FIGURE 3.10: **Resolution of the Rix1-Rea1 reconstruction.** (a) Overall resolution measured at the 0.5 cut-off of the FSC from two semi-independent datasets. (b) Rix1-Rea1 map colored according to its local resolution. Figure adjusted from Barrio-Garcia et al., 2016.

The Rix1-Rea1 map was resolved between 7 and 16 Å. The overall resolution measured by the $FSC_{0.5}$ criterion was 9.5 Å (FIG. 3.10). This allowed visualizing secondary structure features on the core of the particle.

In addition to the Rix1-Rea1 particle, two other sub-classes were obtained through 3D classification of this data-set. The first one corresponded to 24% of the particles and showed density for all biogenesis factors except for Rea1. The second one, composing 42% of the particles was a 60S subunit which did not contain Rea1, the Rix1 complex and Sda1 (FIG. 3.11). Moreover, the density for Rsa4 and H38 was very badly resolved in this class. Besides biogenesis factors occupancy, the other main difference between these classes was the conformation of the L1 stalk. Its inward positioning correlated to the binding of the Rix1 complex, suggesting that L1 is involved in stabilizing it to the pre-60S particle. Importantly, all subpopulations of this data-set showed a rotated 5S RNP and CP, similar to their conformation in the mature state.

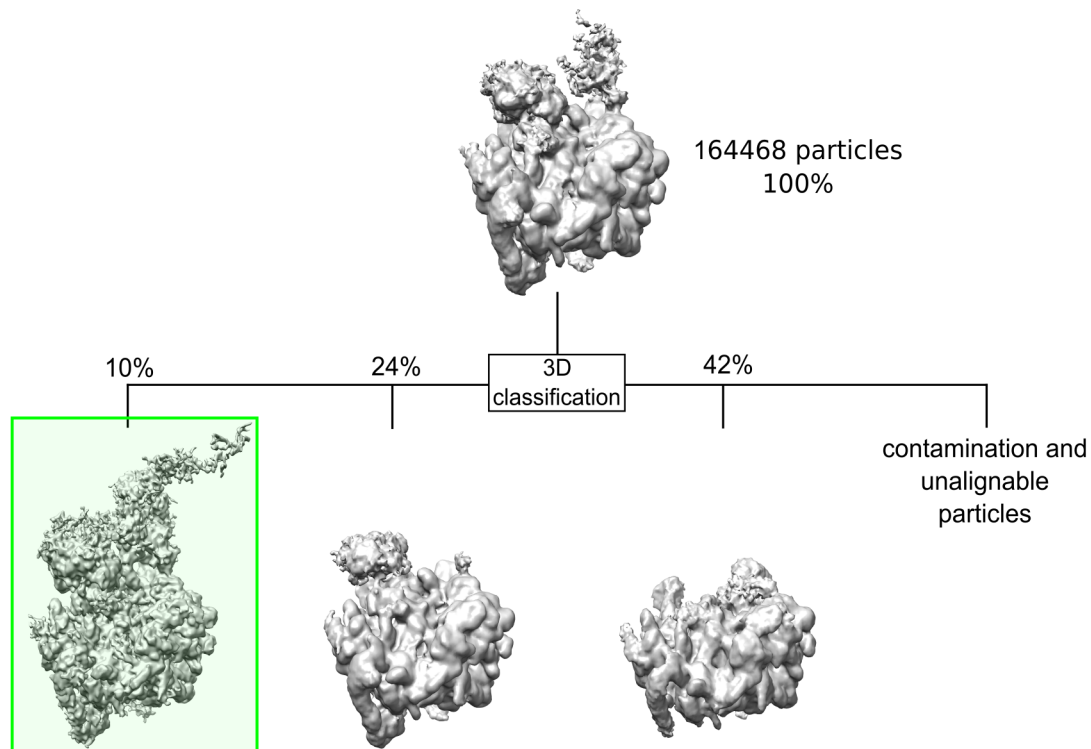


FIGURE 3.11: **Classification of the Rix1-Rea1 dataset.** The class used for the final reconstruction of the Rix1-Rea1 particle is highlighted in green. Figure adjusted from Barrio-Garcia et al., 2016.

3.2.3 Biogenesis factors on the Rix1-Rea1 particle

In general, the core of the Rix1-Rea1 particle resembled the upstream Arx1 particle, not only the rRNA conformation was similar but also the positioning of the previously identified biogenesis factors eIF6, Nog1, Arx1, Mrt4 and Rlp24 (Leidig et al.,

2014; FIG. 3.12). Interestingly, the Rpf2-Rrs1 subcomplex which belongs to the Arx1 particle (Zhang et al., 2007; Asano et al., 2015; Kharde et al., 2015; Madru et al., 2015), was absent from the Rix1–Rea1 particle, supporting the hypothesis that this complex stabilizes the immature conformation of the 5S RNP (Kharde et al., 2015).

As mentioned above, the transition from the Arx1 particle to the Rix1-Rea1 particle involves the acquisition of new biogenesis factors (FIG. 3.12). Firstly, a semi-hollowed sphere-like mass was identified as the Rix1 complex because of its structural resemblance to the negative stain structure of the Rix1–Ipi1 Δ N50–Ipi3 complex (Barrio-Garcia et al., 2016). It contacted the A site finger rRNA helix H38, L1 in its inward conformation, rRNA helix H69, Rea1 and a HEAT repeat protein that was identified here as the biogenesis factor Sda1 (FIG. 3.12, see below).

The Rix1 complex showed secondary structure features in some of its regions (FIG. 3.13a). Two HEAT repeat-like proteins were found, being one on the top of the other, which would only fit size-wise to the two copies of Rix1. Moreover, a characteristic β -propeller density that would correspond to the N-terminal domain of one of the two Ipi3 copies was observed (FIG. 3.13a). Due to the variable resolution of this part of the particle, neither the orientation of these factors nor the identification of Ipi1 and the other Ipi3 copy could be achieved, so a model of the Rix1 complex is not provided here. Nevertheless, the structural features mentioned above supported the identification of the Rix1 complex in the pre-60S particle.

Secondly, a unique ring-like shape was unambiguously identified as the Rea1 AAA⁺ ATPase domain. An elongated flexible density that corresponds to Rea1's tail protruds from it (FIG. 3.12). The ring is placed vertically over the 5S RNP on the intersubunit side, contacting uL5, rRNA helix H38, the UBL domain of Rsa4 and the Rix1 complex (FIG. 3.12, FIG. 3.13b). Notably, a flexible elongated density bridges Rea1 towards the Rix1 complex, being identified as its H2 insertion in domain D2, responsible for the interaction between Rix1 and Rea1 (FIG. 3.13b, left; see 3.2.1). Using the above mentioned information as well as the position of Rea1's tail on the top of the ring, the orientation of Rea1 AAA⁺ ATPase domain was determined and a molecular model based on its homology to dynein was created (Garbarino and Gibbons, 2002). Its orientation on the particle was further confirmed by a small exposed density protruding nearby Rea1's D4 domain, assigned to its H2 insertion motif (FIG. 3.13b, right). This insertion is poorly conserved and non essential for the particle stability (Barrio-Garcia et al., 2016), which supported its location towards the solvent area.

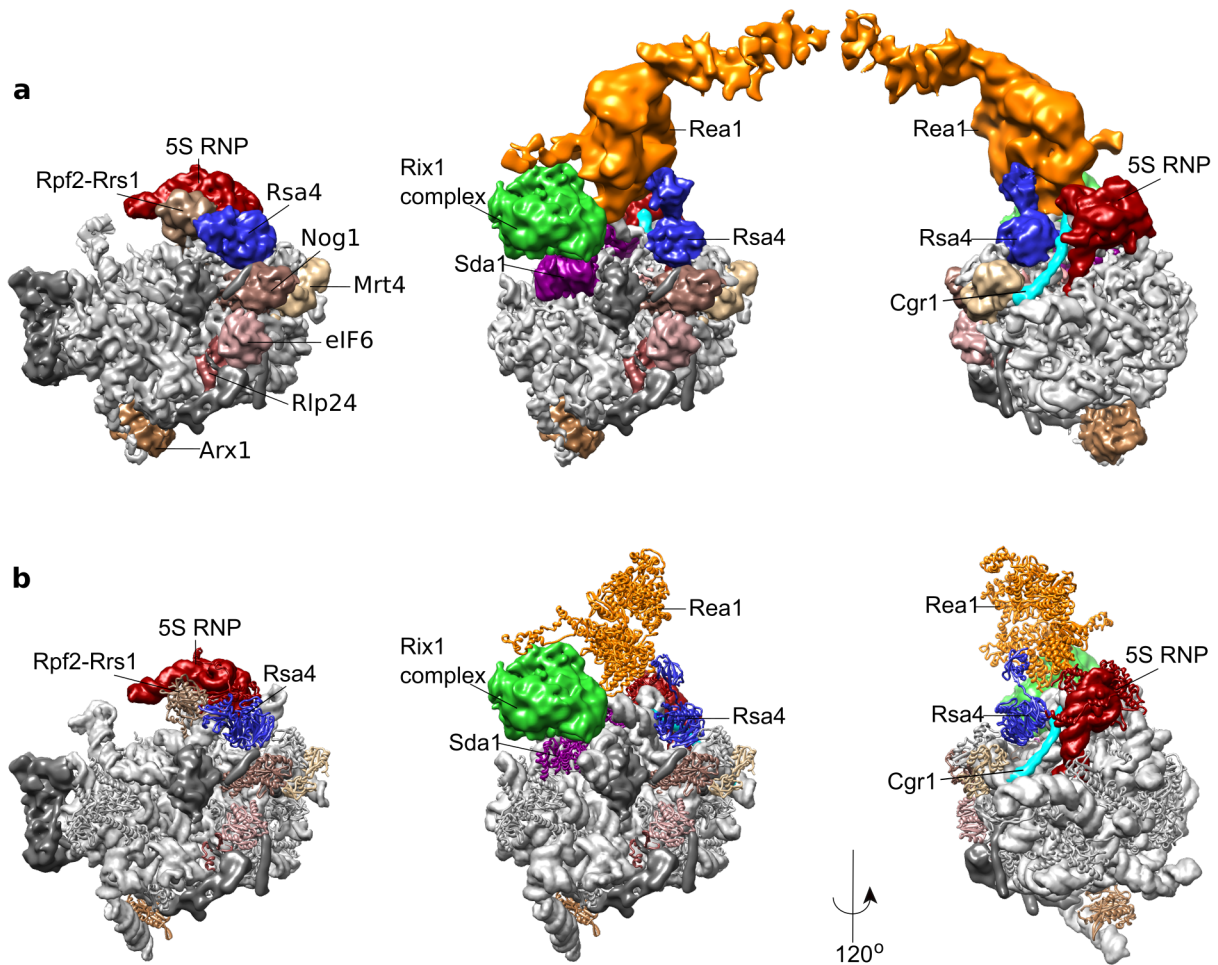


FIGURE 3.12: Identification of biogenesis factors on the Rix1-Rea1 particle. (a) A comparison between segmented maps of the Arx1 particle (left) and the Rix1-Rea1 particle (right and middle) is shown highlighting the 5S RNP in red, Rea1 in orange, the Rix1 subcomplex in green, Rsa4 in blue, Sda1 in dark magenta, Rsa4 in blue, Cgr1 in cyan and the already identified factors on the Arx1 particle in brown (namely Rlp24, Rpf2-Rrs1, Arx1, Mrt4, Nog1 and eIF6). In dark gray are shown non-assigned densities and in light gray the pre-60S subunit. All displayed elements are filtered according to their local resolution. (b) The model for the Arx1 particle (left) is compared to the Rix1-Rea1 particle (right and middle). rRNA is shown as artificial density in light gray and filtered to 8 Å. R-proteins are displayed as ribbons in gray. Those areas of the structure that are not included in the model are shown using the experimental density (in green for the Rix1 complex and dark gray for the unidentified areas). The 5S RNP assembly factors are shown using an identical color code as in (b). Figure adjusted from Barrio-Garcia et al., 2016.

The ribosome-assembly factor Sda1, is a putative HEAT-repeat protein (Dez et al., 2006; Buscemi et al., 2000) which is stoichiometrically bound to the Rix1-Rea1 particle (FIG. 3.9a). HEAT-repeats (Huntingtin, elongation factor 3, protein phosphatase 2A, Tor1) are known to form solenoid protein domains from α -helical structures. Its corresponding density was found right below the Rix1 complex, extending from uL5 to rRNA helix H70. It established close contacts with the L1 stalk in its inward conformation (FIG. 3.13a, right) and rRNA helices H38, H68, H69 and H81. Notably, all predicted α -helices could be traced to rod like densities of the cryo-EM map. Consistent with this interpretation, loss of pre-60S particles is observed when performing affinity-purification of the FtpA-tagged Rix1 when SDA1 gene expression is repressed (Barrio-Garcia et al., 2016), suggesting a scaffolding role for this factor.

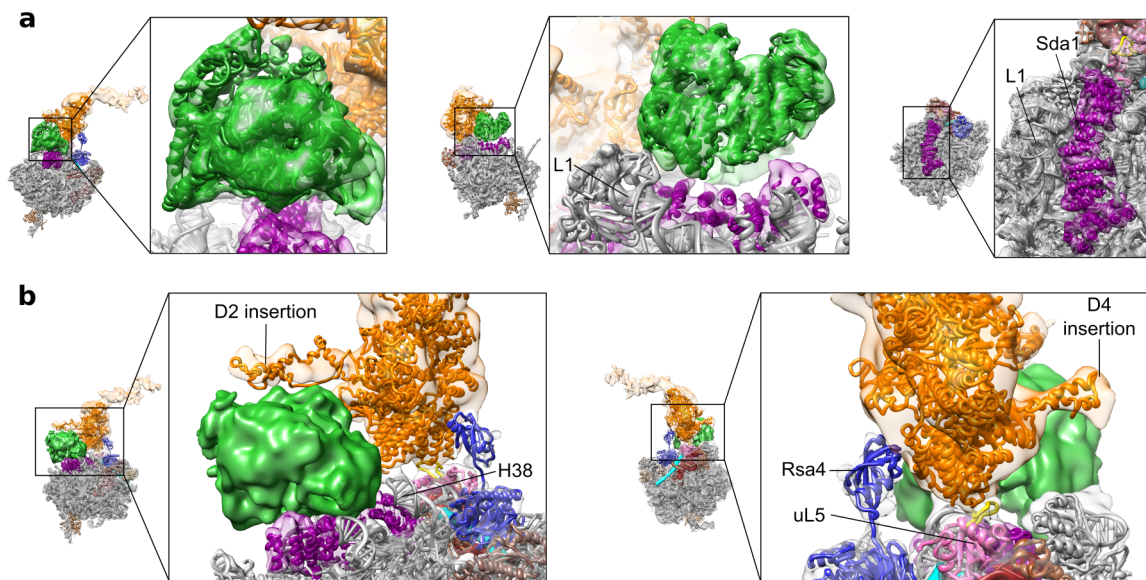


FIGURE 3.13: Interactions of biogenesis factors on the Rix1-Rea1 particle. (a) Identification of the Rix1 complex (green; left and middle) and Sda1 (dark magenta; right) (b) Model and position of hexameric Rea1 AAA⁺ ATPase ring (orange) highlighting its interactions with the Rix1 complex, Rsa4 (blue), uL5 (hot pink and yellow) and the A-site finger rRNA helix H38 (gray). Adjusted from Barrio-Garcia et al., 2016.

An elongated α -helical factor which is about 114 Å long and acts as a wedge between the 5S rRNA, Rsa4 and rRNA helix H38, remained unidentified in the Rix1-Rea1 structure (FIG. 3.12, cyan). However, in the recent high resolution structure of the Arx1 particle by Wu and colleagues (Wu et al., 2016) it has been identified as the C terminus of Cgr1.

Finally, the biogenesis factor Rsa4 was identified, consisting of an N-terminal ubiquitin-like domain and a C-terminal eight-bladed β -propeller domain (Baßler et al., 2014). This was achieved by comparing the reconstructions of the Rix1-Rea1 particle to the Arx1 particle, where Rsa4 is placed near the stalk base, between uL11 and uL18 (on the un-rotated 5S RNP) and its UBL domain pointing towards Rpf2-Rrs1 (see FIG. 3.12, left side; Leidig et al., 2014). Even though in the Rix1-Rea1 particle Rsa4 binds to a similar area, it exchanges its binding partners. Instead of the 5S RNP, it binds rRNA helix H38 (which has a new conformation, see 3.2.4) and the above mentioned biogenesis factor Cgr1. Furthermore, its β -propeller domain shifted about 25 Å to reach its conformation in the Rix1-Rea1 particle and its UBL domain adopts a new conformation towards Rea1's D3 domain, shifting 65 Å when comparing the Arx1 and Rix1-Rea1 particles (FIG. 3.13 and FIG. 3.15)

3.2.4 rRNA remodeling from the Arx1 particle to the mature 60S

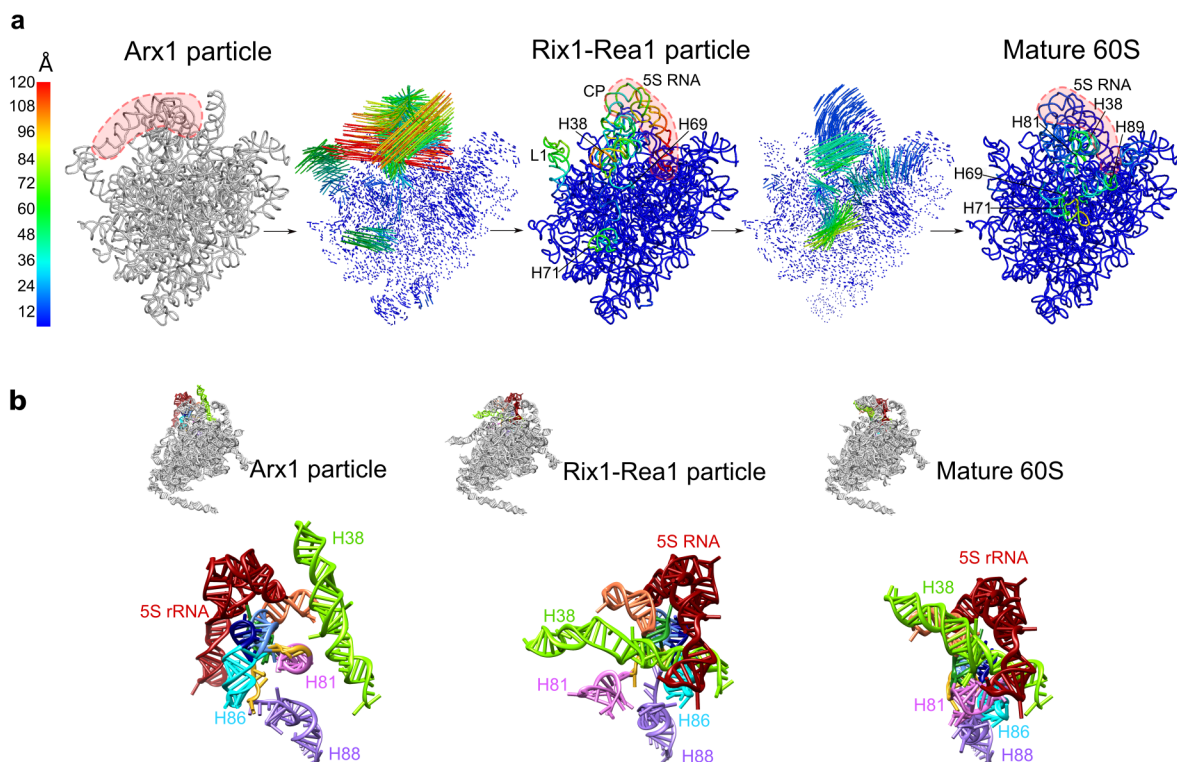


FIGURE 3.14: rRNA maturation from the Arx1 particle to the mature 60S subunit. rRNA conformations in the different biogenesis intermediates are shown for the whole ribosomal subunit (a) and with a focus on the CP (b). See main text (3.2.4) for a detailed description. Adjusted from Barrio-Garcia et al., 2016.

The rRNA conformation of Rix1-Rea1 pre-60S particle was compared to the Arx1 particle and to the mature 60S subunit. This is illustrated in FIG. 3.14, which shows the rRNA structures of the three different states. In between two intermediates, vectors connecting their coordinates are displayed using a color code that varies according to their length (see reference bar on the right side). This heat map highlights the dramatic remodeling step happening during the progression from the Arx1 to the Rix1-Rea1 particle. In addition, rRNA helices H71, H69 and H38 shifted about 50 Å, 15 Å and 100 Å, respectively, in the direction of their mature position. After the Rix1-Rea1 particle, only little rearrangements must occur in order to achieve the final 60S rRNA, despite that there are still a few ribosome biogenesis intermediates between these two states. The biggest remodeling in this case is happening in rRNA helices H38, H69, H71, H81 and H89. These are on the periphery of the 60S subunit and are therefore easily accessible for the last remodeling steps. By focusing on the rRNA helices of the CP (FIG. 3.14b), the large rearrangement which they undergo in the transition from the Arx1 particle to the Rix1-Rea1 particle is emphasized, in contrast to the little remodeling of the CP happening after this step.

3.2.5 CP rotation from the Arx1 to the Rix1-Rea1 particle

The above mentioned conformational change of rRNA helix H38 is of great importance for the mechanism of 5S RNP rotation. Strikingly, H38 in the Arx1 pre-60S particle is positioned in the same place where the tip of the 5S RNA is relocated after rotation has occurred. Therefore, H38 rearrangement towards the intersubunit side is a prerequisite for 5S RNP rotation (FIG. 3.15). Interestingly, in the Rix1-Rea1 particle, H38 contacts both the Rix1 complex and Rea1's D2 domain, being this conformation further stabilized by Cgr1 (FIG. 3.15). Moreover, L3 loop in r-protein uL5 (residues 107 to 124, which was demonstrated to be implicated in Syo1 binding; Calviño et al., 2015; Kressler et al., 2012a) is pointing towards H38 in the Arx1 structure, but in the Rix1-Rea1 reconstruction becomes one of the few binding sites which accurately stabilize Rea1 to the pre-60S particle. More specifically, L3 loop of uL5 contacts Rea1's D3 domain (FIG. 3.15).

These results suggest that H38 not only serves as a placeholder for the 5S RNA, but also that its relocation towards the intersubunit side is a process that happens in parallel to 5S RNP and CP rotation. Necessarily, during H38 rearrangement, Rsa4 unlocks from the 5S RNP, otherwise it could not be bound to H38 and Rea1 in the Rix1-Rea1 pre-60S particle (FIG. 3.15).

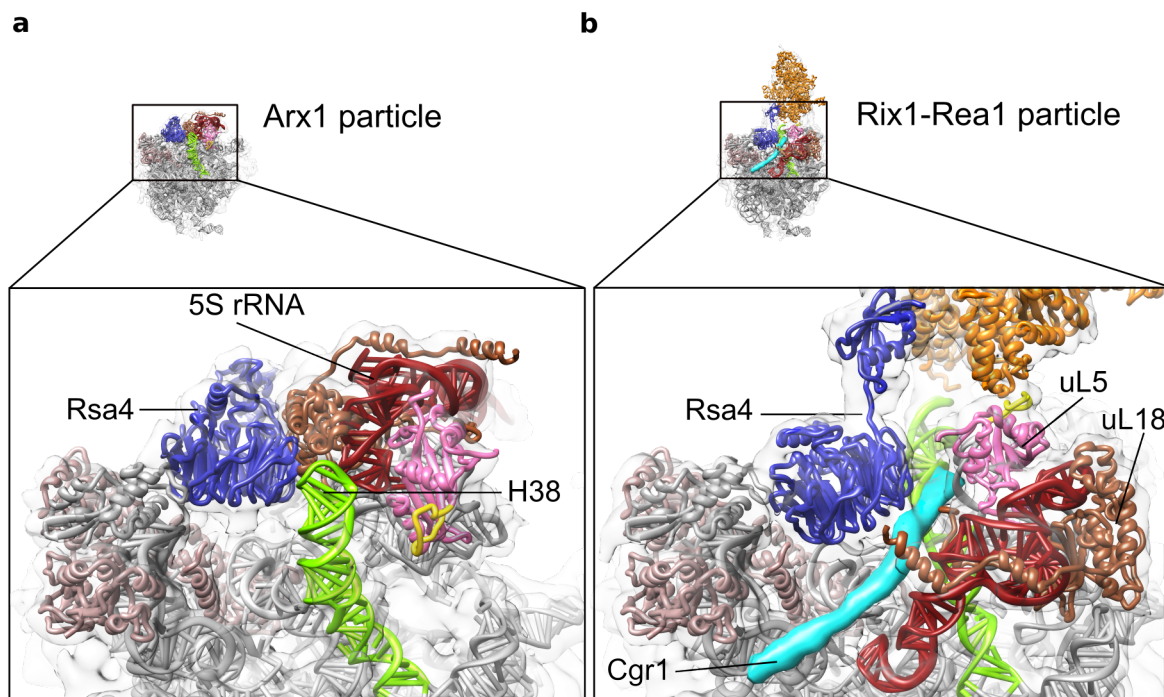


FIGURE 3.15: **Comparison between Arx1 and Rix1-Rea1 particles provides insights into rotation mechanism.** Zoom views of Rsa4, H38 and the 5S RNP comparing their conformation on the Arx1 particle (a) and Rix1-Rea1 particle (b). Blue, Rsa4; orange, Rea1; Red, 5S rRNA; green, H38; brown, uL18; pink, uL5; yellow, uL5 residues 107–124. Adjusted from Barrio-Garcia et al., 2016.

3.2.6 Cryo-EM structure of the Rix1-Rea1 K1089A particle

In order to clarify the involvement of Rea1's ATPase activity into CP remodeling, the cryo-EM structure of a pre-60S particle isolated from a Rea1 mutant was obtained. Since it was suggested that the power stroke exerted by Rea1 when removing Rsa4 from the pre-60S particle could also induce rearrangements on the rRNA helices of the pre-60S (Baßler et al., 2014), a Rix1-Rea1 particle from a Rea1 mutant unable to release Rsa4 was isolated for cryo-EM analysis (FIG. 3.16a). This specific mutation, located in the Walker A site of D3 (Rea1 K1089A), showed dominant lethality (Barrio-Garcia et al., 2016). In addition, pre-60S particles carrying it were not exported to the cytoplasm (Ulbrich et al., 2009; Barrio-Garcia et al., 2016). As a consequence, ribosome half-mers were detected by ribosome profile analysis after overexpression *rea1* K1089A (Barrio-Garcia et al., 2016).

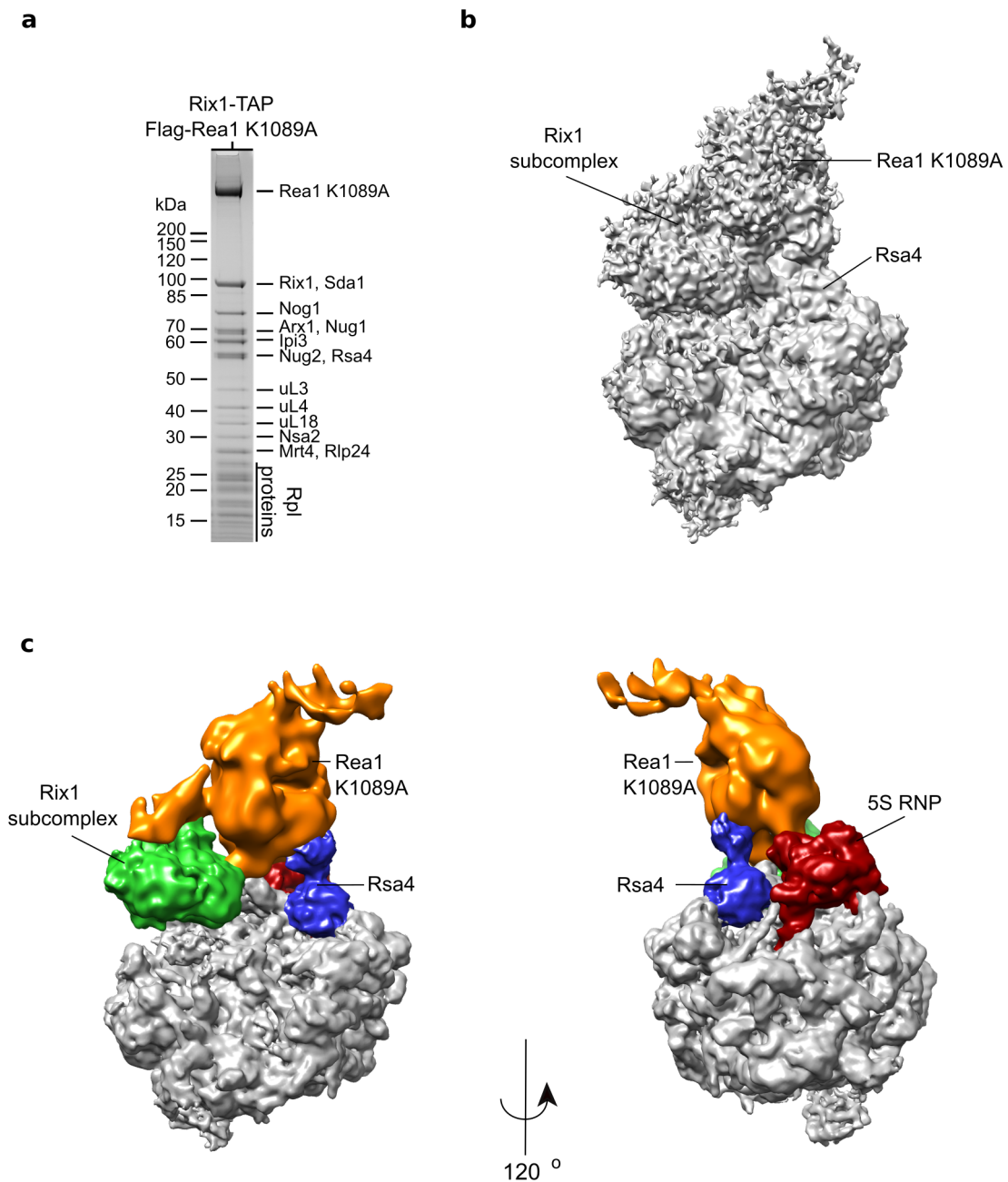


FIGURE 3.16: Cryo-EM structure of the Rix1-Rea1 K1089A particle. (a) Purification of the Rix1–Rea1 K1089A pre-60S particle used for cryo-EM. SDS-PAGE and Coomassie staining were used for the analysis of the sample. (b) Cryo-EM structure of the Rix1-Rea1 K1089A particle, main hallmark structures are identified. (c) Segmentation of the cryo-EM reconstruction of the Rix1–Rea1 K1089A pre-60S particle, different factors are filtered according to their local resolution. Red, 5S rRNP; blue, Rsa4; green, Rix2 complex; orange, Rea1 K1089A. Adjusted from Barrio-Garcia et al., 2016.

The resulting cryo-EM structure was highly similar to the wild type (WT) Rix1-Rea1 particle: the same biogenesis factors bind to the same places at the core of the pre-60S particle; Rix1 and Rea1 K1089A bind on the intersubunit side and are responsible of huge additional densities; the foot structure is absent and the rRNA conformation is essentially the same (FIG. 3.16b). Importantly, 5S RNP rotation has also occurred, reaching to its pseudo-mature position (FIG. 3.16c). These results imply that binding and hydrolysis of ATP in Rea1's D3 is not a prerequisite for 5S RNP rotation.

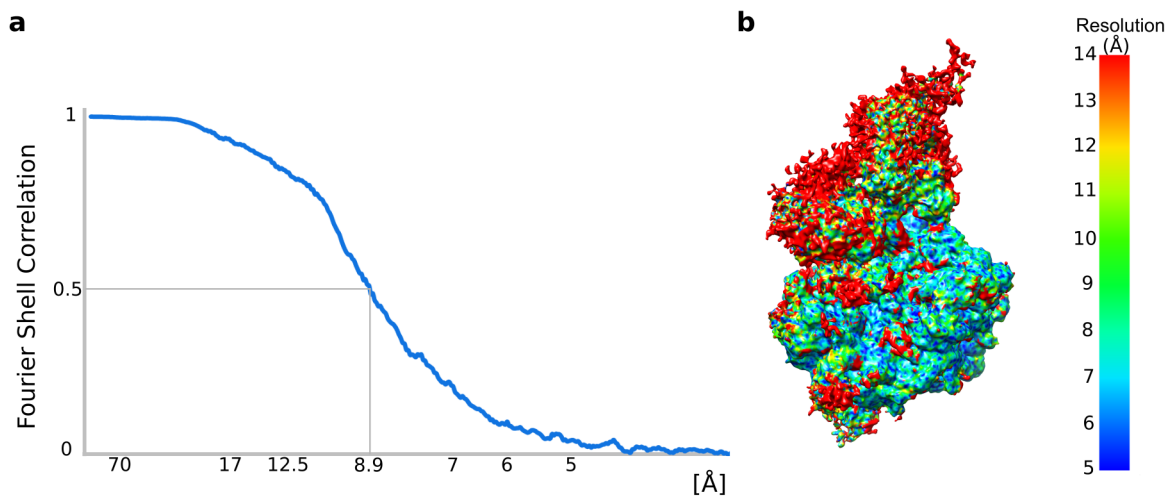


FIGURE 3.17: **Resolution of the Rix1-Rea1 K1098A reconstruction.** (a) Overall resolution measured at the 0.5 cut-off of the FSC from two semi-independent datasets. (b) Rix1-Rea1 K1098A map colored according to its local resolution. Adjusted from Barrio-Garcia et al., 2016.

Similar to the WT, this particle was resolved between 5 and 14 Å and the overall resolution measured by the $FSC_{0.5}$ criterion was 8.9 Å (FIG. 3.17). By 3D classification of this dataset, three main classes were obtained (FIG. 3.18). The first one corresponded to 8% of the particles, which was used for the final reconstruction of the Rix1-Rea1 K1089A particle, as it enriched for both factors of interest (Rix1 and Rea1 K1089A). The second class (20% of the data) also contained both Rix1 and Rea1 K1089A. However, the L1 stalk was not stable and displayed both its in and out

conformation. The third class, corresponding to 40% of the data, lost both Rix1 and Rea1 K1089A and displayed again the two different conformations of L1.

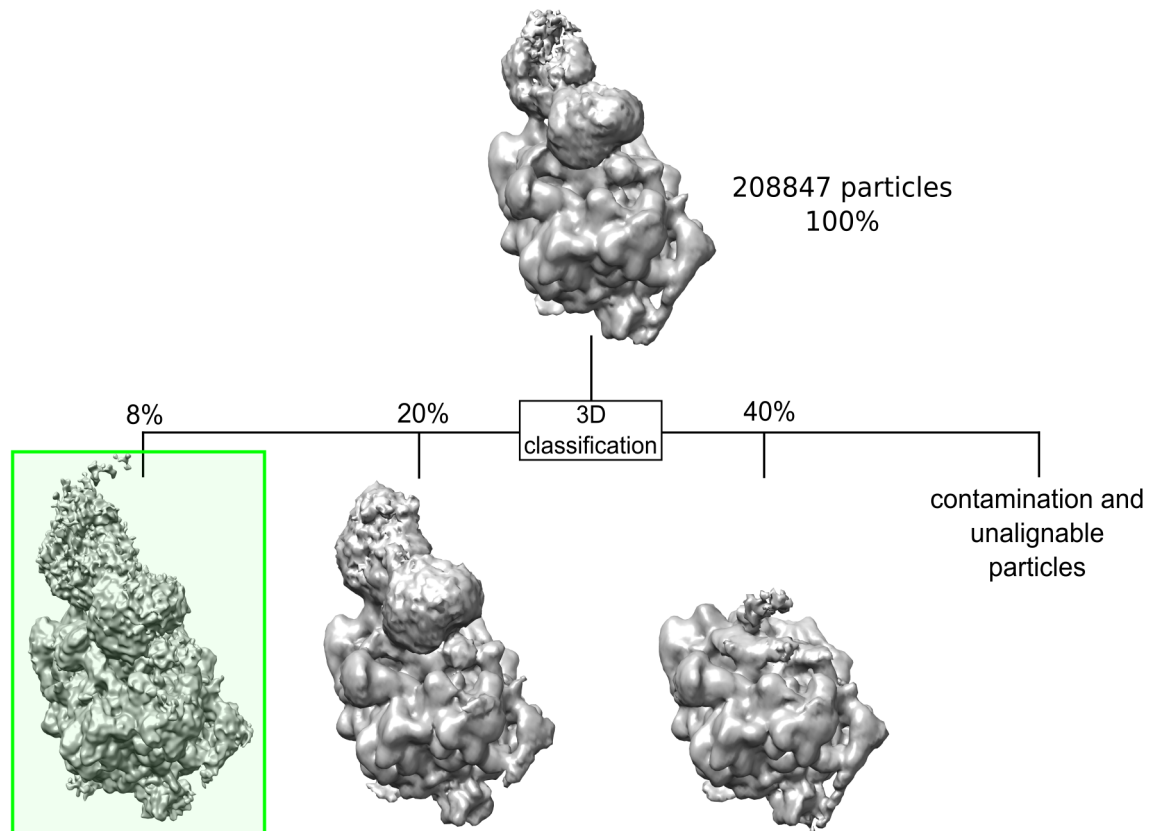


FIGURE 3.18: **Classification of the Rix1-Rea1 K1098A dataset.** The class used for the final reconstruction is highlighted in green. Adjusted from Barrio-Garcia et al., 2016.

3.2.7 Cryo-EM structure of the Rix1 Δ C particle

With the aim to further understand the remodeling mechanism of the CP and Rea1's role, the cryo-EM structure of the Rix1 Δ C particle was solved. As described in 3.2.1, this mutant is unable to recruit Rea1 to the pre-60S (see FIG. 3.19a). Strikingly, the resulting particle was structurally closer to the Arx1 particle than to the Rix1-Rea1 pre-60S intermediate. Not only the CP remained in its immature conformation (correlating with the presence of Rpf2 and Rrs1) but also the foot structure was not removed (FIG. 3.19). The Rix1 Δ C complex, which is certainly part of this mutant intermediates (FIG. 3.19a), did not have the same position as in the WT Rix1-Rea1

particle. Instead, it was flexibly bound to the tip of the 5S RNP in its immature position.

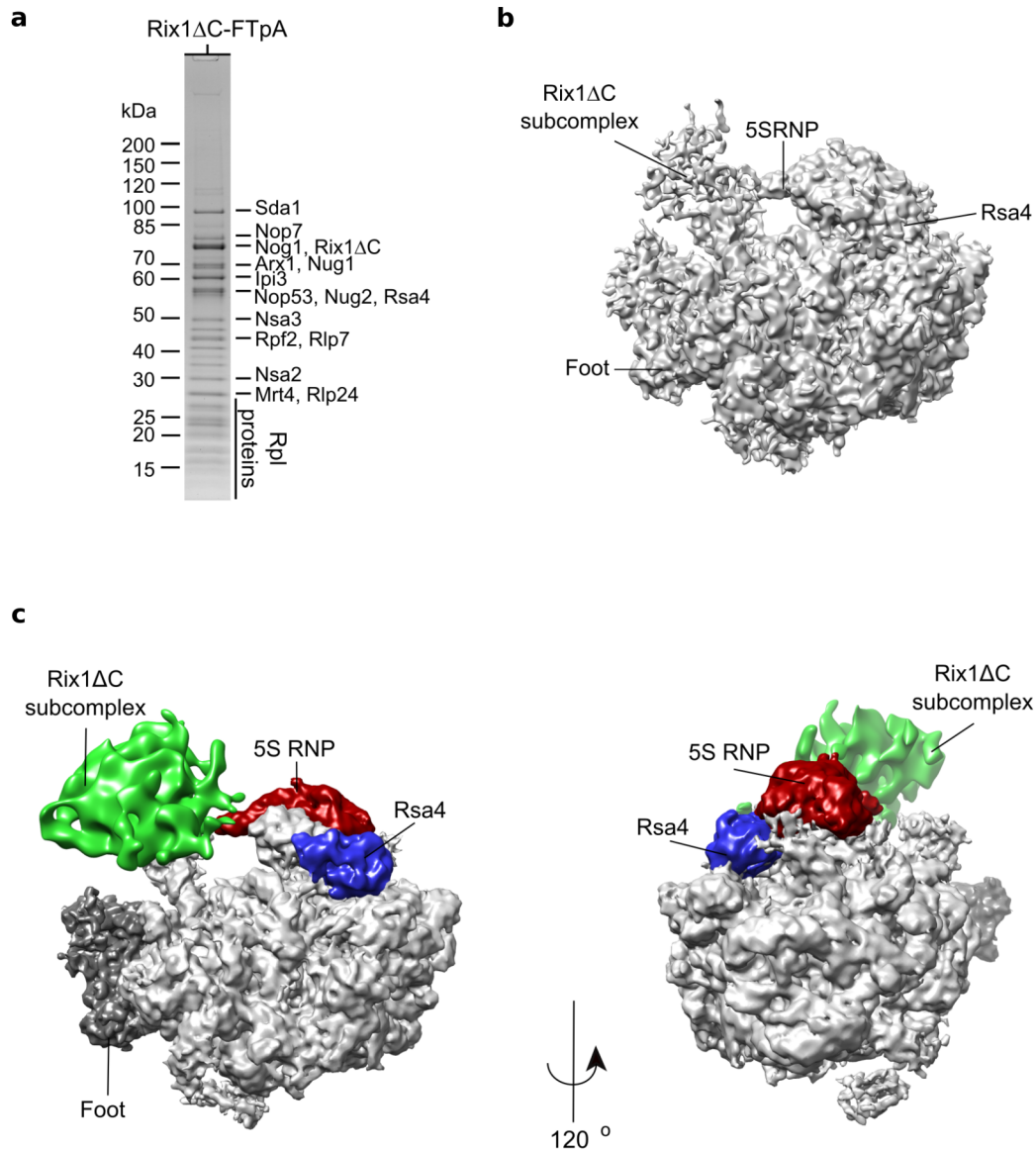


FIGURE 3.19: **Cryo-EM structure of the Rix1 Δ C particle.** (a) Purification of the Rix1 Δ C pre-60S particle used for cryo-EM. SDS-PAGE and Coomassie staining were used for the analysis of the sample. (b) Cryo-EM structure of the Rix1 Δ C particle, main hallmark structures are identified. (c) Segmentation of the cryo-EM reconstruction of the Rix1 Δ C pre-60S particle, different factors are filtered according to their local resolution. Red, 5S rRNP; blue, Rsa4; green, Rix1 complex. Adjusted from Barrio-Garcia et al., 2016.

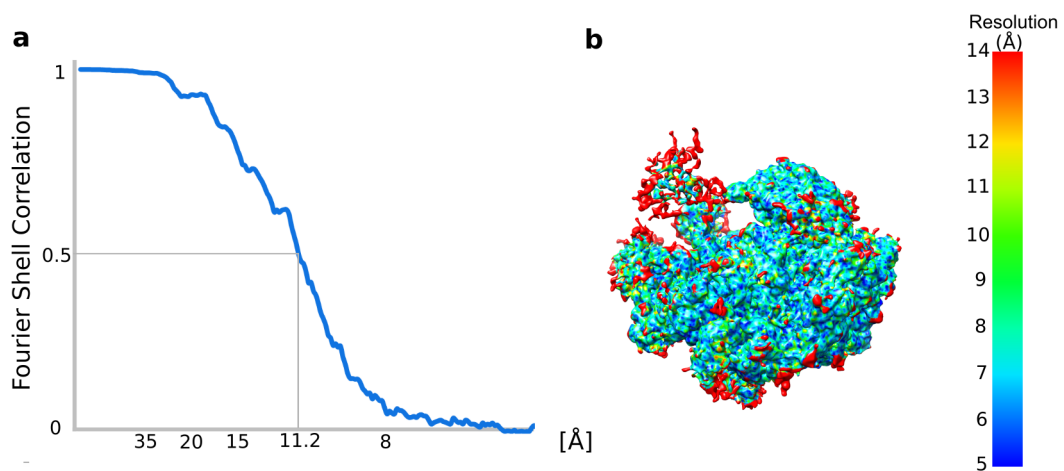


FIGURE 3.20: **Resolution of the Rix1 Δ C reconstruction.** (a) Overall resolution measured at the 0.5 cut-off of the FSC from two semi-independent datasets. (b) Rix1 Δ C map colored according to its local resolution. Adjusted from Barrio-Garcia et al., 2016.

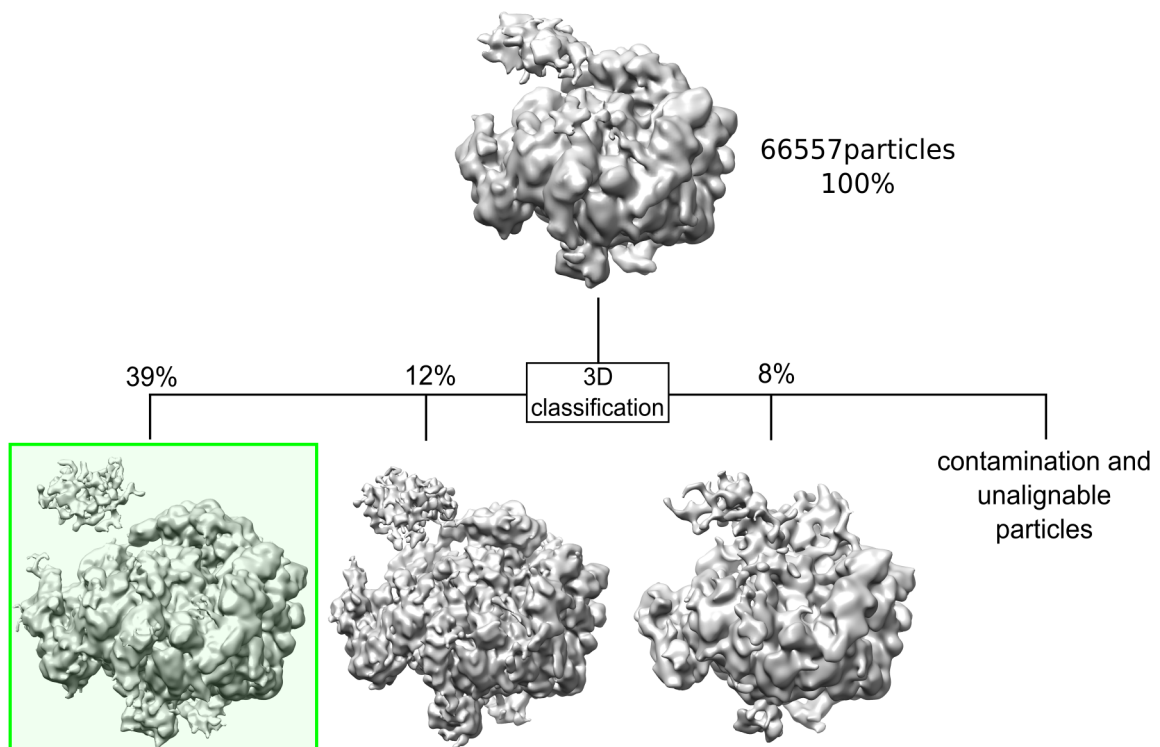


FIGURE 3.21: **Classification of the Rix1 Δ C dataset.** The class used for the final reconstruction is highlighted in green. Adjusted from Barrio-Garcia et al., 2016.

The resolution of this particle varied again between 5 and 14 Å, and the overall resolution measured by the $FSC_{0.5}$ criterion was 11.2 Å (FIG. 3.20). From the three main classes obtained through 3D classification (FIG. 3.21), the largest one (containing about 39% of the particles) was used for the final reconstruction. Interestingly, the class were the density assigned to the Rix1 complex was closest to the 5S RNP (comprising 12% of the data), does not show density for Rsa4. Moreover, the third class which only contained 8% of the total amount of particles, showed a mature 5S RNP (FIG. 3.21).

In summary, these data suggested that recruitment of both the Rix1 subcomplex and Rea1 to the pre-60S particle, but not Rea1's ATPase activity, drives efficient 5S RNP and CP maturation.

4 Discussion

4.1 Structurally impaired ribosomes can engage in translation

Throughout this dissertation it has been highlighted that a number of quality control checkpoints have the role to ensure the production of properly assembled and functional ribosomes. However, some defects in the ribosome biogenesis pathway are overlooked by these checkpoints, giving rise to several human diseases linked to mutations in r-proteins or ribosome biogenesis factors (Kressler et al., 2010). In the first project presented in this thesis it is shown that big structural impairments of the ribosome can also be ignored by all quality control mechanisms. Here it is demonstrated that pre-60S particles containing the completely unprocessed ITS2 and all the biogenesis factors of the foot, can be exported to the cytoplasm and produce translationally active ribosomes FIG. 3.5. These results are in agreement with the findings by Rodríguez-Galán and colleagues showing that ribosomes containing 7S rRNA can engage in translation (Rodríguez-Galán et al., 2015).

In addition, the present study proves that these faulty ribosomes enrich tRNAs in their A/P and P/E hybrid states, corresponding to a pre-translocation intermediate (FIG. 3.6). Moreover, biochemical analysis showed that Tae2 and Ltn1 are recruited to the impaired 60S subunits after a splitting event. Therefore, the fact that these ribosomes are not completely processed leads to translational stress, which is sensed by the cell to stimulate subunit splitting and recruitment of the RQC factors to the 60S, as it happens to trigger mRNA quality control pathways after ribosome stalling. Nevertheless, the cryo-EM structure of the Nop53 Las1-depleted 80S particle did not show any direct indication of stalling provoked by the foot. The finding that these impaired 80S subunits accumulate tRNAs in hybrid states rather indicates that translocation cannot be carried out efficiently, causing pauses in the translation process. This is further supported by the fact that lethality observed in double mutants targeting Las1, Ltn1, Ski2 and Ski7 in cells incubated by translocation inhibitors (Anshuk

Sharkar, personal communication). Importantly, Ski7 and Ski2 (part of the Ski complex composed of Ski2, Ski3 and Ski8) are required for 3' to 5' exosome-dependent mRNA degradation (Shoemaker and Green, 2012).

Why translocation is not efficient in this particle? Comparing the structures of the mature ribosome and the Nop53 Las1-depleted 80S particle, the only difference is that ES19 is slightly shifted because of its interaction with the foot, but this ES does not have a known role in translation. This area is not far from the three-way junction below the L1 stalk, which has been shown to be involved in translocation (Fei et al., 2008). Interestingly, in the Nop53 Las1-depleted 80S particle, the L1 stalk is in its inward conformation but in empty 80S class, it does not have a defined position. Therefore, a direct contact between L1 and the foot could not be found. The first possible reason that explains this translocation problem would be that the foot is obstructing the movement of ES27 from its two conformations (FIG. 4.1), but even though this ES was shown to be essential for cell survival in *T. thermophila* (Jeeninga et al., 1997; Sweeney et al., 1994) and implicated in coordinating ribosomes at the TE (Bradatsch et al., 2012; Greber et al., 2012; Leidig et al., 2013), its specific roles during translation are still not clear.

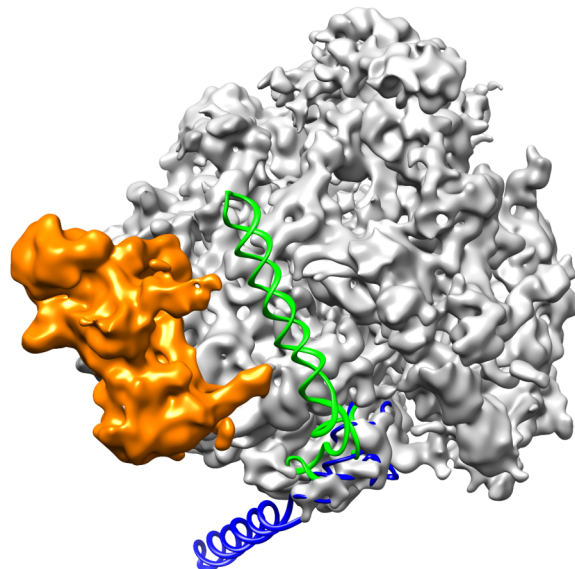


FIGURE 4.1: **Foot obstructing the path of ES27.** The map for the Nop53 Las1-depleted 80S particle highlighting the foot in orange and the structural models of ES27 in their respective "in" (green) and "out" (blue) conformations are shown (PDB IDs 3IZF and 3IZD Armache et al., 2010).

The second possible reason arises by analysing the structure of actively translating polysomes (Myasnikov et al., 2014). The fit of the Nop53 Las1-depleted 80S particle into the polysome structure, demonstrates that the foot would clash with the small subunit of the next ribosome (FIG. 4.2). Therefore, the foot structure would impair the rotation of the small subunit and consequently translocation would not be carried out efficiently.

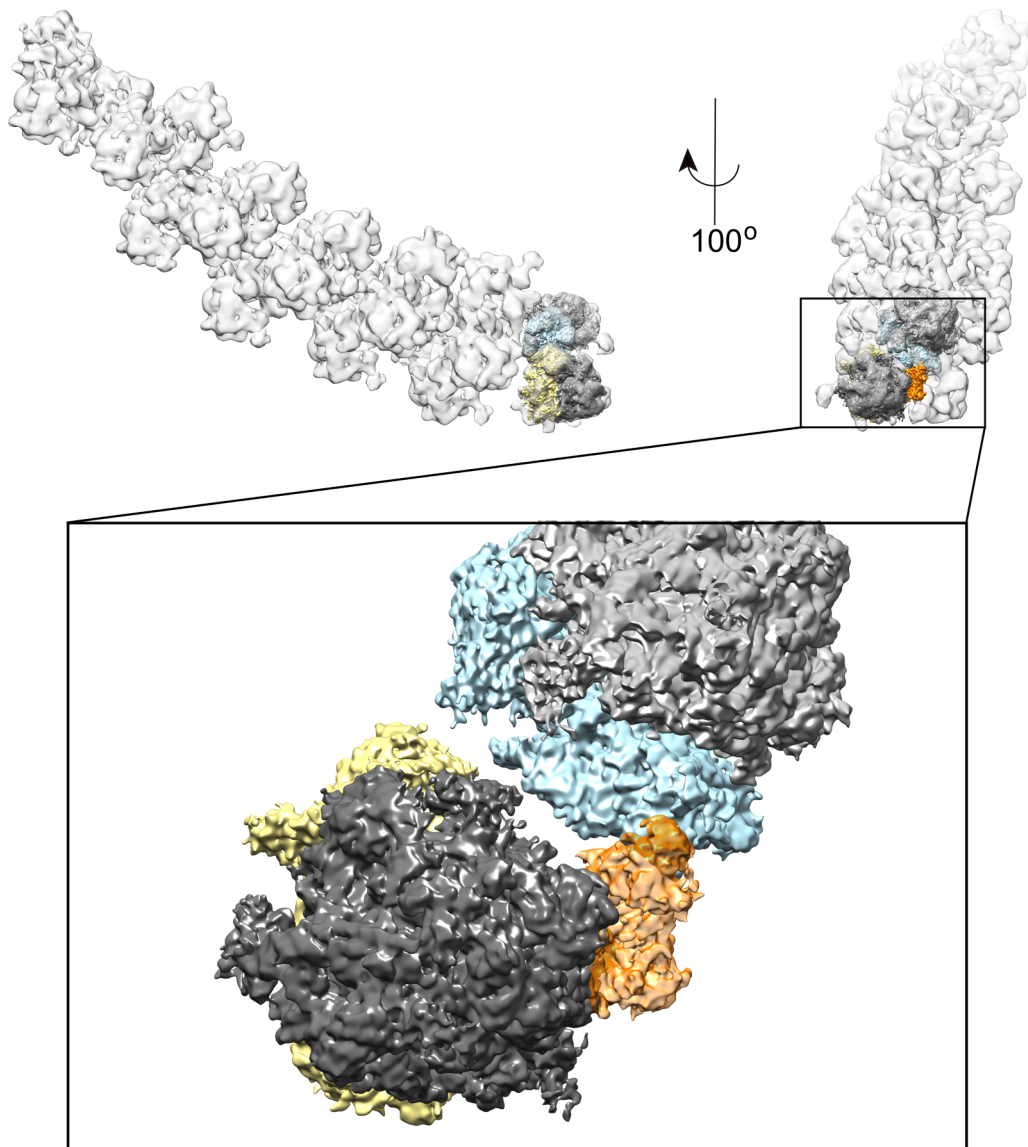


FIGURE 4.2: Foot clashing within polysomes. The map for the Nop53 Las1-depleted 80S particle is fitted into the polysome density (EMDB-2790) highlighting the foot in orange; the small subunit in yellow and light-blue; and the large subunit in gray.

The mechanism by which this translocation-inefficient ribosomes are detected is not clear yet. What appears to be certain is that even though the ribosome biogenesis quality control system fails to detect these improperly processed ribosomes, downstream events are carried out in order to prevent deficient translation, as indicated by RQC co-enrichment in this sample (FIG. 3.1). Correspondingly, depletion of LAS1 resulted in a nucleolar stress characterized by a G1-phase arrest and stabilization of the tumor suppressor p53 (Castle et al., 2010). Moreover, genetic interactions between a Las1 mutant and Ski2 and Ski7 were found by Anshuk Sharkar (personal communication) suggesting that the mRNAs engaging in translation with such defective machinery are also targeted for degradation.

The logical consequence of the fact that these faulty ribosomes are recognized is that the 60S subunit should also be degraded. In order to verify this and to elucidate whether these particles are substrates of NRD, further experiments should be carried out in the future (see Future Perspective).

4.2 Biogenesis factors in the Rix1-Rea1 particle

In this project several biogenesis factors have been structurally characterized and unambiguously positioned on the pre-60S subunit, revealing significant insights into their respective activities.

Firstly, Rea1, the largest protein in the yeast genome (Garbarino and Gibbons, 2002), was precisely localized in the nascent 60S. The assigned position was not only in agreement with previous structural studies (2D negative stain images; Nissan et al., 2004; Ulbrich et al., 2009) but also with the available biochemical data, showing an interaction with the UBL domain of Rsa4, which is important for the recruitment of Rea1 to the pre-60S particles (Barrio-Garcia et al., 2016). Nevertheless, the fact that an unambiguous orientation was found for Rea1 is mostly due to the very characteristic features of this huge enzyme, which were visible in the cryo-EM structure presented in this thesis (see section 3.2.3 and figures 3.12 and 3.13b).

Rea1 constitutes one of the two AAA⁺ ATPases that form a hexameric ring. The other one is dynein, to which Rea1 is distantly related (Garbarino and Gibbons, 2002). Even though it was at first speculated that Rea1 could have a role in nuclear pre-60S transport (Nissan et al., 2004) the similarity of Rea1 to dynein is restricted to the motor domain (Garbarino and Gibbons, 2002), which would rather speak for a common way to induce conformational changes on the ring domain in order to exert

a mechanical force. Rea1 was shown to be involved in the release of biogenesis factors in an ATP-dependent manner on two different pre-60S intermediates, first in the nucleolus and then in the nucleoplasm (Ulbrich et al., 2009; Baßler et al., 2010). This function was recently extended by Matsuo and colleagues, as they demonstrated that Rea1's AAA⁺ activity is coupled to the binding of GTP to Nug2, which suggests a checkpoint role for this machinery before nuclear export (Matsuo et al., 2014). The present study further extends and deepens on Rea1's activities. Here it is shown that Rea1 is required for CP and 5S RNP rotation and that proper maturation of the CP is what Nug2 and Rea1 are checking before export to the cytoplasm is allowed (see 4.4). Since the transition of pre-60S particles from the nucleolus to the nucleus is coupled to the release of the Ytm1-Erb1-Nop7 subcomplex by Rea1 (Baßler et al., 2010), it is tempting to speculate that Rea1 has also a checkpoint role in the nucleolus, and thus, structurally characterizing such an early pre-60S intermediate would be very revealing.

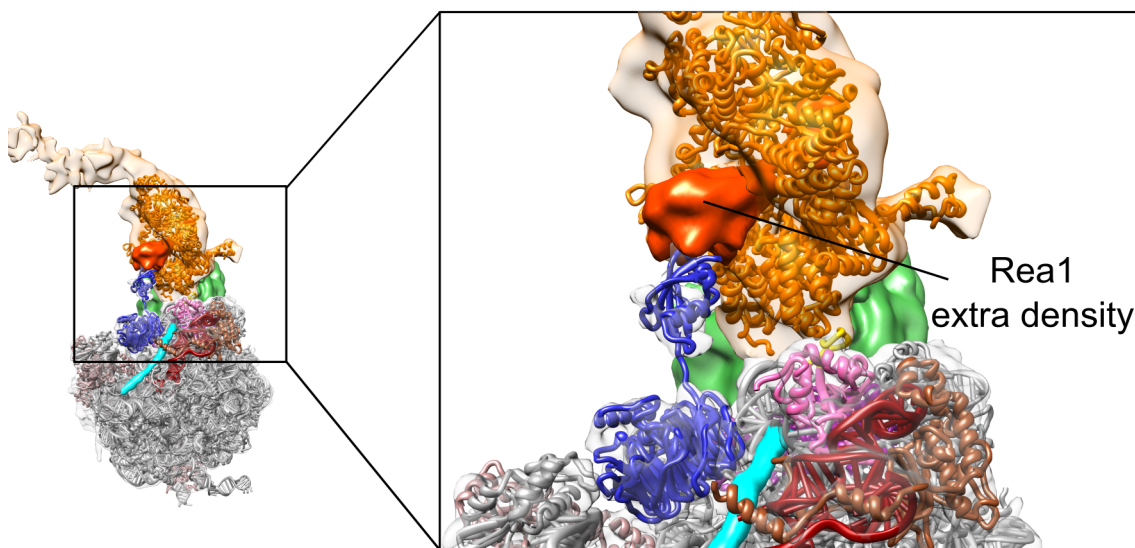


FIGURE 4.3: **Rsa4's UBL domain interacts with an unexplained density of Rea1.** Highlighted in dark orange is the density of Rea1 that is not explained by the model.

Rsa4 is an essential nucleoplasmic biogenesis factor present specifically in the early Arx1 and the Rix1-Rea1 particles (Ulbrich et al., 2009). Strikingly, the interaction found between the UBL domain of Rsa4 and Rea1 in the context of the Rix1-Rea1 particle was not the same as the one first observed through yeast 2-hybrid experiments, which involved the MIDAS domain of Rea1 (Ulbrich et al., 2009). It

was shown that by mutating residue E144 in Rsa4, this interaction (Rsa4's UBL domain with Rea1's MIDAs) is hindered and ATP-dependent release of Rsa4 does not occur (Ulbrich et al., 2009). Remarkably, Rsa4's UBL domain undergoes important rearrangements and changes its binding partners in the transit from the Arx1 particle to the Rix1-Rea1 particle (FIG. 3.15). However, instead of binding Rea1 through its MIDAS domain, Rsa4 interacts with a region of Rea1 that was left unexplained by the provided model (see FIG. 4.3). Since the remaining parts of Rea1 are already assigned to specific segments of the cryo-EM map, it could be hypothesized that this unexplained density belongs to Rea1's N-terminal domain. Nevertheless, due to the lack of resolution in this area this interpretation could not be proven so far. In any case, putting together the preceding data from Ulbrich and colleagues with the Arx1 and Rix1-Rea1 cryo-EM structures, it seems that Rsa4 is highly dynamic, not only altering the conformation of its UBL relative to its β -propeller domain, but also changing its binding partners several times. This is done in a stepwise manner during important checkpoint-remodeling steps of the pre-60S pathway (see section 4.4).

Next, the Rix1 complex was identified and assigned to a specific density of the Rix1-Rea1 structure. Little information was available for the Rix1 complex before this study. Neither its specific roles in pre-60S maturation nor how it is structurally arranged were clear. Here, the involvement of Rix1 on Rea1's recruitment to the pre-60S was discovered, as well as that this step is crucial for CP remodeling (see section 3.2.7). In mammals, the PELP1-TEX10-WDR18 complex (homologue of the Rix1 complex) was shown to interact with Las1 and pre-60S particles before ITS2 cleavage, suggesting that the Rix1 complex is also involved in the maturation of nucleolar intermediates (Castle et al., 2012). Since Rea1 is likewise involved in stripping biogenesis factors in the nucleolus, it would be interesting to investigate whether there is a common mechanism happening both in the nucleolus and the nucleoplasm, through which the Rix1 complex brings Rea1 to the pre-60S intermediates.

Even though a big effort was made to characterize the Rix1 complex with biochemical and cross linking restraints, its molecular model could not be provided for two main reasons: i) the resolution in this area was not good enough and ii) the interpretation of the biochemical restraints was difficult because the complex contains two copies of Ipi1 and Rix1. Despite that, although not being unambiguous (only the density of one of the two Ipi3 copies was seen and the density for Ipi1 is not well defined), the most plausible model for the Rix1 complex based on the cryo-EM density and the biochemical restraints, is described in FIG. 4.4. In this arrangement, the two

copies of Rix1 would be placed vertically one on top of each other, being stabilized to the maturing 60S subunit by L1, Sda1 and the H2 insertion of Rea1. They contact the two Ipi3 copies on one side and Ipi1 on the other side. The circle is closed by the interaction between Ipi1 and one of the Ipi3 copies (FIG. 4.4). In this configuration, Ipi1 would contact the nascent particle not only through Sda1, but also through the D2 lid domain of Rea1 and rRNA helices H69 and H38. Nevertheless, in order to provide a reliable molecular model for the Rix1 complex, a higher resolution structure will be needed in the future (see Future Perspective).

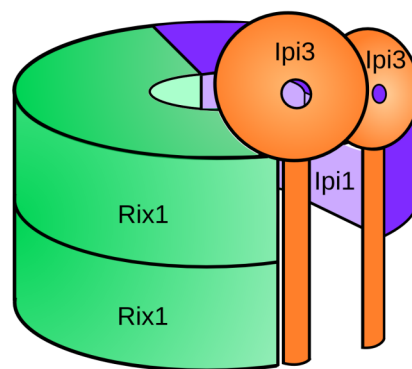


FIGURE 4.4: **Model of the Rix1 complex organization.**

Finally, the HEAT-repeat protein Sda1 was found in the cryo-EM structure of the Rix1-Rea1 particle and a model for every predicted helix was built (see section 3.2.3 and FIG. 3.13). Sda1 was first described as a pre-60S biogenesis factor required for nuclear export (Baßler et al., 2001; Dez et al., 2006), although it remained unclear whether it is needed for the export process itself or for the pre-60S to acquire export competence (Dez et al., 2006). In this study, it is demonstrated that Sda1 has an important role in recruiting and scaffolding both the Rix1 complex and Rea1 to the pre-60S subunit, which is ultimately needed for CP protuberance maturation and export competence acquisition.

4.3 Model improvement using high-resolution structures of pre-60S intermediates

The model for the early Arx1 particle has been remarkably improved and completed with the recent high-resolution cryo-EM structure of this intermediate purified

through Nug2 (Wu et al., 2016). Because most of the biogenesis factors in the Arx1 particle are also present in the Rix1-Rea1 particle, a more detailed understanding of the latter can be achieved through the comparison between the two structures. In addition, the structure by Greber and colleagues of a cytoplasmic intermediate (Greber et al., 2016) can be used to localize Alb1 and improve the model of its cofactor Arx1.

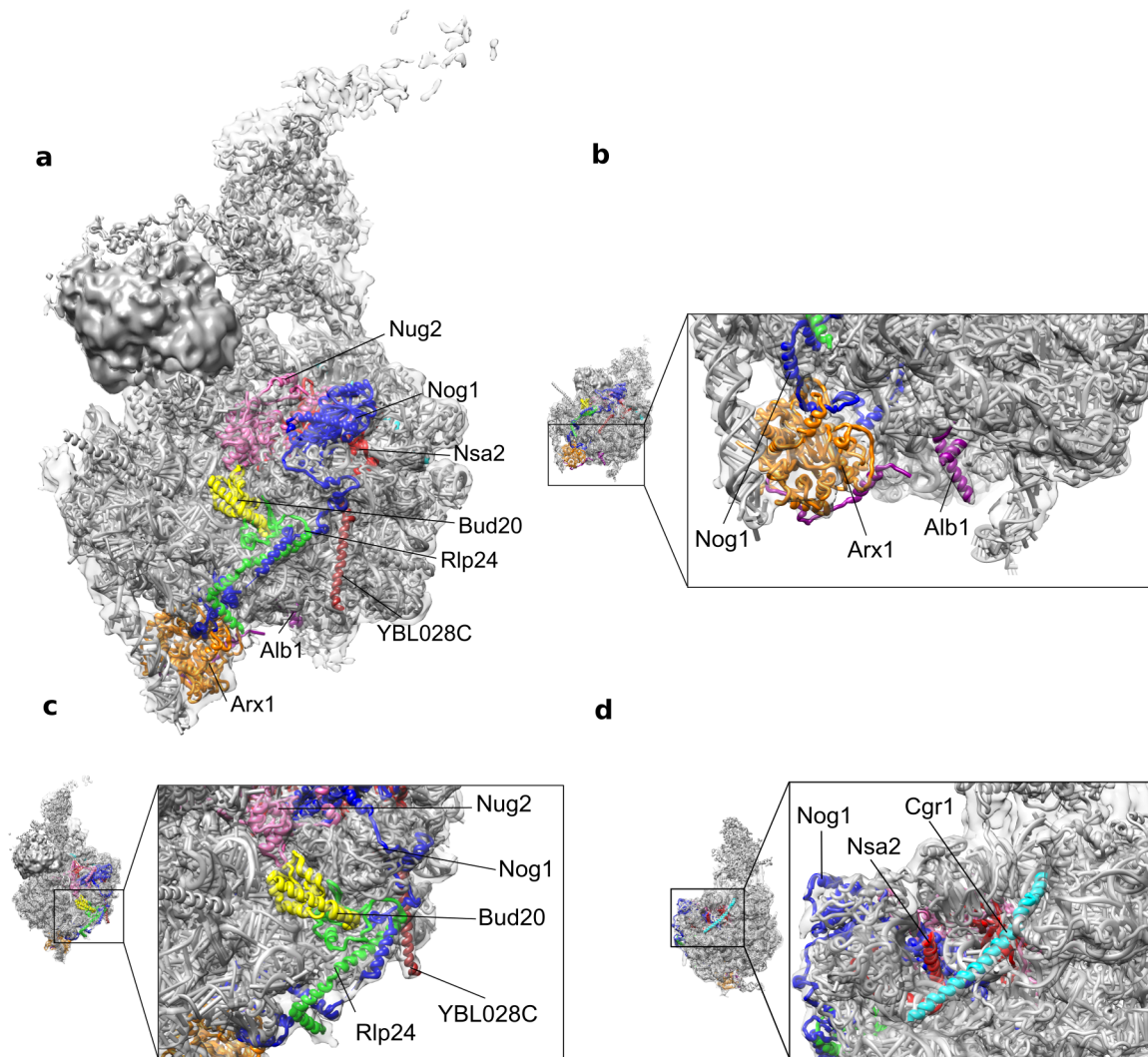


FIGURE 4.5: Biogenesis factors identified or improved using recent high resolution structures. (a) The Rix1-Rea1 map is fitted with its corresponding models (gray). Biogenesis factors that were completed or identified using the recently available high resolution structures are highlighted with different colors (PDB IDs 3JCT and 5APO). Except Cgr1, all these proteins were rigid body fitted into the Rix1-Rea1 density. (b) Zoom on the TE showing the fit for Arx1, Alb1 and Nog1. (c) Zoom on Rlp24, Bud20, YBL028C, Nug2 and Nog1. (d) Zoom on Nsa2, Nug2 and Cgr1.

Thus, all densities that were not assigned in the Rix1-Rea1 structure (see FIG. 3.12, dark gray), can now be explained by a specific biogenesis factor (FIG. 4.5). Initially, Cgr1, Nug2, Nsa2, Bud20, YBL028C and Alb1 were not identified in the Rix1-Rea1 particle due to the lack of restraints and resolution. All these factors except Cgr1 (which has an extended conformation in the context of the Rix1-Rea1 particle) could be rigid body fitted into the Rix1-Rea1 map using their respective models from Wu et al., 2016 and Greber et al., 2016 (FIG. 4.5; PDB IDs 3JCT and 5APO). By following this procedure, only three conflicting parts are found: Nug2 would clash with rRNA H71, Nsa2 with H89 and YBL028C with the r-protein eL3 in the model provided for the Rix1-Rea1 particle. However, this is likely due to the fact that in these areas the model was not correct. The base of H89 consists of single stranded rRNA and its model can be improved using the high resolution structure by Wu and colleagues. Similarly, the model for eL3 could be corrected to avoid the clash with YBL028C. In the case of H71 a correction would be more difficult, since this helix is flexible and in the Rix1-Rea1 structure it does not have the same conformation as in the Arx1 particle (FIG. 3.14). Interestingly, Nug2 does not establish a contact with Rea1. Therefore, the observed coupling between the two enzymes (Matsuo et al., 2014) seems to occur either in an indirect way, or after a conformational change induced by GTP binding to Nug2 which would bring Rea1 and Nug2 in close proximity.

Although Nog1, Rlp24 and Arx1 were already identified in the Rix1-Rea1 particle, large portions of these proteins were not included in the Rix1-Rea1 model. However, more complete models of these proteins were provided in the higher resolution cryo-EM maps of the Arx1 and Rei1 particles. These could also be rigid body fitted in the Rix1-Rea1 density, giving a clarification for the entire cryo-EM map (FIG. 4.5). Notably the C-terminal domain of Nog1, which is inserted into the TE, could also be observed in the Rix1-Rea1 intermediate (FIG. 4.5b).

4.4 Remodeling mechanism of the CP

By comparing the structures of two consecutive pre-ribosomal intermediates, a mechanistic model for the transition between them has been provided in this study. Particularly, the CP of the pre-60S subunit is substantially remodeled in the progression from the Arx1 to the Rix1-Rea1 particle. This rotation of the CP constitutes the last big remodeling step happening on the 60S maturation pathway (FIG. 3.14).

The Arx1 particle constitutes the substrate for Rix1, Rea1 and Sda1 (FIG. 4.6). When Rea1 is not recruited to the pre-60S particles due to the lack of the C-terminal

domain of Rix1, the Rix1 complex seems to bind near the tip of the 5S RNA and Rpf2-Rrs1 (see section 3.2.7 and FIG. 3.19). This initial binding of the Rix1 complex appears to destabilize the contact between Rsa4 and the 5S RNP, which is a requirement for the rotation of the CP. This is because rRNA H38 has to move towards the intersubunit side passing between Rsa4 and the 5S RNP, since it occupies the place to which the 5S RNA reaches in its semi-final position (FIG. 3.15). Because in its "unlock" state Rsa4 is loosely bound to the particle and in the Rix1 Δ C particle lacks Rea1 to be further stabilized, it may easily fall off and that is probably why Rsa4 is absent on 12% of the particles of this dataset (FIG. 3.21).

Nevertheless, the Rix1 complex without Rea1 is not sufficient for efficient 5S RNP rotation as demonstrated by the cryo-EM structure by the Rix1 Δ C particle (FIG. 3.19). Importantly, only about 8% of the particles of this dataset gave rise to a 3D reconstruction where the rotation has already been carried out (FIG. 3.21), which could be the reason why the rix1 Δ C mutant causes a slow-growth phenotype but is not lethal (Barrio-Garcia et al., 2016). Whether this is a consequence of obtaining substoichiometric amounts of Rea1 in the purification (see FIG. 3.19) or if the combined action of the Rix1 complex with other biogenesis factors present in the particle could also lead to a very inefficient rotation of the CP, remained unclear. What seems to be certain is that Rea1's recruitment to the pre-60S is essential for effective rotation of the 5S RNP, and that this process is coupled to the movement of rRNA H38 towards the intersubunit space (FIG. 4.6). Interestingly, Wu and colleagues recently showed that the repositioning of H38 involves the conformational change of the C-terminus of Cgr1, which transits from a bent helix to a straightened form (Wu et al., 2016), suggesting that this factor also takes part in the remodeling of the CP.

The cryo-EM structure of the dominant lethal Rix1-Rea1 K1089A mutant, which is unable to release Rsa4 and is blocked in nuclear export (Barrio-Garcia et al., 2016), demonstrated that ATP binding and hydrolysis in Rea1's D3 is not required for 5S RNP relocation. Importantly, Rea1's D2, D3, D4 and D5 contain all residues essential for ATP activity in their canonical forms, and only the Walker B motif in D1 and D6 protomers is deviant (Garbarino and Gibbons, 2002). As a consequence, the possibility that CP rotation depends on the ATPase binding/hydrolysis of some other protomer cannot be excluded, although this seems unlikely since the remodeling of the 5S RNP appears to be a prerequisite for Rea1 to stably dock to the pre-60S. This is inferred by observing the cryo-EM structure of the Rix1-Rea1 particle, where Rea1 binds to Rsa4, L3 loop in r-protein uL5 and rRNA H38, all of them in their respective

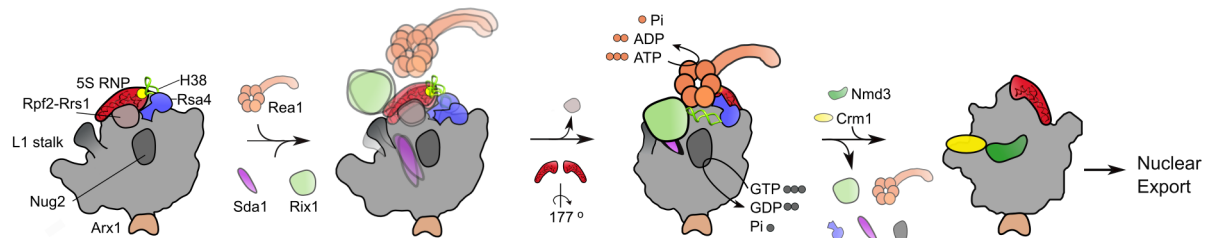


FIGURE 4.6: **Nucleoplasmic maturation of pre-60S particles.** Figure from Barrio-Garcia et al., 2016.

relocated positions (FIG. 3.13).

Only after Rea1 is firmly bound to the maturing particles, correct maturation of the CP can be sensed by Nug2 and Rea1, which then hydrolyse their respective nucleotide triggering the release of this huge machinery and allowing the export of the pre-60S particles to the cytoplasm (Matsuo et al., 2014, FIG. 4.6). Notably, during 3D classification of the Rix1-Rea1 particle, it was found that 42% of the data did not show clear density for Rix1, Cgr1, Rea1, Sda1 and Rsa4 (FIG. 3.11). Whether this class consisted of particles where the mentioned proteins were lost unspecifically after purification (for example during transportation or grid making, as it seems to be the case for 24% of the particles of the Rix1-Rea1 particle that lost Rea1 and 40% of the particles that lost both Rix1 and Rea1 in the Rix1-Rea1 K1098A dataset), or if it comprises a particle where disassembly of these factors was carried out by Rea1 due to an ATP contamination, could not be clarified in this study. However, the second option would correlate better to the fact that this subclass in the WT dataset does not show a clear density for Rsa4 and H38. Still, in order to get a more detailed understanding into the exact consequences of ATP hydrolysis by Rea1 further experiments should be carried out (see Future Perspective).

The Rpf2-Rrs1 complex was suggested to stabilize the immature configuration of the CP by inserting the C-terminal domain of Rrs1 through the three-way junction connecting helices H80, H82 and H88 of 25S rRNA (Kharde et al., 2015). This was in disagreement with the hypothesis by Madru and colleagues, as they assigned the same density to the disordered C-terminal domain of Rpf2 (Madru et al., 2015). The

high resolution structure of the early Arx1 particle indicated that this density corresponds to Rrs1's C-terminal domain, which wraps around the above mentioned three-way junction (FIG. 4.7, Wu et al., 2016), supporting the interpretation by Kharde and colleagues that the release of the Rpf2-Rrs1 complex could play a role in the rotation of the CP. However, despite that the C-terminus of Rix1 is required for the disassembly of this complex (as inferred from the Rix1 Δ C particle), the mechanistic details of this process are not clear yet.

In summary, the findings presented in this dissertation indicate that the maturation of the CP is achieved by the cooperative action of several biogenesis factors, including: Rea1, Rix1, Rsa4, Sda1, Cgr1 and the Rpf2-Rrs1 complex.

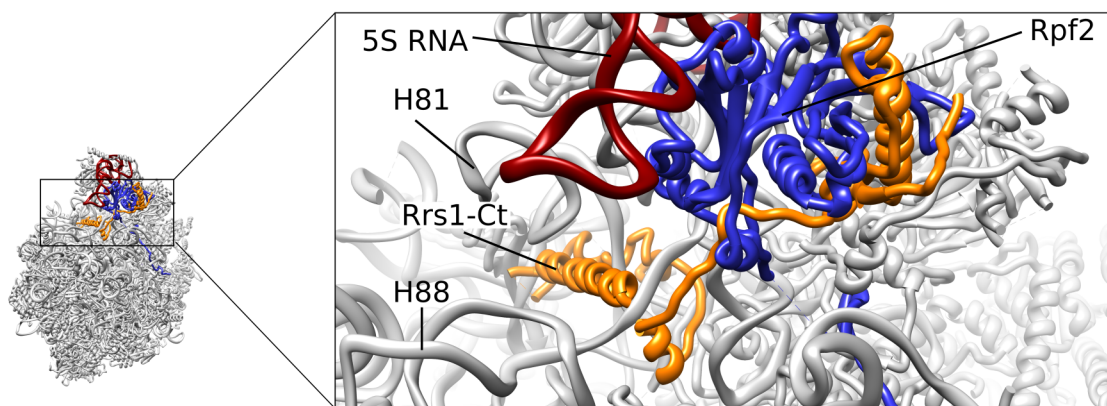


FIGURE 4.7: **The Rpf2-Rrs1 complex stabilizes the immature conformation of the CP.** The structure shown corresponds to PDB ID 3JCT (Wu et al., 2016).

4.5 Foot removal in the transit from the Arx1 to Rix1-Rea1 particle

The cryo-EM structures presented in this study suggest that there is a correlation between stable binding of the Rix1-Rea1 complex to the pre-60S particles and the removal of the foot structure (see FIG. 3.9, FIG. 3.16 and FIG. 3.19). However, with the available data it is difficult to draw any conclusions into how this process takes place, since neither the Rix1 complex nor Rea1 are in close proximity to the foot in the context of the Rix1-Rea1 particle. Moreover, after 3D classification of the Nug2 particle, Wu and colleagues found a subclass that contained Rix1, Rea1

and the foot structure (Wu et al., 2016), which makes the previous correlation to seem inconsistent. Thus, further investigations should be carried out in order to mechanistically understand how the foot is removed.

5 Conclusions

The results obtained for the Nop53 Las1-depleted sample reveal that a large structural alteration of the 60S which arises from a defect in the biogenesis pathway may be ignored by all quality control checkpoints. Therefore, impaired subunits are exported to the cytoplasm where they form 80S ribosomes. Although these ribosomes are able to translate, an enrichment of A/P and P/E hybrid tRNAs is observed using cryo-EM analysis, suggesting that translocation is not efficient. This is recognized by the cell, leading to the dissociation of the 40S subunit and the recruitment of the RQC to the 60S. Summarizing, here it is proven that ribosomes bearing large structural defects may nevertheless be translationally active, but inefficient translation is detected in the cytoplasm where quality control mechanisms are activated. Eventually, the products of these ribosomes are degraded by the RQC system, which defines a wider range of action for this machinery.

The work on the Rix1-Rea1 particle presented in this thesis provides a model for the rotation mechanism of the CP. The architecture of this particle shows that after binding of the Rix1-Rea1 complex, the CP and the 5S RNP display full rotation towards the mature conformation. The comparison of the rRNA in the Arx1, Rix1-Rea1 and mature states demonstrates that this remodeling step is the largest one happening at the end of the pre-60S maturation pathway. After the Rix1-Rea1 intermediate, little rearrangements of the rRNA are required to achieve the final 60S structure.

Analysis of the Rix1 Δ C particle showed that the C-terminus of Rix1 recruits Rea1 to the pre-ribosome and that this is a requirement for efficient CP rotation. In addition, the architecture of the Rix1-Rea1 K1098A intermediate containing a mutation in Rea1 which makes it unable to trigger the release of Rsa4, is almost identical to the WT, showing full rotation of the CP. Thus, 5S RNP relocation towards the mature state is independent from Rsa4 release. A close comparison between the Arx1 and Rix1-Rea1 particles suggests that the remodeling of the CP is a complex multilateral process, which involves: binding of the Rix1-Rea1 complex, release of Rpf2-Rrs1,

unlocking of Rsa4 from the 5S RNP to allow the movement of H38 towards the intersubunit side and a conformational change in Cgr1 which stabilizes H38 in the above mentioned position.

Importantly, only after rotation has occurred, Rea1 can stably bind to the pre-60S particle. Hence, Rea1 together with Nug2 proofread the proper maturation of the CP before biogenesis factors can be released and nuclear export is allowed. Thus, a dual function for this checkpoint machinery is suggested: first monitoring the correct arrangement of this hallmark site of the 60S subunit and secondly, triggering the release of biogenesis factors, which drives further progression in the maturation pathway.

Taken together, here it is shown that some structural features at important functional sites of the ribosome (as is the case of the CP and the intersubunit side), are carefully checked by quality control mechanisms avoiding nuclear export of faulty particles; but others with less impact on translation (like the 5' end of the 25S), lack a quality control mechanism during the ribosome biogenesis pathway. Nevertheless, if defects in ribosome production lead to inefficient translation, surveillance mechanisms are ultimately activated in the cytoplasm.

6 Future Perspective

Two main questions remained unanswered regarding the Nop53 Las1-depleted particle. The first question is how are these structurally deficient ribosomes initially recognized so that subsequent surveillance mechanisms are activated. The second one is about their degradation. Further biochemical experiments should be done in order to clarify whether these particles are targets 25S NRD, which will provide a deeper understanding about this degradation system. If this turns to be the case, this particle would be an ideal candidate to perform structural studies involving NRD, which will be helpful since the mechanisms underlying this machinery are poorly understood.

As discussed in section 4.3, in order to make a better model of the Rix1-Rea1 particle the recently available high-resolution maps of pre-60S intermediates (Wu et al., 2016; Greber et al., 2016) can be used. However, the models of Sda1, Rea1 and the Rix1 complex are not part of this improvement, leaving important questions about this machinery unanswered. Therefore, high resolution structures of the Rix1 complex and Rea1 will be useful to understand the mechanistic details of Rea1's recruitment, 5S RNP rotation, the release of biogenesis factors from the pre-60S by Rea1 and the assembly of the Rix1-complex itself. Since the Rix1 complex and Rea1 are large in size, this can be done using both by X-Ray crystallography and cryo-EM. Another possibility is to improve the resolution of the whole cryo-EM map; however, since the Rix1 complex and Rea1 are on the periphery of the pre-60S and are more flexible than the rest of the particle, an improvement of their models using this approach does not seem to be realistic. Nevertheless, because Sda1 has a very stable binding to the pre-60S, this factor could benefit from this approach.

The exact consequences of ATP hydrolysis by Rea1 are still unclear, and even though the binding of Rea1 seems to trigger the rotation of the CP, it could not be disproved in this study that this process also requires ATP hydrolysis on some other ATPase protomer of Rea1 different than D3. In order to elucidate these questions, it

will be interesting to structurally characterize *in vitro* reconstituted Rix1-Rea1 particles in the future, obtained by mixing Arx1 particles with the Rix1 complex, Sda1 and Rea1. The cryo-EM analysis should then be done before and after incubation with ATP and an ATP analogue. This may also reveal details into how the foot structure is removed after the Rix1-Rea1 complex is recruited.

Structural information is not available yet for many intermediates in the ribosome maturation pathway. Thus, obtaining the cryo-EM structures of other native particles, specially the earlier ones, will immensely help to further understand how ribosomes are produced.

In a broader perspective, little is known about the maturation of human ribosomes, even though this process is clinically relevant. Therefore, a similar approach as the presented here should be carried out in the future in order to structurally and mechanistically characterize human pre-ribosomes.

Appendix

```

D1-DYNEIN/1-222 1 YKFEYIGPERLIYTP LLLIGFATL TDSLHQKYGGCFGPAAGTGKTEITVKAFGQNLGRV--VVVFNCD 66
D1-REA1/1-284 1 -----VSRLRQLGRKIQNSTPIMLIGKAGSGKTFLINELSKYMGCHDSIVKIHLG 50
D2-REA1/1-282 1 -----SLRLMEQISVCIQMTEPVLLVGETGTGKTTVVQQLAKMLAKK--LTVINVS 49
D3-REA1/1-259 1 -----EKNMNNLYRATSGKRFPVLIQGP TSSGKTSMIKYLADITGHK--FVRINNH 49
D4-REA1/1-259 1 -----MRRLSVLVSSCLKNKEPVLLVGETGCGKTTICQLLAQFMGRE--LITLNAH 49
D5-REA1/1-266 1 -----ASNLYRVVRA-MQVHKPILLEGSPGVGKTSLITALANITGNK--LTRINLS 48
D6_REA1/1-245 1 -----NVAVYESVLKAINNMP LVLVGRGNSGKTEITIRFLASILGFR--VDVFSMN 49

D1-DYNEIN/1-222 67 -----DSFDYQVLSRLLVGIITQIGAWGCFDEFNRLDEKVL SAVSANIQQIQNG-LQV 117
D1-REA1/1-284 51 EOTDAKLLIGTYTSGDK----PGTFEWRAGVLATAVKEGRWLI EDIDKAPT DVLSILLSLLEK--- 110
D2-REA1/1-282 50 QOTETGDL LGGYKPVNS-108-SFVFNVFGSLVKTI RAGEWLLLDENVLATAIDTLESISDLLTEPDS 115
D3-REA1/1-259 50 EHTDLQELGTYVTD-----TGKLSFKEGVLVEALRKYWI VLDELNLAPTDVLEALNRLLDN-- 109
D4-REA1/1-259 50 QNTETGDI LGAQRPVR--58--VLFEWSDGLIQAMRTGNFFLLDEISLADDSVLERLNSVLE-P-E 110
D5-REA1/1-266 49 EOTDLVDFLFGADAPGE-----RSGEFLWHDAPFLRAMKKGEWLLDEMNLASQS VLEGLNACLDHR-- 109
D6_REA1/1-245 50 SDIDSMIDLGGYEQVDL--91--VKFEWFDGMLVKAVEKQHWLILDNANLCSPSVLDRLNLSLEID-- 111

D1-DYNEIN/1-222 118 -GKSHITLLEEETPLSPHTAVFITLNP GYNG--RSELPENLKK-----SFREFSMKSPQSGTIAEM 175
D1-REA1/1-284 111 RELTIPSRG-----ETVKAANGFQLISTVRINEDHQ--KDSNKTINLNMIGMRIWNVIELEPSEE 170
D2-REA1/1-282 116 RSILLSEKGD---AE-PIKAHPDFRIFACMNPATDVG-KRDLPMGIRS-----RFTEIYVHSPERD 171
D3-REA1/1-259 110 RELFIPETQ-----EVVHPHPDFLLFATQNPPIYGGRIILSRAFRN-----RFLELHFDIIPQD 164
D4-REA1/1-259 111 RSLLLAEQGS---SDSLVTASENFQFATMNPGGDYG-KKELSPALRN-----RFTEIWWPSMEDF 167
D5-REA1/1-266 110 GEAYIPELD-----ISFSCHPNFLVFAAQNPQYQGGGRKGLPKSFVN-----RFSVVFIDMLTSD 164
D6_REA1/1-245 112 GSLLINECSQEDGQPRVLPKHPNFRFLTMDPKYGELSRR----AMRN-----RGVEIYIDELHSR 168

D1-DYNEIN/1-222 176 ILQIM-----GFEDSKSLASKIVHFLELLSSK-----CSSMN---HYHFLGRTLK 217
D1-REA1/1-284 171 DLTHILAQ-K-----FPLTNLIPKLI DSYKNVKS---IYMNTKF-----ISLNKGAHTRVVS 219
D2-REA1/1-282 172 ITDL-----LSIDKYIGKYSVSEWVGNDIAELYLEAKLSDNNTIVDGSNQP HFS 224
D3-REA1/1-259 165 ELEITLRE---R---C-QIAPS YAKKIVEVY-RQLS-----IERSASRLFQKNS--FAT 209
D4-REA1/1-259 168 NDVNMIVSS-----RLL EDLKDLANPIVKFSEWF GKKLGGGNATS-----GVIS 211
D5-REA1/1-266 165 DLLLIAKH---L---YSPTEPDI IAKMIKLM-STLE-----DQVCKRKLWGNSSPWEFVN 212
D6_REA1/1-245 169 STAFDRITLGFELGENIDFVSDDGILKK-IKLNEDMSIP LKHYP--SYLSRPF CIF-----AQ 224

D1-DYNEIN/1-222 218 GVLRN----- 222
D1-REA1/1-284 220 VDLTKLGERLDILFKNNGINKPDQLIQSSYYSIFSEAADCFAAIGEFKALEPITQAI GESLD- 284
D2-REA1/1-282 225 IRTLRTLLYVTDI IH-----IYGLRRSLY-D-GFCMSFLTLLDQKKSEAILKRVIEKFTLGRLK 282
D3-REA1/1-259 210 LRD LFRWALRDVAGYE-----QLAASGY--MLLAERCRTPOEKVTVKKLEKVMKVK----- 259
D4-REA1/1-259 212 LRDILAWWEIFINKVFP-----KIQNKSTALI-QGAASMVFI DALGTNNTAYLAE----- 259
D5-REA1/1-266 213 LRDILRWLKL LN-QYS-----ICEDVDVDFVDIIVKQRFRTISDKNKAQLLEIDIFGKF----- 266
D6_REA1/1-245 225 VHDILLLSDE-----EP I EES-----LAAVI----- 245

```

FIGURE A.1: Alignment between Rea1's AAA⁺ domains and Dynein AAA1 module. Numbers (198, 58 and 91) indicate the amount of residues (not displayed) for H2 insertion motifs in D2, D4 and D6

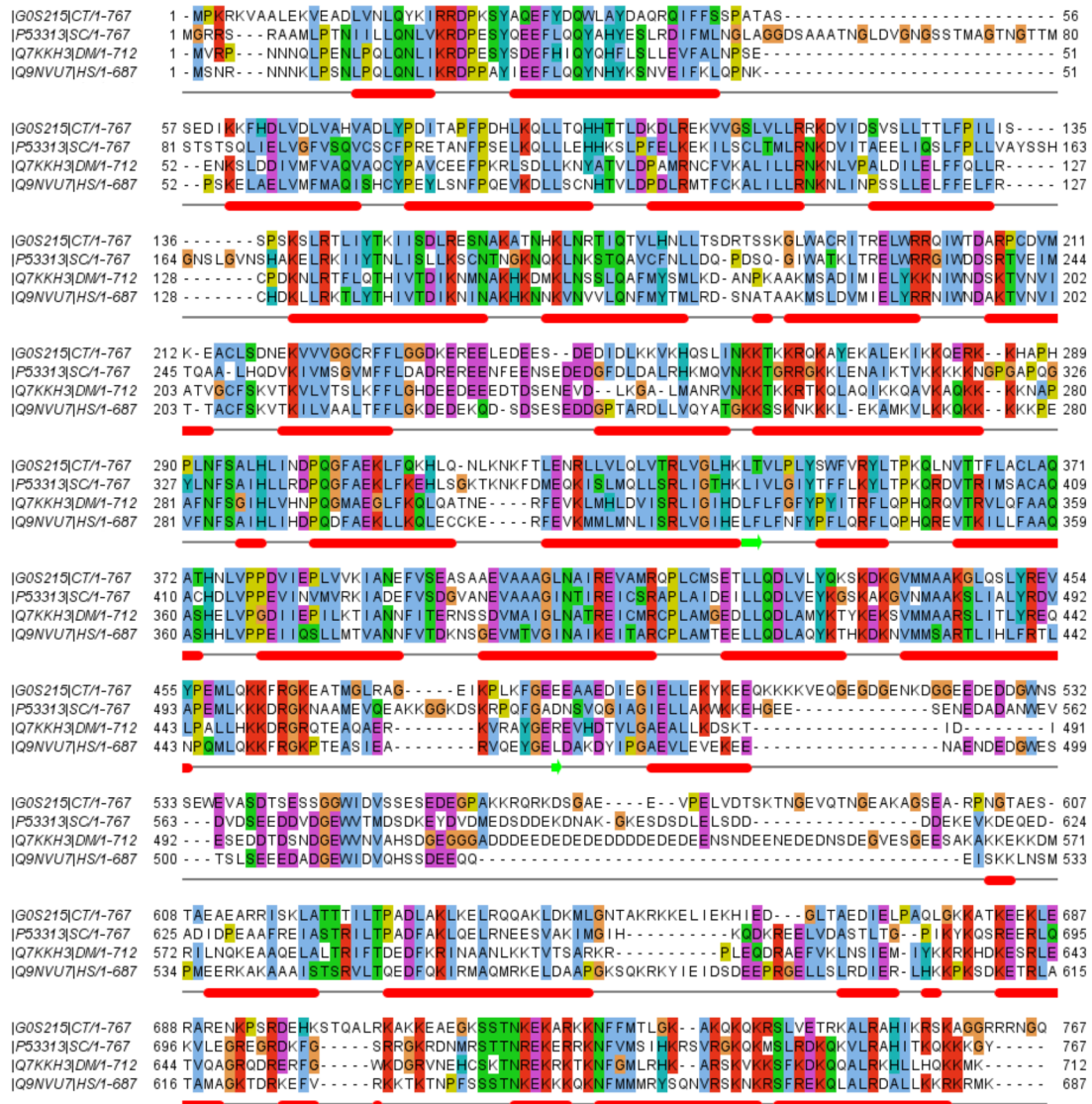


FIGURE A.2: *Sda1* secondary structure and sequence conservation. Alignment of *Sda1* sequences from *C. thermophilum* (CT), *S. cerevisiae*, *D. melanogaster* (DM) and *H. sapiens* (HS). Predicted α -helices for *S. cerevisiae* are shown in red (jnetpred).

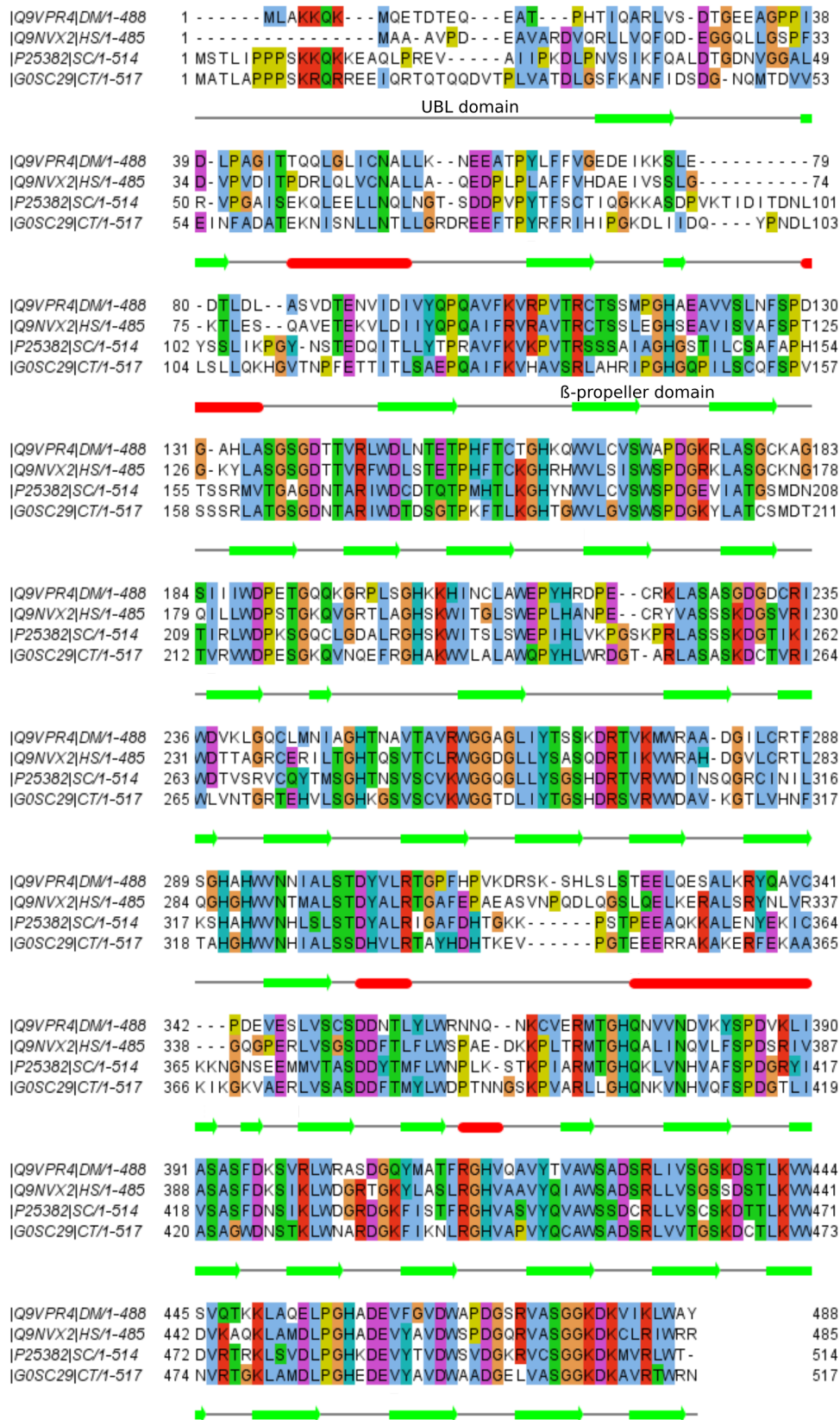


FIGURE A.3: Rsa4 secondary structure and sequence conservation. Alignment of Rsa4 sequences from *D. melanogaster* (DM), *H. sapiens* (HS), *S. cerevisiae* and *C. thermophilum* (CT). α -helices and β -sheets derived from PDB ID 4WJS are shown in red and green respectively.

List of Abbreviations

μg	Microgram
μl	Microliter
μM	Micromolar
3D	Three-dimensional
aa-tRNA	Aminoacyl-tRNA
A-site	Aminoacyl-site
ATP	Adenosine triphosphate
CAT tail	C-terminal Ala/Thr tail
<i>C. thermophilum</i>	Chaetomium thermophilum
CC	Cross-correlation
CTF	Contrast transfer function
CP	Central protruberance
cryo-EM	Cryo-electron microscopy
<i>D. discoideum</i>	Dictyostelium discoideum
D1, D2, D3, D4, D5, D6	Domains 1, 2, 3, 4, 5 and 6 on Rea1's AAA ⁺ domain
DC	Decoding center
<i>D. melanogaster</i>	Drosophila melanogaster
DNA	Deoxyribonucleic acid
DTT	Dithiothreitol
<i>E. coli</i>	Escherichia coli
ES	Expansion segment
E-site	Exit-site
ETS1, ETS2	External transcribed spacers 1 and 2
FG	Phenylalanine-glycine
FSC	Fourier shell correlation

GTP	Guanosine triphosphate
<i>H. sapiens</i>	Homo sapiens
H2	Helix 2 insertion motif (Rea1)
HEAT	Huntingtin, elongation factor 3, protein phosphatase 2A, Tor1
ITS1, ITS2	Internal transcribed spacers 1 and 2
kDa	Kilodalton
MDa	Megadalton
MDFE	Molecular dynamics flexible fitting
mg	Milligram
MIDAS	Metal ion-dependent adhesion site
mM	Millimolar
mRNA	Messenger RNA
NC	Nascent chain
NRD	Non-functional rRNA decay
NLS	Nuclear localization signal
NPC	Nuclear pore complex
OD	Optical density
PAGE	Polyacrylamide gel electrophoresis
PDB	Protein data bank
pre-rRNA	precursor rRNA
P-site	Peptidyl-site
PTC	Peptidyl transferase center
r.p.m.	Revolutions per minute
RAC	Ribosome associated complex
RNP	Ribonucleoprotein
r-proteins	Ribosomal proteins
RQC	Ribosome quality control
rRNA	Ribosomal RNA
S (unit)	Svedberg unit
<i>S. cerevisiae</i>	Saccharomyces cerevisiae
SDS	Sodium dodecyl sulfate
snoRNA	Small nucleolar RNA
snoRNP	Small nucleolar RNP
<i>T. thermophila</i>	Tetrahymena thermophila

TAP	Tandem affinity purification
TCA	Trichloroacetic acid
TE	Tunnel exit
tRNA	Transfer RNA
UBL	Ubiquitin-Like
WT	Wild type
XL-MS	Cross-linking and mass-spectrometry
YPD	Yeast extract peptone dextrose
YPG	Yeast extract peptone glycerol

References

- Adams, P. D. et al. (2010). “PHENIX: a comprehensive Python-based system for macromolecular structure solution”. In: *Acta Crystallogr.* 66, pp. 213–21. DOI: 10.1107/S0907444909052925.
- Anger, A. M. et al. (2013). “Structures of the human and drosophila 80S ribosome”. In: *Nature* 497, pp. 80–85. DOI: 10.1038/nature12104.
- Armache, J.-P. et al. (2010). “Cryo-EM structure and rRNA model of a translating eukaryotic 80S ribosome at 5.5 Å resolution”. In: *Proc. Natl. Acad. Sci. U. S. A.* 107, pp. 19748–19753. DOI: 10.1073/pnas.1009999107.
- Armistead, J. and B. Triggs-Raine (2014). “Diverse diseases from a ubiquitous process: The ribosomopathy paradox”. In: *FEBS Lett.* 588, pp. 1491–1500. DOI: 10.1016/j.febslet.2014.03.024.
- Asano, N. et al. (2015). “Structural and functional analysis of the Rpf2-Rrs1 complex in ribosome biogenesis”. In: *Nucleic Acids Res.* 43, pp. 4746–4757. DOI: 10.1093/nar/gkv305.
- Ban, N. et al. (2000). “The complete atomic structure of the large ribosomal subunit at 2.4 Å resolution”. In: *Science (80-.)*. 289, pp. 905–920. DOI: 10.1126/science.289.5481.905.
- Ban, N. et al. (2014). “A new system for naming ribosomal proteins”. In: *Curr. Opin. Struct. Biol.* 24, pp. 165–169. DOI: 10.1016/j.sbi.2014.01.002.
- Bange, G. et al. (2013). “New twist to nuclear import: When two travel together”. In: *Commun. Integr. Biol.* 6, pp. 1–9. DOI: 10.4161/cib.24792.
- Barrio-Garcia, C. et al. (2016). “Architecture of the Rix1-Rea1 checkpoint machinery during pre-60S-ribosome remodeling”. In: *Nat. Struct. Mol. Biol.* 23, pp. 37–44. DOI: 10.1038/nsmb.3132.
- Baßler, J. et al. (2001). “Identification of a 60S Preribosomal Particle that Is Closely Linked to Nuclear Export”. In: *Mol. Cell* 8.3, pp. 517–529. DOI: 10.1016/S1097-2765(01)00342-2.

- Baßler, J. et al. (2010). “The AAA-ATPase Rea1 drives removal of biogenesis factors during multiple stages of 60S ribosome assembly”. In: *Mol. Cell* 38, pp. 712–721. DOI: 10.1016/j.molcel.2010.05.024.
- Baßler, J. et al. (2014). “A network of assembly factors is involved in remodeling rRNA elements during preribosome maturation”. In: *J. Cell Biol.* 207, pp. 481–498. DOI: 10.1083/jcb.201408111JCB.
- Becker, T. et al. (2012). “Structural basis of highly conserved ribosome recycling in eukaryotes and archaea”. In: *Nature* 482, pp. 501–6. DOI: 10.1038/nature10829.
- Beckmann, R. et al. (2001). “Architecture of the Protein-Conducting Channel Associated with the Translating 80S Ribosome”. In: *Cell* 107.3, pp. 361–372. DOI: 10.1016/S0092-8674(01)00541-4.
- Behrmann, E. et al. (2015). “Structural snapshots of actively translating human ribosomes”. In: *Cell* 161, pp. 845–857. DOI: 10.1016/j.cell.2015.03.052.
- Ben-Shem, A. et al. (2011). “The structure of the eukaryotic ribosome at 3.0 Å resolution”. In: *Science (80-.)*. 334, pp. 1524–1529. DOI: 10.1126/science.1212642.
- Blanchard, S. C. et al. (2004). “tRNA dynamics on the ribosome during translation”. In: *Proc. Natl. Acad. Sci. U. S. A.* 101, pp. 12893–12898. DOI: 10.1073/pnas.0403884101.
- Bradatsch, B. et al. (2007). “Arx1 functions as an unorthodox nuclear export receptor for the 60S preribosomal subunit”. In: *Mol. Cell* 27, pp. 767–779. DOI: 10.1016/j.molcel.2007.06.034.
- Bradatsch, B. et al. (2012). “Structure of the pre-60S ribosomal subunit with nuclear export factor Arx1 bound at the exit tunnel”. In: *Nat. Struct. Mol. Biol.* 19, pp. 1234–1241. DOI: 10.1038/nsmb.2438.
- Brandman, O. and R. S. Hegde (2016). “Ribosome-associated protein quality control”. In: *Nat. Struct. Mol. Biol.* 23, pp. 7–15. DOI: 10.1038/nsmb.3147.
- Brandman, O. et al. (2012). “A ribosome-bound quality control complex triggers degradation of nascent peptides and signals translation stress”. In: *Cell* 151, pp. 1042–1054. DOI: 10.1016/j.cell.2012.10.044.
- Buscemi, G et al. (2000). “The *Saccharomyces cerevisiae* SDA1 gene is required for actin cytoskeleton organization and cell cycle progression”. In: *J. Cell Sci.* 113, pp. 1199–1211.
- Bussiere, C. et al. (2012). “Integrity of the P-site is probed during maturation of the 60S ribosomal subunit”. In: *J. Cell Biol.* 197, pp. 747–759. DOI: 10.1083/jcb.201112131.

- Butterfield, R. J. et al. (2014). “Congenital lethal motor neuron disease with a novel defect in ribosome biogenesis”. In: *Neurology* 82, pp. 1322–1330. DOI: 10.1212/WNL.0000000000000305.
- Calviño, F. R. et al. (2015). “Symportin 1 chaperones 5S RNP assembly during ribosome biogenesis by occupying an essential rRNA-binding site”. In: *Nat. Commun.* 6, p. 6510. DOI: 10.1038/ncomms7510.
- Castle, C. D. et al. (2010). “Las1L is a nucleolar protein required for cell proliferation and ribosome biogenesis”. In: *Mol. Cell. Biol.* 30.18, pp. 4404–4414. DOI: 10.1128/MCB.00358-10.
- Castle, C. D. et al. (2012). “LAS1L interacts with the mammalian Rix1 complex to regulate ribosome biogenesis”. In: *Mol. Biol. Cell* 23.4, pp. 716–728. DOI: 10.1091/mbc.E11-06-0530.
- Chen, J. Z. and N. Grigorieff (2006). “SIGNATURE: A single-particle selection system for molecular electron microscopy”. In: *J. Struct. Biol.* 157, pp. 168–173. DOI: 10.1016/j.jsb.2006.06.001.
- Choe, Y.-J. et al. (2016). “Failure of RQC machinery causes protein aggregation and proteotoxic stress”. In: *Nature* 531, pp. 191–195. DOI: 10.1038/nature16973.
- Cole, S. E. et al. (2009). “A convergence of rRNA and mRNA quality control pathways revealed by mechanistic analysis of nonfunctional rRNA decay”. In: *Mol. Cell* 34, pp. 440–450. DOI: 10.1016/j.molcel.2009.04.017.
- Connolly, K. and G. Culver (2009). “Deconstructing ribosome construction”. In: *Trends Biochem. Sci.* 34, pp. 256–263. DOI: 10.1016/j.tibs.2009.01.011.
- Cruz, J. de la et al. (2015). “Functions of ribosomal proteins in assembly of eukaryotic ribosomes in vivo”. In: *Annu. Rev. Biochem.* 84, pp. 93–129. DOI: 10.1146/annurev-biochem-060614-033917.
- Dai, M. S. and H. Lu (2008). “Crosstalk between c-Myc and ribosome in ribosomal biogenesis and cancer”. In: *J. Cell. Biochem.* 105, pp. 670–677. DOI: 10.1002/jcb.21895.
- Dai, M. S. et al. (2007a). “Feedback regulation of c-Myc by ribosomal protein L11”. In: *Cell Cycle* 6, pp. 2735–2741. DOI: 10.4161/cc.6.22.4895.
- Dai, M.-S. et al. (2007b). “Inhibition of c-Myc activity by ribosomal protein L11”. In: *EMBO J.* 26, pp. 3332–3345. DOI: 10.1038/emboj.2009.70.
- Defenouillère, Q. et al. (2013). “Cdc48-associated complex bound to 60S particles is required for the clearance of aberrant translation products”. In: *Proc. Natl. Acad. Sci. U. S. A.* 110, pp. 5046–5051. DOI: 10.1073/pnas.1221724110.

- Demoinet, E. et al. (2007). “The Hsp40 chaperone Jjj1 is required for the nucleocytoplasmic recycling of preribosomal factors in *Saccharomyces cerevisiae*”. In: *RNA* 13, pp. 1570–1581. DOI: 10.1261/rna.585007.
- Dever, T. E. and R. Green (2015). “The elongation, termination, and recycling: Phases of translation in eukaryotes”. In: *Cold Spring Harb. Perspect Biol*, pp. 1–16. DOI: 10.1101/cshperspect.a013706.
- Dez, C. et al. (2004). “Npa1p, a component of very early pre-60S ribosomal particles, associates with a subset of small nucleolar RNPs required for peptidyl transferase center modification”. In: *Mol. Cell. Biol.* 24, pp. 6324–37. DOI: 10.1128/MCB.24.14.6324-6337.2004.
- Dez, C. et al. (2006). “Surveillance of nuclear-restricted pre-ribosomes within a subnucleolar region of *Saccharomyces cerevisiae*”. In: *EMBO J.* 25, pp. 1534–46. DOI: 10.1038/sj.emboj.7601035.
- Dinman, J. D. (2009). “The eukaryotic ribosome: Current status and challenges”. In: *J. Biol. Chem.* 284, pp. 11761–11765. DOI: 10.1074/jbc.R800074200.
- Donati, G. et al. (2013). “5S ribosomal RNA is an essential component of a nascent ribosomal precursor complex that regulates the Hdm2-p53 checkpoint”. In: *Cell Rep.* 4, pp. 87–98. DOI: 10.1016/j.celrep.2013.05.045.
- Eswar, N. et al. (2006). “Comparative protein structure modeling using Modeller”. In: *Curr. Protoc. Bioinforma.* 5, pp. 1–47. DOI: 10.1002/0471250953.bi0506s15.
- Fatica, A. et al. (2002). “Ssf1p prevents premature processing of an early pre-60S ribosomal particle”. In: *Mol. Cell* 9, pp. 341–351. DOI: 10.1016/S1097-2765(02)00458-6.
- Fatica, A. et al. (2004). “PIN domain of Nob1p is required for D-site cleavage in 20S pre-rRNA”. In: *Rna* 10, pp. 1698–1701. DOI: 10.1261/rna.7123504.
- Fei, J. et al. (2008). “Coupling of ribosomal L1 stalk and tRNA dynamics during translation elongation”. In: *Mol. Cell* 30, pp. 348–359. DOI: 10.1016/j.molcel.2008.03.012.
- Frank, J and R. K. Agrawal (2000). “A ratchet-like inter-subunit reorganization of the ribosome during translocation”. In: *Nature* 406, pp. 318–322. DOI: 10.1038/35018597.
- Frank, J. (2002). “Single-particle imaging of macromolecules by cryo-electron microscopy”. In: *Annu. Rev. Biophys. Biomol. Struct.* 31, pp. 303–319. DOI: 10.1146/annurev.biophys.31.082901.134202.

- Frank, J. and M Radermacher (1996). "SPIDER and WEB : Processing and visualization of images in 3D electron microscopy and related fields". In: *J. Struct. Biol.* 116, pp. 190–199.
- Freed, E. F. et al. (2010). "When ribosomes go bad: diseases of ribosome biogenesis". In: *Mol. Biosyst.* 6, pp. 481–93. DOI: 10.1039/b919670f.
- Fromont-Racine, M. et al. (2003). "Ribosome assembly in eukaryotes". In: *Gene* 313, pp. 17–42. DOI: 10.1016/S0378-1119(03)00629-2.
- Fujii, K. et al. (2009). "A role for ubiquitin in the clearance of nonfunctional rRNAs". In: *Genes Dev.* 23, pp. 963–974. DOI: 10.1101/gad.1775609.
- Fujii, K. et al. (2012). "40S subunit dissociation and proteasome-dependent RNA degradation in nonfunctional 25S rRNA decay". In: *EMBO J.* 31, pp. 2579–2589. DOI: 10.1038/emboj.2012.85.
- Gadal, O. et al. (2001). "Nuclear export of 60s ribosomal subunits depends on Xpo1p and requires a nuclear export sequence-containing factor, Nmd3p, that associates with the large subunit protein Rpl10p". In: *Mol. Cell. Biol.* 21, pp. 3405–15. DOI: 10.1128/MCB.21.10.3405-3415.2001.
- Garbarino, J. E. and I. Gibbons (2002). "Expression and genomic analysis of midasin, a novel and highly conserved AAA protein distantly related to dynein". In: *BMC Genomics* 3.1, p. 18. DOI: 10.1186/1471-2164-3-18.
- Gartmann, M. et al. (2010). "Mechanism of eIF6-mediated inhibition of ribosomal subunit joining". In: *J. Biol. Chem.* 285, pp. 14848–14851. DOI: 10.1074/jbc.C109.096057.
- Gasse, L. et al. (2015). "Coordinated ribosomal ITS2 RNA processing by the Las1 complex integrating endonuclease, polynucleotide kinase, and exonuclease activities". In: *Mol. Cell* 60, pp. 808–815. DOI: 10.1016/j.molcel.2015.10.021.
- Grandi, P. et al. (2002). "90S pre-ribosomes include the 35S pre-rRNA, the U3 snoRNP, and 40S subunit processing factors but predominantly lack 60S synthesis factors". In: *Mol. Cell* 10, pp. 105–115. DOI: 10.1016/S1097-2765(02)00579-8.
- Granneman, S. et al. (2011). "A cluster of ribosome synthesis factors regulate pre-rRNA folding and 5.8S rRNA maturation by the Rat1 exonuclease". In: *EMBO J.* 30, pp. 4006–4019. DOI: 10.1038/emboj.2011.256.
- Grant, T. and N. Grigorieff (2015). "Measuring the optimal exposure for single particle cryo-EM using a 2.6 Å reconstruction of rotavirus VP6." In: *Elife* 4, pp. 1–19. DOI: 10.7554/eLife.06980.

- Greber, B. J. et al. (2012). “Cryo-EM structures of Arx1 and maturation factors Rei1 and Jjj1 bound to the 60S ribosomal subunit”. In: *Nat. Struct. Mol. Biol.* 19, pp. 1228–1233. DOI: 10.1038/nsmb.2425.
- Greber, B. J. et al. (2016). “Insertion of the biogenesis factor Rei1 probes the ribosomal tunnel during 60S maturation”. In: *Cell* 164, pp. 1–12. DOI: 10.1016/j.cell.2015.11.027.
- Grigorieff, N. (2007). “FREALIGN: High-resolution refinement of single particle structures”. In: *J. Struct. Biol.* 157, pp. 117–125. DOI: 10.1016/j.jsb.2006.05.004.
- Groft, C. M. et al. (2000). “Crystal structures of ribosome anti-association factor IF6”. In: *Nat Struct Biol* 7, pp. 1156–1164. DOI: 10.1038/82017.
- Hedges, J. et al. (2005). “Release of the export adapter, Nmd3p, from the 60S ribosomal subunit requires Rpl10p and the cytoplasmic GTPase Lsg1p”. In: *EMBO J.* 24, pp. 567–79. DOI: 10.1038/sj.emboj.7600547.
- Henras, A. K. et al. (2008). “The post-transcriptional steps of eukaryotic ribosome biogenesis”. In: *Cell. Mol. Life Sci.* 65, pp. 2334–2359. DOI: 10.1007/s00018-008-8027-0.
- Henras, A. K. et al. (2015). “An overview of pre-ribosomal RNA processing in eukaryotes”. In: *Wiley Interdiscip. Rev. RNA* 6, pp. 225–242. DOI: 10.1002/wrna.1269.
- Hinnebusch, A. G. and J. R. Lorsch (2012). “The mechanism of eukaryotic translation initiation: New insights and challenges”. In: *Cold Spring Harb. Perspect Biol* 4, pp. 1–25. DOI: 10.1101/cshperspect.a011544.
- Hung, N.-J. and A. W. Johnson (2006). “Nuclear recycling of the pre-60S ribosomal subunit-associated factor Arx1 depends on Rei1 in *Saccharomyces cerevisiae*.” In: *Mol. Cell. Biol.* 26, pp. 3718–27. DOI: 10.1128/MCB.26.10.3718-3727.2006.
- Jackson, R. J. et al. (2010). “The mechanism of eukaryotic translation initiation and principles of its regulation”. In: *Nat. Rev. Mol. Cell Biol.* 10, pp. 113–127. DOI: 10.1038/nrm2838.
- Janke, C. et al. (2004). “A versatile toolbox for PCR-based tagging of yeast genes: New fluorescent proteins, more markers and promoter substitution cassettes”. In: *Yeast* 21, pp. 947–962. DOI: 10.1002/yea.1142.
- Jeeninga, R. E. et al. (1997). “Variable regions V13 and V3 of *Saccharomyces cerevisiae* contain structural features essential for normal biogenesis and stability of 5.8S and 25S rRNA.” In: *RNA* 3, pp. 476–88.
- Kappel, L. et al. (2012). “Rlp24 activates the AAA-ATPase Drg1 to initiate cytoplasmic pre-60S maturation”. In: *J. Cell Biol.* 199, pp. 771–782. DOI: 10.1083/jcb.201205021.

- Kemmler, S. et al. (2009). “Yvh1 is required for a late maturation step in the 60S biogenesis pathway”. In: *J. Cell Biol.* 186, pp. 863–880. DOI: 10.1083/jcb.200904111.
- Kharde, S. et al. (2015). “The structure of Rpf2-Rrs1 explains its role in ribosome biogenesis.” In: *Nucleic Acids Res.* 43, pp. 7083–95. DOI: 10.1093/nar/gkv640.
- Klinge, S. et al. (2011). “Crystal structure of the eukaryotic 60S ribosomal subunit in complex with initiation factor 6”. In: *Science (80-.)*. 334, pp. 941–948.
- Kon, T. et al. (2012). “The 2.8 Å crystal structure of the dynein motor domain”. In: *Nature* 484, pp. 345–350. DOI: 10.1038/nature10955.
- Kornprobst, M. et al. (2016). “Architecture of the 90S Pre-ribosome: A structural view on the birth of the eukaryotic ribosome”. In: *Cell* 166, pp. 380–393. DOI: 10.1016/j.cell.2016.06.014.
- Kos, M. and D. Tollervey (2010). “Yeast pre-rRNA processing and modification occur cotranscriptionally”. In: *Mol. Cell* 37, pp. 809–820. DOI: 10.1016/j.molcel.2010.02.024.
- Kressler, D. et al. (2012a). “Synchronizing nuclear import of ribosomal proteins with ribosome assembly”. In: *Science (80-.)*. 338, pp. 666–671. DOI: 10.1126/science.1226960.
- Kressler, D. et al. (2008). “The AAA ATPase Rix7 powers progression of ribosome biogenesis by stripping Nsa1 from pre-60S particles”. In: *J. Cell Biol.* 181, pp. 935–944. DOI: 10.1083/jcb.200801181.
- Kressler, D. et al. (2010). “Driving ribosome assembly”. In: *Biochim. Biophys. Acta* 1803, pp. 673–683. DOI: 10.1016/j.bbamcr.2009.10.009.
- Kressler, D. et al. (2012b). “The power of AAA-ATPases on the road of pre-60S ribosome maturation - Molecular machines that strip pre-ribosomal particles”. In: *Biochim. Biophys. Acta* 1823, pp. 92–100. DOI: 10.1016/j.bbamcr.2011.06.017.
- Kucukelbir, A. et al. (2014). “Quantifying the local resolution of cryo-EM density maps”. In: *Nat. Methods* 11, pp. 63–5. DOI: 10.1038/nmeth.2727.
- Lafontaine, D. L. J. and D Tollervey (2001). “The function and synthesis of ribosomes”. In: *Nat. Rev. Mol. Cell Biol.* 2, pp. 514–20. DOI: 10.1038/35080045.
- Lafontaine, D. L. J. et al. (1998). “Yeast 18S rRNA dimethylase Dim1p: a quality control mechanism in ribosome synthesis?” In: *Mol. Cell. Biol.* 18, pp. 2360–2370.
- Lafontaine, D. L. J. (2015). “Noncoding RNAs in eukaryotic ribosome biogenesis and function”. In: *Nat. Struct. & Mol. Biol.* 22, pp. 11–19. DOI: 10.1038/nsmb.2939.
- LaRiviere, F. J. et al. (2006). “A late-acting quality control process for mature eukaryotic rRNAs”. In: *Mol. Cell* 24, pp. 619–626. DOI: 10.1016/j.molcel.2006.10.008.

- Lebreton, A. et al. (2006). "A functional network involved in the recycling of nucleocytoplasmic pre-60S factors". In: *J. Cell Biol.* 173, pp. 349–360. DOI: 10.1083/jcb.200510080.
- Leidig, C. et al. (2013). "Structural characterization of a eukaryotic chaperone — the ribosome-associated complex". In: *Nat Struct Biol* 20, pp. 23–30. DOI: 10.1038/nsmb.2447.
- Leidig, C. et al. (2014). "60S ribosome biogenesis requires rotation of the 5S ribonucleoprotein particle". In: *Nat. Commun.* 5, p. 3491. DOI: 10.1038/ncomms4491.
- Li, X. et al. (2013). "Electron counting and beam-induced motion correction enable near-atomic-resolution single-particle cryo-EM". In: *Nat. Methods* 10, pp. 584–90. DOI: 10.1038/nmeth.2472.
- Lo, K. Y. et al. (2009). "Ribosome stalk assembly requires the dual-specificity phosphatase Yvh1 for the exchange of Mrt4 with P0". In: *J. Cell Biol.* 186, pp. 849–862. DOI: 10.1083/jcb.200904110.
- Lo, K. Y. et al. (2010). "Defining the pathway of cytoplasmic maturation of the 60S ribosomal subunit". In: *Mol. Cell* 39, pp. 196–208. DOI: 10.1016/j.molcel.2010.06.018.
- Longtine, M. S. et al. (1998). "Additional modules for versatile and economical PCR-based gene deletion and modification in *Saccharomyces cerevisiae*". In: *Yeast* 14.10, pp. 953–961. DOI: 10.1002/(SICI)1097-0061(199807)14:10<953::AID-YEA293>3.0.CO;2-U.
- Lyumkis, D. et al. (2014). "Structural basis for translational surveillance by the large ribosomal subunit-associated protein quality control complex". In: *Proc. Natl. Acad. Sci. U. S. A.* 111, pp. 15981–6. DOI: 10.1073/pnas.1413882111.
- Madru, C. et al. (2015). "Chaperoning 5S RNA assembly". In: *Genes Dev.* 29, pp. 1432–1446. DOI: 10.1101/gad.260349.115.
- Matsuo, Y. et al. (2014). "Coupled GTPase and remodelling ATPase activities form a checkpoint for ribosome export." In: *Nature* 505, pp. 112–6. DOI: 10.1038/nature12731.
- Melnikov, S. et al. (2012). "One core, two shells: bacterial and eukaryotic ribosomes". In: *Nat. Struct. Mol. Biol.* 19, pp. 560–567. DOI: 10.1038/nsmb.2313.
- Meyer, A. E. et al. (2010). "The cytosolic J-protein, Jjj1, and Rei1 function in the removal of the pre-60 S subunit factor Arx1". In: *J. Biol. Chem.* 285, pp. 961–968. DOI: 10.1074/jbc.M109.038349.
- Moazed, D and H. F. Noller (1989). "Intermediate states in the movement of transfer RNA in the ribosome". In: *Nature* 342, pp. 142–8. DOI: 10.1038/342142a0.

- Mougey, E. B. et al. (1993). "The terminal balls characteristic of eukaryotic rRNA transcription units in chromatin spreads are rRNA processing complexes". In: *Genes Dev.* 7.8, pp. 1609–1619. DOI: 10.1101/gad.7.8.1609.
- Moy, T. I. and P. A. Silver (2002). "Requirements for the nuclear export of the small ribosomal subunit". In: *J. Cell Sci.* 115, pp. 2985–2995.
- Myasnikov, A. G. et al. (2014). "The molecular structure of the left-handed supra-molecular helix of eukaryotic polyribosomes." In: *Nat. Commun.* 5, p. 5294. DOI: 10.1038/ncomms6294.
- Nierhaus, K. H. and F Dohme (1974). "Total Reconstitution of Functionally Active 50S Ribosomal Subunits from Escherichia coli". In: *Proc. Natl. Acad. Sci.* 71.12, pp. 4713–4717. DOI: 10.1073/pnas.71.12.4713.
- Nishimura, K. et al. (2009). "An auxin-based degron system for the rapid depletion of proteins in nonplant cells". In: *Nat. Methods* 6, pp. 917–922. DOI: 10.1038/nmeth.1401.
- Nissan, T. A. et al. (2002). "60S pre-ribosome formation viewed from assembly in the nucleolus until export to the cytoplasm". In: *EMBO J.* 21, pp. 5539–5547.
- Nissan, T. A. et al. (2004). "A pre-ribosome with a tadpole-like structure functions in ATP-dependent maturation of 60S subunits". In: *Mol. Cell* 15, pp. 295–301. DOI: 10.1016/j.molcel.2004.06.033.
- Nissen, P. et al. (2000). "The structural basis of ribosome activity in peptide bond synthesis". In: *Science (80-.)*. 289, pp. 920–930. DOI: 10.1126/science.289.5481.920.
- Oeffinger, M. et al. (2004). "A pre-ribosome-associated HEAT-repeat protein is required for export of both ribosomal subunits". In: *Genes Dev.* 18, pp. 196–209. DOI: 10.1101/gad.285604.
- Oskarsson, T. and A. Trumpp (2005). "The Myc trilogy: Lord of RNA polymerases". In: *Nat. Cell Biol.* 7, pp. 215–217. DOI: 10.1038/ncb0305-215.
- Pertschy, B. et al. (2007). "Cytoplasmic recycling of 60S preribosomal factors depends on the AAA protein Drg1". In: *Mol. Cell. Biol.* 27, pp. 6581–6592. DOI: 10.1128/MCB.00668-07.
- Pertschy, B. et al. (2009). "RNA helicase Prp43 and its co-factor Pfa1 promote 20 to 18S rRNA processing catalyzed by the endonuclease Nob1". In: *J. Biol. Chem.* 284, pp. 35079–35091. DOI: 10.1074/jbc.M109.040774.
- Peske, F. et al. (2005). "Sequence of steps in ribosome recycling as defined by kinetic analysis". In: *Mol. Cell* 18, pp. 403–412. DOI: 10.1016/j.molcel.2005.04.009.

- Petry, S. et al. (2008). "The termination of translation". In: *Curr. Opin. Struct. Biol.* 18, pp. 70–77. DOI: 10.1016/j.sbi.2007.11.005.
- Pettersen, E. F. et al. (2004). "UCSF Chimera - A visualization system for exploratory research and analysis". In: *J. Comput. Chem.* 25, pp. 1605–1612. DOI: 10.1002/jcc.20084.
- Pisarev, A. V. et al. (2007). "Recycling of eukaryotic posttermination ribosomal complexes". In: *Cell* 131, pp. 286–299. DOI: 10.1016/j.cell.2007.08.041.
- Preis, A. et al. (2014). "Cryoelectron microscopic structures of eukaryotic translation termination complexes containing eRF1-eRF3 or eRF1-ABCE1". In: *Cell Rep.* 8, pp. 59–65.
- Rabl, J. et al. (2011). "Crystal structure of the eukaryotic 40S ribosomal subunit in complex with initiation factor 1". In: *Science* 331, pp. 730–736. DOI: 10.1126/science.1198308.
- Rigaut, G et al. (1999). "A generic protein purification method for protein complex characterization and proteome exploration". In: *Nat. Biotechnol.* 17, pp. 1030–1032. DOI: 10.1038/13732.
- Rodríguez-Galán, O. et al. (2015). "Immature large ribosomal subunits containing the 7S pre-rRNA can engage in translation in *Saccharomyces cerevisiae*". In: *RNA Biol.* 12, pp. 838–846. DOI: 10.1080/15476286.2015.1058477.
- Rodríguez-Mateos, M. et al. (2009). "Role and dynamics of the ribosomal protein P0 and its related trans-acting factor Mrt4 during ribosome assembly in *Saccharomyces cerevisiae*". In: *Nucleic Acids Res.* 37, pp. 7519–7532. DOI: 10.1093/nar/gkp806.
- Rohou, A. and N. Grigorieff (2015). "CTFFIND4: Fast and accurate defocus estimation from electron micrographs". In: *J. Struct. Biol.* 192, pp. 216–221. DOI: 10.1016/j.jsb.2015.08.008.
- Rosenthal, P. B. and R. Henderson (2003). "Optimal determination of particle orientation, absolute hand, and contrast loss in single-particle electron cryomicroscopy". In: *J. Mol. Biol.* 333, pp. 721–745. DOI: 10.1016/j.jmb.2003.07.013.
- Schäfer, T. et al. (2003). "The path from nucleolar 90S to cytoplasmic 40S pre-ribosomes". In: *EMBO J.* 22, pp. 1370–1380. DOI: 10.1093/emboj/cdg121.
- Schäfer, T. et al. (2006). "Hrr25-dependent phosphorylation state regulates organization of the pre-40S subunit". In: *Nature* 441, pp. 651–5. DOI: 10.1038/nature04840.

- Scheres, S. H. W. (2012). “RELION: Implementation of a Bayesian approach to cryo-EM structure determination”. In: *J. Struct. Biol.* 180.3, pp. 519–530. DOI: 10.1016/j.jsb.2012.09.006.
- Schlutzen, F. et al. (2000). “Structure of functionally activated small ribosomal subunit at 3.3 Å resolution”. In: *Cell* 102, pp. 615–623.
- Schmeing, T. M. et al. (2009). “The crystal structure of the ribosome bound to EF-Tu and aminoacyl-tRNA”. In: *Science (80-.)*. 326, pp. 688–695. DOI: 10.1126/science.1179700.
- Schütz, S. et al. (2014). “A RanGTP-independent mechanism allows ribosomal protein nuclear import for ribosome assembly”. In: *Elife* 79, pp. 1–24. DOI: 10.7554/eLife.03473.
- Selmer, M. et al. (2006). “Structure of the 70S ribosome complexed with mRNA and tRNA”. In: *Science (80-.)*. 313, pp. 1935–1942. DOI: 10.1089/zeb.2014.0984.
- Senger, B. et al. (2001). “The nucle(ol)ar Tif6p and Efl1p are required for a late cytoplasmic step of ribosome synthesis”. In: *Mol. Cell* 8, pp. 1363–1373. DOI: 10.1016/S1097-2765(01)00403-8.
- Sengupta, J. et al. (2010). “Characterization of the nuclear export adaptor protein Nmd3 in association with the 60S ribosomal subunit”. In: *J. Cell Biol.* 189, pp. 1079–1086. DOI: 10.1083/jcb.201001124.
- Shajani, Z. et al. (2011). “Assembly of bacterial ribosomes”. In: *Annu. Rev. Biochem.* 80, pp. 501–26. DOI: 10.1146/annurev-biochem-062608-160432.
- Shao, S. et al. (2015). “Structure and assembly pathway of the ribosome quality control complex”. In: *Mol. Cell* 57, pp. 433–444. DOI: 10.1016/j.molcel.2014.12.015.
- Shchepachev, V. and D. Tollervy (2016). “Motoring toward pre-60S-ribosome export”. In: *Nat. Struct. Mol. Biol.* 23.1, pp. 3–4. DOI: 10.1038/nsmb.3154.
- Shen, P. S. et al. (2015). “Rqc2p and 60S ribosomal subunits mediate mRNA-independent elongation of nascent chains”. In: *Science (80-.)*. 347, pp. 75–78.
- Shine, J and L Dalgarno (1974). “The 3'-terminal sequence of Escherichia coli 16S ribosomal RNA: complementarity to nonsense triplets and ribosome binding sites”. In: *Proc. Natl. Acad. Sci. U. S. A.* 71, pp. 1342–1246. DOI: 10.1073/pnas.71.4.1342.
- Shoemaker, C. J. and R. Green (2012). “Translation drives mRNA quality control”. In: *Nat. Struct. Mol. Biol.* 19, pp. 594–601. DOI: 10.1038/nsmb.2301.

- Söding, J. et al. (2005). “The HHpred interactive server for protein homology detection and structure prediction”. In: *Nucleic Acids Res.* 33, pp. 244–248. DOI: 10.1093/nar/gki408.
- Sonenberg, N. and A. G. Hinnebusch (2009). “Regulation of translation initiation in eukaryotes: Mechanisms and biological targets”. In: *Cell* 136, pp. 731–745. DOI: 10.1016/j.cell.2009.01.042.
- Spahn, C. M. T. et al. (2001). “Structure of the 80S ribosome from *Saccharomyces cerevisiae* - tRNA-ribosome and subunit-subunit interactions”. In: *Cell* 107, pp. 373–386. DOI: 10.1016/S0092-8674(01)00539-6.
- Steitz, T. a. (2008). “A structural understanding of the dynamic ribosome machine”. In: *Nat. Rev. Mol. Cell Biol.* 9, pp. 242–253. DOI: 10.1038/nrm2352.
- Strunk, B. S. and K. Karbstein (2009). “Powering through ribosome assembly”. In: *RNA* 15, pp. 2083–2104. DOI: 10.1261/rna.1792109.
- Strunk, B. S. et al. (2011). “Ribosome assembly factors prevent premature translation initiation by 40S assembly intermediates”. In: *Science (80-.)*. 333, pp. 1449–1454. DOI: 10.1126/science.1208245.
- Strunk, B. S. et al. (2012). “A translation-like cycle is a quality control checkpoint for maturing 40S ribosome subunits”. In: *Cell* 150, pp. 111–121. DOI: 10.1016/j.cell.2012.04.044.
- Sweeney, R et al. (1994). “An rRNA variable region has an evolutionarily conserved essential role despite sequence divergence”. In: *Mol. Cell. Biol.* 14, pp. 4203–15. DOI: 10.1128/MCB.14.6.4203.Updated.
- Trabuco, L. G. et al. (2008). “Flexible fitting of atomic structures into electron microscopy maps using molecular dynamics”. In: *Structure* 16, pp. 673–683. DOI: 10.1016/j.str.2008.03.005.
- Traub, P and M Nomura (1968). “Structure and function of *E. coli* ribosomes. V. Reconstitution of functionally active 30S ribosomal particles from RNA and proteins”. In: *Proc. Natl. Acad. Sci. U. S. A.* 59, pp. 777–784. DOI: 10.1073/pnas.59.3.777.
- Tschochner, H. and E. Hurt (2003). “Pre-ribosomes on the road from the nucleolus to the cytoplasm”. In: *Trends Cell Biol.* 13, pp. 255–263. DOI: 10.1016/S0962-8924(03)00054-0.
- Udem, S. a. and R Warner (1973). “The cytoplasmic maturation of a ribosomal precursor ribonucleic acid in yeast”. In: *J. Biol. Chem.* 248, pp. 1412–1416.

- Ulbrich, C. et al. (2009). “Mechanochemical removal of ribosome biogenesis factors from nascent 60S ribosomal subunits”. In: *Cell* 138, pp. 911–922. DOI: 10.1016/j.cell.2009.06.045.
- Voorhees, R. M. and V Ramakrishnan (2013). “Structural basis of the translational elongation cycle”. In: *Annu. Rev. Biochem.* 82, pp. 203–236. DOI: 10.1146/annurev-biochem-113009-092313.
- Warner, J. R. (1999). “The economics of ribosome biosynthesis in yeast”. In: *Trends Biochem. Sci.* 24, pp. 437–440. DOI: 10.1016/S0968-0004(99)01460-7.
- Weis, F. et al. (2015). “Mechanism of eIF6 release from the nascent 60S ribosomal subunit”. In: *Nat. Struct. Mol. Biol.* 22, pp. 914–919. DOI: 10.1038/nsmb.3112.
- West, M. et al. (2005). “Defining the order in which Nmd3p and Rpl10p load onto nascent 60S ribosomal subunits”. In: *Mol. Cell. Biol.* 25, pp. 3802–13. DOI: 10.1128/MCB.25.9.3802-3813.2005.
- Wilson, D. N. and J. H. D. Cate (2012). “The structure and function of the eukaryotic ribosome”. In: *Cold Spring Harb. Perspect Biol* 4:a011536, pp. 1–18. DOI: 10.1101/cshperspect.a011536.
- Wimberly, B. T. et al. (2000). “Structure of the 30S ribosomal subunit”. In: *Nature* 407, pp. 327–39. DOI: 10.1038/35030006.
- Woolford, J. L. and S. J. Baserga (2013). “Ribosome biogenesis in the yeast *Saccharomyces cerevisiae*”. In: *Genetics* 195, pp. 643–681. DOI: 10.1534/genetics.113.153197.
- Wu, S. et al. (2016). “Diverse roles of assembly factors revealed by structures of late nuclear pre-60S ribosomes”. In: *Nature* 534, pp. 133–137. DOI: 10.1038/nature17942.
- Zavialov, A. V. et al. (2005). “Splitting of the posttermination ribosome into subunits by the concerted action of RRF and EF-G”. In: *Mol. Cell* 18, pp. 675–686. DOI: 10.1016/j.molcel.2005.05.016.
- Zhang, J. et al. (2007). “Assembly factors Rpf2 and Rrs1 recruit 5S rRNA and ribosomal proteins rpL5 and rpL11 into nascent ribosomes”. In: *Genes Dev.* 21, pp. 2580–2592. DOI: 10.1101/gad.1569307.
- Zheng, J. et al. (2015). “Structure of human MDM2 complexed with RPL11 reveals the molecular basis of p53 activation”. In: *Genes Dev.* 29, pp. 1524–1534. DOI: 10.1101/gad.261792.115.

Acknowledgements

I had a great time in the Beckmann Lab and I really want to thank Prof. Roland Beckmann to give me this opportunity. Specially because he did it despite my lack of biochemistry background and because he has always been very encouraging and supportive.

I would like to thank Prof. Karl-Peter Hopfner and Dr. Daniel Wilson for being part of my thesis advisory committee, for all the nice suggestions and for being so friendly and accessible.

I am deeply thankful to Dr. Thomas Becker for correcting this dissertation and for taking so nicely care of me as a poor physicist. . . he taught me almost everything I can do in the wet-lab. The rest I learnt from the brilliant Chris. Lukas's help on processing the Rix1-Rea1 particle during his practicum was crucial. I thank him as well as Stephan, Christoph, Andre and Stefan for sharing their very useful scripts. Many thanks to Alexei for finding all possible typos in any thing I wrote during my PhD. Thanks to Marco, Anne, Yui, Bertrand, Kadda, Ting, Martin, Daniel, Andy and J.P for all the help at work and all the fun times.

My special appreciation goes to Prof. Ed Hurt, Dr. Matthias Thoms and Anshuk Sharkar from the Hurt Lab at Heidelberg University. I really enjoyed working with their team. This thesis would not have been possible without their beautiful purifications of pre-60S intermediates and all the knowledge about ribosome biogenesis they shared with us.

Many thanks to Charlotte Ungewickell and Dr. Otto Berninghausen for their indispensable care of the microscopes, grid making and data collection; to Heidi Sieber, Andrea Gilmozzi, Joana Musial and Susi Rieder for the great job they do in the lab; and to everyone in the Beckmann and Wilson Labs (including the older and newer generations) for the very enjoyable environment.

I also want to thank the Graduate School GRK1721 for their funding and the all people being part of it for their efforts in creating such a stimulating programme.

Sin lugar a duda, la persona más importante para que esta tesis haya llegado a su fin es Sebastian, le doy las gracias por su apoyo indispensable. A mis padres y a mi hermano les agradezco infinitamente su cariño, su sentido del humor y la sencillez con la que me han enseñado a disfrutar de la vida. Mi interés por la ciencia se debe sobretodo a ellos. Ines, Ana, Mariel, Jezabel, Nico, Justina y Peter son responsables de muchísimos buenos ratos en Múnich y espero que en el futuro los sigamos teniendo allá donde estemos. Isa se merece una mención especial, gracias a ella decidí buscar un doctorado en Alemania. A Mateo le agradezco sus playlists motivacionales para escribir la tesis. Al resto de mi gran familia, a las HBKs, a mis amigos de toda la vida y a los fisiquillos, les agradezco que estén ahí y que sean el principal motivo para que siempre quiera volver a casa.

Curriculum Vitae

Personal Details

Name Clara Barrio García
 Date of birth 8.10.1987
 Place of birth Madrid, Spain
 Nationality Spanish

Education

- 2012–Current **Doctoral Researcher**, *Gene Center, Ludwig Maximilians University*, Munich (Germany).
 Doctoral Thesis Titled: "Structural view on 60S ribosome biogenesis: remodeling and quality control mechanisms". Under the supervision of Prof. Dr. Roland Beckmann
- 2011–2012 **Master in Biophysics**, *Universidad Autónoma de Madrid*, Madrid (Spain).
- 2010–2011 **Imperial College International Diploma**, *Imperial College London*, London (UK).
 One year placement studying Physics within an Erasmus Programme
- 2005–2011 **Graduate in Physics**, *Universidad Autónoma de Madrid*, Madrid (Spain).

Courses and Conferences

- 2015 **EMBO Conference on Ribosome Synthesis**, Brussels (Belgium).
- 2013 **Cold Spring Harbor Protein Purification Course**, Cold Spring Harbor, NY (USA).

Publications

- 2016 **Barrio-Garcia C**, Thoms M, Flemming D, Kater L, Berninghausen O, Baßler J, Beckmann R, Hurt E. Architecture of the Rix1-Rea1 checkpoint machinery during pre-60S-ribosome remodeling. *Nature Structural and Molecular Biology*.
- 2014 Bassler J, Paternoga H, Holdermann I, Thoms M, Granneman S, **Barrio-Garcia C**, Nyarko A, Lee W, Stier G, Clark SA, Schraivogel D, Kallas M, Beckmann R, Tollervey D, Barbar E, Sinning I, Hurt E. A network of assembly factors is involved in remodeling rRNA elements during preribosome maturation. *Journal of Cell Biology*.
- 2014 Preis A, Heuer A, **Barrio-Garcia C**, Hauser A, Eyler DE, Berninghausen O, Green R, Becker T, Beckmann R. Cryoelectron microscopic structures of eukaryotic translation termination complexes containing eRF1-eRF3 or eRF1-ABCE1. *Cell Reports*.
- 2014 Gogala M, Becker T, Beatrix B, Armache JP, **Barrio-Garcia C**, Berninghausen O, Beckmann R. Structures of the Sec61 complex engaged in nascent peptide translocation or membrane insertion. *Nature*.
- 2012 Hervás R, Galera-Prat A, Gómez-Sicilia A, Losada-Urzáiz F, Fernández M, Fernández-Bravo D, Santana E, **Barrio-Garcia C**, Melero C, Carrión-Vazquez M. Nanomechanics of proteins, both Folded and Disordered. Chapter 1 of *Single-Molecule Studies of Proteins*, Springer.